HIGHWAY RESEARCH RECORD

Number 48

Measurements and Relationships of Soil Stress and Strength

5 Reports

Presented at the
43rd ANNUAL MEETING
January 13-17, 1964

HIGHWAY RESEARCH BOARD
of the
Division of Engineering and Industrial Research
National Academy of Sciences—
National Research Council
Washington, D. C.
1964

Department of Soils, Geology and Foundations

Eldon J. Yoder, Chairman
Joint Highway Research Project
Purdue University, Lafayette, Indiana

COMMITTEE ON STRESS DISTRIBUTION IN EARTH MASSES

(As of December 31, 1963)

H. Bolton Seed, Chairman
Department of Civil Engineering
University of California, Berkeley

Richard G. Ahlvin, Chief Engineer, Special Projects Section, Waterways Experiment Station, Vicksburg, Mississippi
E. S. Barber, Consulting Engineer, Soil Mechanics and Foundations, Arlington, Virginia
B. E. Colley, Portland Cement Association, Skokie, Illinois
Melvin T. Davisson, University of Illinois, Urbana
Lawrence A. DuBose, Testing Service Corporation, Lombard, Illinois
Austin H. Emery, Associate Soils Engineer, Bureau of Soil Mechanics, New York State Department of Public Works, Albany
Jacob Feld, Consulting Engineer, New York, N. Y.
F. N. Finn, Technical Director, Products Engineering, Golden Bear Oil Company, Bakersfield, California
Hamilton Gray, Chairman, Department of Civil Engineering, Ohio State University, Columbus
Milton E. Harr, Associate Professor of Soil Mechanics, School of Civil Engineering, Purdue University, Lafayette, Indiana
R. G. Hennes, Department of Civil Engineering, University of Washington, Seattle
W. S. Housel, University of Michigan, Ann Arbor
T. F. McMahon, U. S. Bureau of Public Roads, Washington, D. C.
Robert L. McNeill, Supervisor, Soil Dynamics, Shock Tube Laboratory, University Station, Albuquerque, New Mexico
Carl L. Monismith, University of California, Berkeley
J. O. Osterberg, Civil Engineering Department, Northwestern University, Evanston, Illinois
F. E. Richart, Jr., University of Michigan, Ann Arbor
Robert L. Schiffman, Soil Engineering Division, Massachusetts Institute of Technology, Cambridge
Werner E. Schmid, Assistant Professor, Department of Civil Engineering, Princeton University, Princeton, New Jersey
F. H. Scrivner, Pavement Research Engineer, Texas Transportation Institute, A and M College of Texas, College Station

Contents

STRENGTH-CONSISTENCY INDICES FOR A COHESIVE SOIL

Raymond J. Krizek and Robert L. Kondner 1

EVALUATION OF THE LABORATORY VANE SHEAR TEST

R. D. Goughnour and J. R. Sallberg. 19

PIEZOELECTRIC GAGES FOR DYNAMIC SOIL STRESS MEASUREMENT

E. T. Selig and E. Vey. 34

EFFECT OF STRESS HISTORY ON STRENGTH OF COHESIVE SOILS

W. H. Perloff, Jr., and J. O. Osterberg 49

LOAD-TIME RELATIONSHIPS IN DIRECT SHEAR OF SOIL

H. C. Saxe, L. D. Graves, and B. B. Schimming 72

Strength-Consistency Indices For a Cohesive Soil

RAYMOND J. KRIZEK and ROBERT L. KONDNER
Respectively, Assistant Professor and Associate Professor of Civil Engineering, Northwestern University

Stress-strain response data from approximately 200 constant strain-rate, uniaxial, compression tests on a remolded, plastic clay are analyzed to determine an analytic form of stress-strain relation in terms of strength-consistency indices. These indices are the compressive strength and failure strain of the soil. Variables included in the study are stress, strain, compressive strength, failure strain, moisture content, material history and preparation procedure. The methods of preparation are compaction and extrusion and the various imposed histories include creep, vibration (repeated load applications), overconsolidation and desiccation. Illustrative examples from the literature include the effects of variable strain rate and confining stress and are presented to demonstrate the usefulness of the strength-consistency indices in control and testing of materials.

•A PROBLEM of considerable importance in control and testing of materials, as well as the practical aspects of many phases of highway construction, is that of estimating the response of a cohesive soil at a particular consistency or strength under a particular set of environmental circumstances from the response for the same set of circumstances but at a different moisture content or consistency of the soil. One approach to this problem is the use of strength-consistency indices based on the compressive strength and failure strain of the soil as determined by a constant rate of strain test. The potential usefulness of this approach is illustrated by the stress-strain response of a particular remolded plastic clay at various conditions of consistency and history.

The variables involved in this study are stress, strain, compressive strength, failure strain, moisture content, material history and method of preparation. Specimens were prepared by extrusion and compaction processes. Extruded specimens were subjected to a variety of histories, including creep, vibration (repeated load applications), overconsolidation and desiccation.

Each of the imposed histories attempts to reproduce actual field conditions encountered in dealing with such materials. For example, the specimens subjected to vibratory histories undergo a maximum of approximately 100,000 load applications prior to testing. Such a repeated load history is extremely important in rational highway pavement design. The creep histories may be related to a progressive-type failure phenomenon often associated with highway embankments. A desiccation history may be imposed in the field by alternate wet and dry periods or variations in the ground water table, both during construction and during performance. Overconsolidation history may be imposed on a soil by current causes, such as an embankment surcharge, existing structure, or desiccation, as well as by geologic causes, such as glaciers. The use of extrusion and compaction preparation processes allows for the comparison of results between different soil particle orientations as imposed by various field placement methods.

Paper sponsored by Committee on Stress Distribution in Earth Masses.

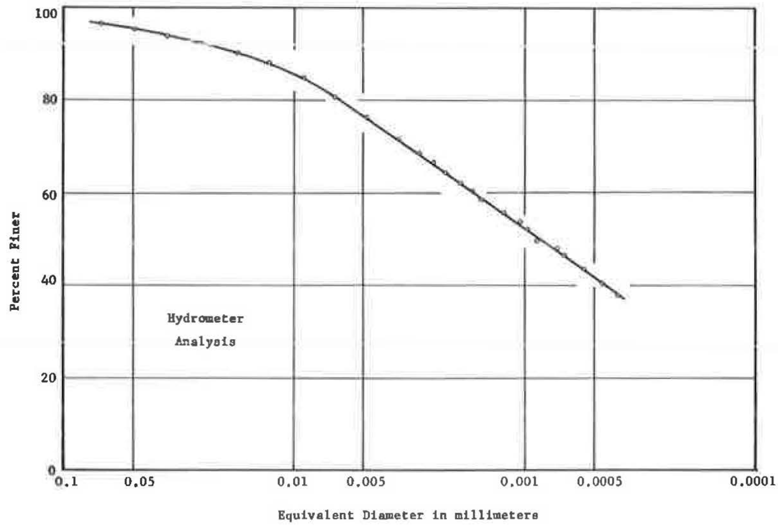

Figure 1. Grain size distribution.

Uniaxial compression tests were then conducted on all specimens and stress-strain response is expressed in analytic form as a function of the strength-consistency indices. These characteristic indices are given for various soil specimens at different moisture contents. Particular emphasis is directed to the significant difference in strength between compacted and extruded specimens, all other factors (density, moisture content, void ratio, etc.) being very nearly the same.

Following the development of the analytic form for stress-strain response, the usefulness of such indices in control and testing of materials is illustrated for some aspects of creep and vibratory loading phenomena and for triaxial and variable strain-rate test data obtained from the literature. Other test procedures for obtaining strength-consistency indices are discussed.

MATERIAL INVESTIGATED

The soil investigated is a remolded, plastic clay sold commercially under the name Jordan Buff by the United Clay Mines Corp., Trenton, N. J. Figure 1 shows the particle size distribution as determined by hydrometer analysis. The characteristics of the clay are: liquid limit, 46 percent; plastic limit, 30 percent; shrinkage limit, 20 percent; plasticity index, 16 percent; and specific gravity, 2.74.

EXPERIMENTAL PROCEDURE

Preparation of Specimens

The soil specimens were prepared from a dry, powdered form by mixing with a predetermined amount of distilled water. After the clay and water were satisfactorily blended, by hand and by mechanical mixer, specimens were formed by either compaction or extrusion.

In the compaction process, the clay-water mixture was subjected to standard Proctor compactive energy of 12,400 ft-lb per cu ft. After the required compaction test information (Fig. 2) was obtained from the mold, three cylindrical specimens 3.65 cm in diameter were cored from each mold by use of specially constructed sampling tubes. The specimens were then removed from the tubes and placed in miter boxes where they were trimmed with a wire saw to lengths of 8.20 cm (giving a length-diameter ratio of 2.25) and immediately tested.

In the extrusion process, the clay-water mixture was passed through a "Vac-Aire" sample extruder similar to that used by Schmertmann and Osterberg (1) and described

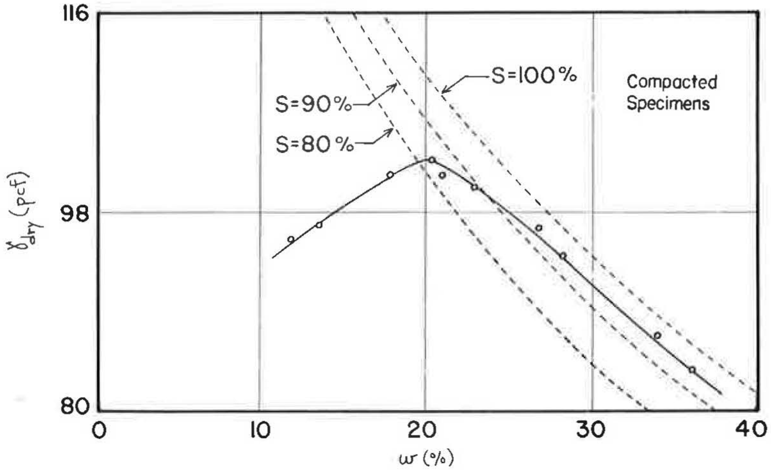

Figure 2. Dry density vs moisture content: compacted specimens.

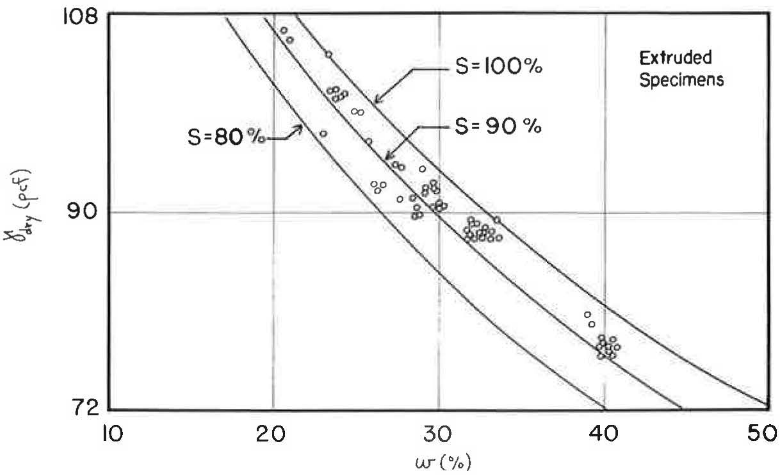

Figure 3. Dry density vs moisture content: extruded specimens.

in detail by Matlock, Fenske and Dawson (2). Depending on the moisture content at which it was mixed, the clay was passed through the extruder two or three times. It was found that the soil mixture decreased in moisture content about 0.5 to 1 percent with each extrusion because of the heat generated. During the last extrusion, as the clay passed through the 3.65-cm diameter die, it was cut into lengths greater than 8.20 cm. The resulting curve of dry density vs moisture content for the extruded specimens is shown in Figure 3. Some of these extruded specimens were placed in the miter box, trimmed with a wire saw to a length of 8.20 cm and immediately tested. However, most specimens were covered with five or six coats of a flexible wax and stored vertically in a single layer at approximately 100 percent RH.

The wax was composed of a mixture of paraffin and petrolatum (trade name, Standard Oil Co., Chicago, Ill.) and provided a protective coating that was not susceptible to large shrinkage upon cooling, not brittle, and could be peeled from the specimen with ease. By maintaining the wax at a temperature a few degrees above its melting point, the driving-off of the more volatile hydrocarbons was prevented. The loss of these hydrocarbons would tend to cause a more permeable and brittle coating upon cooling.

After the wax was removed, the extruded specimens were subjected to various histories to determine their effect on the stress-strain response characteristics. Such histories include overconsolidation, desiccation, creep and vibration. In addition, thixotropic effects were studied for more than a year.

The overconsolidation history was induced by placing a trimmed specimen (L, 8.20 cm; d, 3.65 cm) encased in filter paper in a standard triaxial compression cell and subjecting it to hydrostatic pressure for several days. Lateral confinement was obtained using glycerine as the chamber fluid within a lucite cell. Pressures obtained by applying air pressure to the chamber fluid were measured with a Bourdon pressure gage. All the specimens were free-draining and volume changes were measured by use of a pipette connected to the specimen through the base of the chamber. Axial deformations of the specimens were measured with an indicator dial having a sensitivity of 0.001 in. Overconsolidation pressures varied between 3 and 5 kg per sq cm and were applied for 3 to 7 days. After the consolidation pressure was removed, the specimens were permitted to rebound under conditions of free drainage before testing.

The desiccation history was obtained by removing the wax coating from the specimens and exposing them to a relatively uniform environmental atmosphere for prescribed periods of time. The specimens then were rewaxed and stored in a humid room for at least 10 days to provide reasonable time for a homogeneous redistribution of moisture. They were then stripped of their wax cover, placed in a miter box, trimmed and tested. The creep history was imposed on the trimmed specimens by subjecting them to a constant load in unconfined compression for approximately 20,000 min (2 wk). The loads were then removed and the specimens were allowed to rebound for approximately 10,000 min (1 wk). During this time a protective coating of two membranes with petrolatum on the outer membrane maintained the loss of moisture in the specimens at approximately 0.25 percent. After this history, the membrane coverings were removed and the specimens were tested.

The vibratory history was given to the trimmed specimens by subjecting them to a static stress of approximately 0.54 kg per sq cm and superimposing sinusoidally varying dynamic strain amplitudes of approximately 50,100 and 200 μ-in. per in. for time periods of 1, 4, 16 and 64 min. The frequency of oscillation was 25 cps. Under these conditions, failure would have occurred at approximately 400 μ-in. per in. The specimens exposed for 16 and 64 min were covered with a single uncoated membrane to reduce moisture losses. The vibratory apparatus used for this purpose has been described in detail by Kondner and Krizek (3). Following this history, the rubber membranes were removed and the specimens were immediately tested.

Thixotropic effects were investigated by testing extruded specimens at various intervals throughout a period of approximately 15 mo from the date of extrusion.

Description of Test

After the prescribed history was imposed on the specimens, they were subjected to a constant rate of axial strain test in unconfined compression to determine stress-strain response. These tests were conducted in a standard triaxial compression cell without lateral pressure with a custom-built gear-type testing machine where the rate of deformation was 0.122 cm per min. The use of the triaxial cell helped to reduce drying of the specimen during the test. The degree of deformation of the specimen was obtained by measuring the motion of the upper platen with an indicator dial, and the value of the compressive load was obtained from a proving ring placed in series with the test specimen.

Axial strain of the specimen was determined by dividing the measured deformation by the initial length. Axial stress was determined by dividing the measured compressive load by the corrected specimen area as computed by a uniform, constant-volume area correction. Initial measurements of the specimens were always those associated with the beginning of the unconfined compression test, not the beginning of the load history.

The compressive strength and strain at failure are used as convenient indices for specifying the strength and consistency characteristics of the various specimens. The compressive strength, q, is the maximum axial stress attained in an unconfined com-

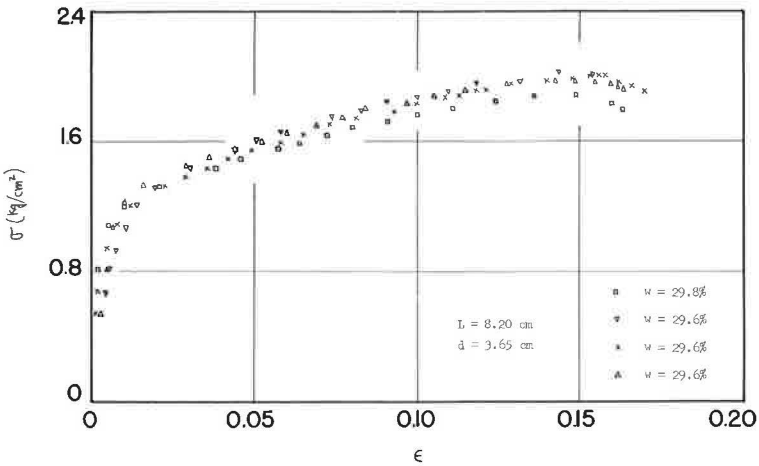

Figure 4. Typical stress-strain response for unconfined compression tests.

pression test or the maximum deviator stress attained in a triaxial test (each based on a constant-volume area correction). The strain at failure, ϵ_f, is the strain associated with the compressive strength on a stress-strain plot.

EXPERIMENTAL RESULTS

General Stress-Strain Response

For any test program to possess a high degree of reliability, it is necessary to be able to duplicate any given test within a reasonable amount of experimental error. To illustrate that this requirement has been satisfied in this test program, the results of four virtually identical tests on four different specimens are shown in Figure 4 in the form of axial stress vs axial strain. Most other tests throughout the program were conducted two or three times to insure duplicability under other conditions.

To investigate the effect of moisture content on the stress-strain response, unconfined compression test data on five different specimens at five different moisture contents (21.0, 25.2, 29.6, 32.9 and 40.4 percent) are shown in Figure 5. As may be anticipated, moisture content plays a significant role in the constitutive response. If the same data are plotted in the form of the ratio of stress to unconfined compressive strength (stress-strength parameter) vs the ratio of strain to strain at failure (strain-failure parameter) (Fig. 6), all five curves of Figure 5 seem to describe one curve in Figure 6. The apparent absence of any phenomenological order would suggest that unconfined compression data presented in this form may be considered explicitly independent of moisture content within the range considered. Of course, the effect of moisture content is implicit in the unconfined compressive strength and failure strain of a soil. Moisture content is not the only variable whose influence is implicitly expressed in the consistency indices q and ϵ_f.

If the data of Figure 6 are replotted in the form of the reciprocal of the secant modulus vs the strain-failure parameter (Fig. 7), the response can be approximated by a straight line whose equation is

$$\frac{\epsilon\, q}{\epsilon_f\, \sigma} = a + b\frac{\epsilon}{\epsilon_f} \tag{1}$$

Eq. 1 can be rearranged into the equation of a two-constant hyperbola, as follows:

$$\frac{\sigma}{q} = \frac{\dfrac{\epsilon}{\epsilon_f}}{a + b\dfrac{\epsilon}{\epsilon_f}} \tag{2}$$

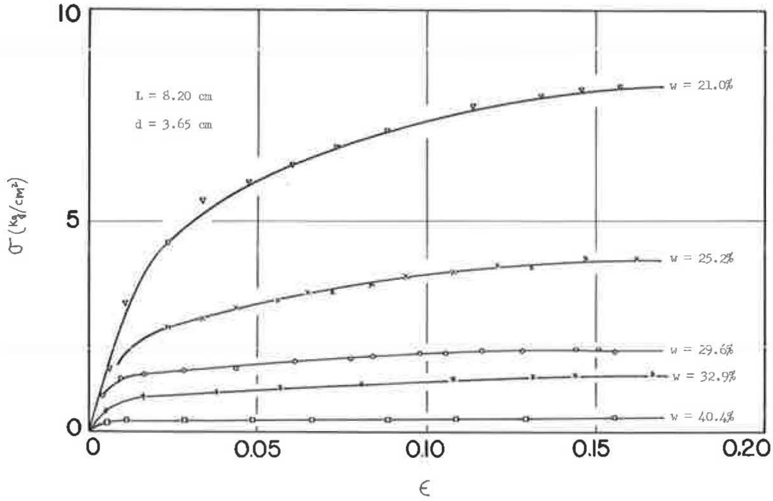

Figure 5. Stress vs strain: different moisture content.

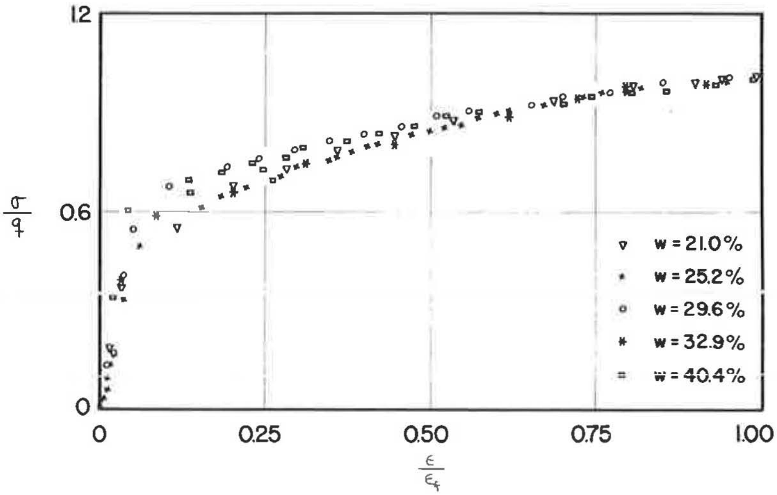

Figure 6. Stress-strength parameter vs strain-failure parameter: different moisture content.

in which 1/a represents the initial slope of the stress-strength parameter vs strain-failure parameter curve and 1/b represents the theoretical ultimate value of the stress-strength parameter as the strain-failure parameter increases to infinity. The actual ultimate value of the stress-strength parameter is, of course, unity. In the region of large strains, the curve is very flat and actual failure conditions are somewhat subjective. The usefulness and application of such a hyperbolic formulation have been shown by Kondner and Krizek (4) and Kondner (5, 6).

Types of Failure

The predominant type of failure encountered was along a plane inclined approximately 45° to the axis of the specimen. Many of the specimens exhibited base failures; that is, the failure plane intersected the base of the specimen. For the specimens with high

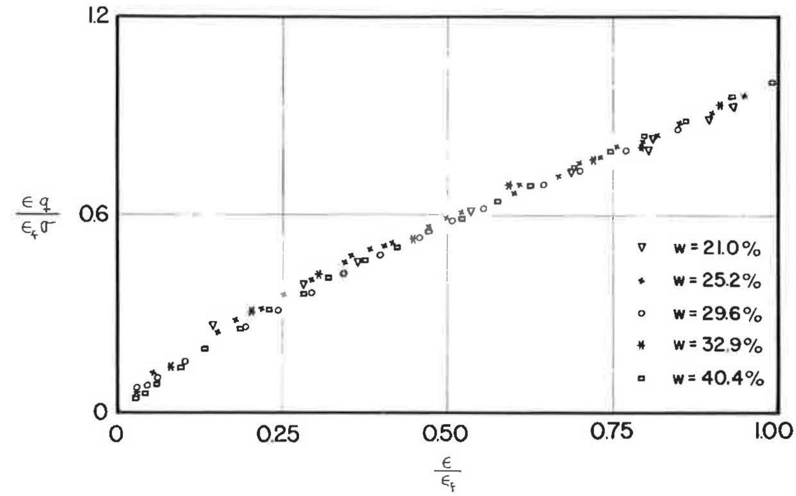

Figure 7. Transformed hyperbolic stress-strain response: different moisture content.

moisture contents (in the neighborhood of 40 percent), many failures were of a "bulging" nature, in which the specimen gradually increases in diameter as it shortens in length, even at very high values of axial strain.

Constitutive Response

Extruded Specimens.—

Extrusion History Alone.—Approximately 60 tests were performed on specimens subjected solely to the extrusion preparation process. Because of the high pressures encountered in this process, some preconsolidation stress may also exist in the specimens. If present, such stresses are probably of relatively consistent magnitude in all specimens at a particular moisture content, and their effects are considered insofar as they contribute to the over-all strength characteristics of the soil. These extruded specimens were tested at various intervals from immediately to 15 mo after extrusion. Curing of specimens for extended periods of time allows migration of water to insure a uniform distribution of moisture content throughout the specimen. Also, effects due to thixotropy have ample time to develop. A constant-strain-rate unconfined compression test was conducted on each specimen and representative data for moisture contents from approximately 21.0 to 41.2 percent are plotted in transformed hyperbolic form in Figure 8. All data seem to describe a single straight line and effects in the normalized stress-strain response due to migration of water or thixotropy are either very small or of the same order as experimental error.

Overconsolidation History.—Ten extruded specimens with high moisture contents (approximately 40 percent) were subjected to overconsolidation stresses up to 5 kg per sq cm for periods up to 7 days. During this time, measurements were obtained and void ratio, moisture content and degree of saturation were calculated. The specimens were tested immediately in unconfined compression and normalized stress-strain results are shown in Figure 9. The loci of all points tend to trace out a single curve. At the time of the unconfined test, the specimens ranged in moisture content from approximately 33.4 to 38.0 percent.

Desiccation History.—Approximately 30 extruded specimens were desiccated for periods up to 25 hr. Initial moisture contents before desiccation were approximately 40 and 32 percent, whereas final moisture contents after desiccation ranged down to 8.4 percent. The rate of desiccation was found to be approximately 1 percent change in moisture content per 100 min. After a curing period of at least 10 days to allow for a homogeneous redistribution of moisture content, specimens were tested in unconfined compression. Normalized constitutive response data are shown in Figure 10.

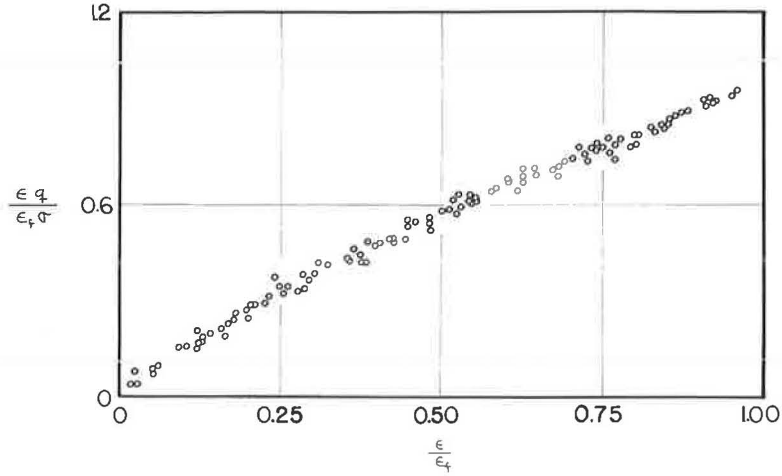

Figure 8. Transformed hyperbolic stress-strain response: extrusion history alone.

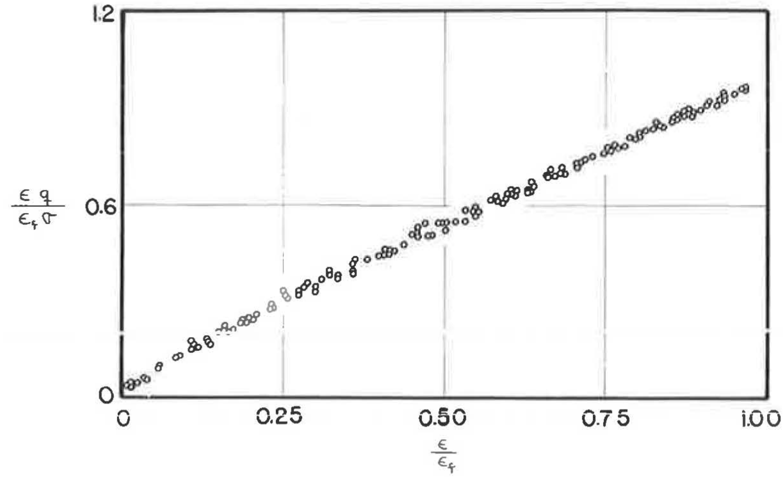

Figure 9. Transformed hyperbolic stress-strain response: overconsolidation history.

Vibratory History.—Fifteen extruded specimens with moisture contents from approximately 26.1 to 32.7 percent were subjected to vibratory histories in which a prescribed cycle of deformation was applied approximately 1,500 to 96,000 times. The strain amplitudes correspond to stress amplitudes of approximately 20 to 60 percent of the stress value required to cause failure under the given test conditions. The specimens then were tested in unconfined compression and normalized stress-strain results are shown in Figure 11.

Creep History.—Thirty-five extruded specimens with moisture contents varying from 23.2 to 40.6 percent were subjected for 2 wk to applied constant loads up to approximately 75 percent of the compressive strength of the soil; then the load was removed and each specimen was rebounded for 1 wk. Following this, uniaxial compression tests were conducted on the specimens and normalized data in transformed hyperbolic form are shown in Figure 12.

Compacted Specimens.—Approximately 40 compacted specimens (using the standard Proctor energy) of the same geometrical configuration as the extruded ones were tested

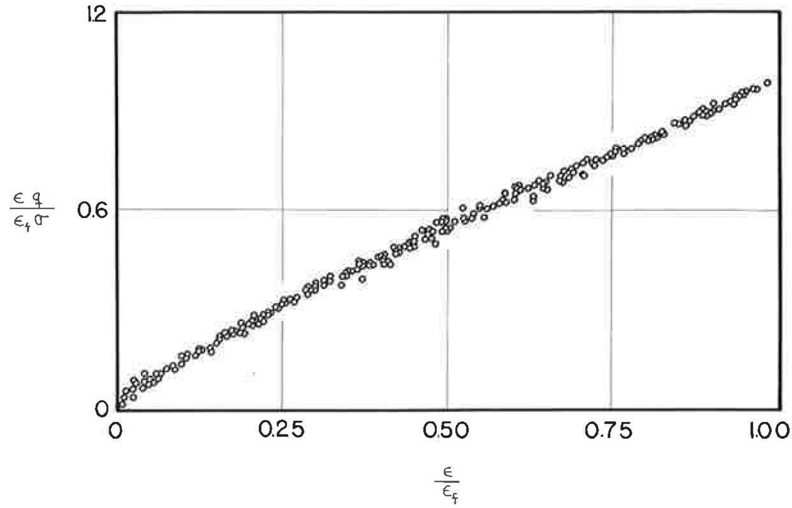

Figure 10. Transformed hyperbolic stress-strain response: desiccation history.

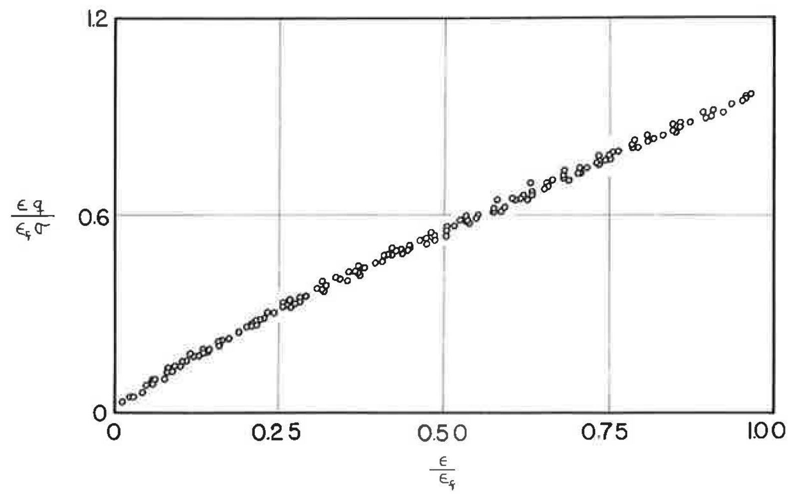

Figure 11. Transformed hyperbolic stress-strain response: vibratory history.

in unconfined compression immediately after they were cored from the mold. Moisture contents ranged from approximately 21.1 to 36.6 percent and normalized stress-strain response for these specimens is shown in Figure 13. Once again it can be seen that the data seem to trace out a straight line (except for the region of small strain); however, the line so described has a different slope and intercept from the corresponding plots for extruded specimens.

Analytic Representation

An examination of the constitutive response for all extruded specimens including any imposed history (Figs. 8-12) indicates that it can be represented within a reasonable amount of experimental error by a single equation of the form of Eq. 2. For this case, the coefficients a and b become 0.08 and 0.92, respectively. Thus, the analytic ex-

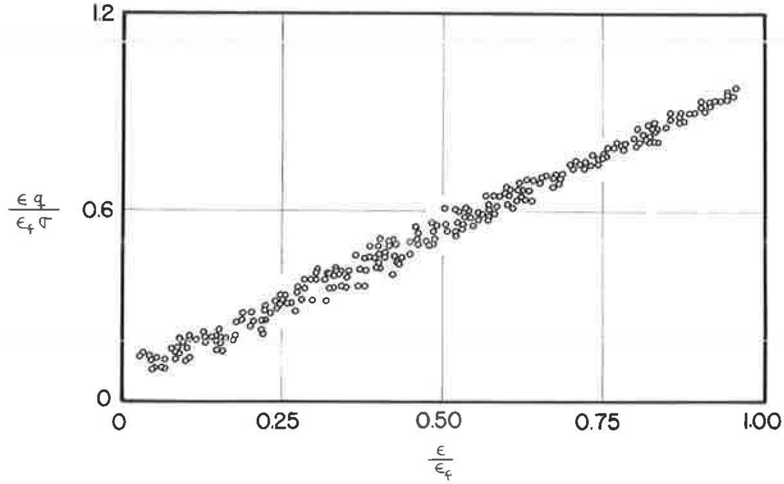

Figure 12. Transformed hyperbolic stress-strain response: creep history.

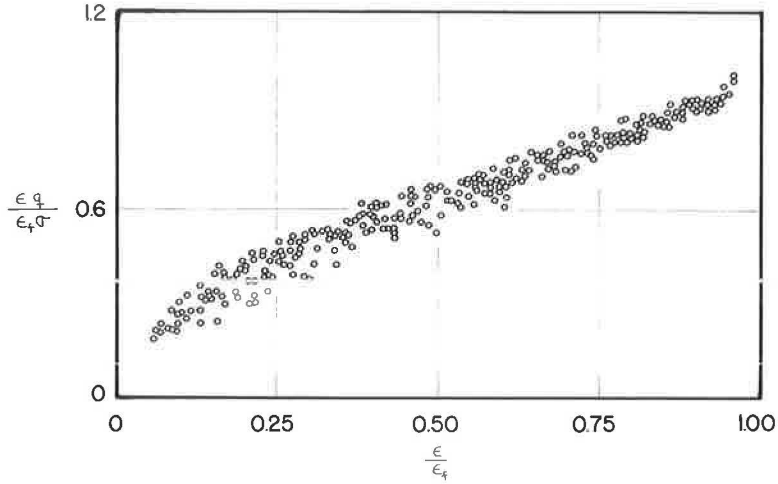

Figure 13. Transformed hyperbolic stress-strain response: compacted specimens.

pression for the extruded specimens can be written

$$\frac{\sigma}{q} = \frac{\frac{\epsilon}{\epsilon_f}}{0.08 + 0.92\,\frac{\epsilon}{\epsilon_f}} \tag{3}$$

For the compacted specimens (Fig. 13), the coefficients a and b may be approximated by 0.24 and 0.74, respectively. Hence, the representative analytic equation becomes

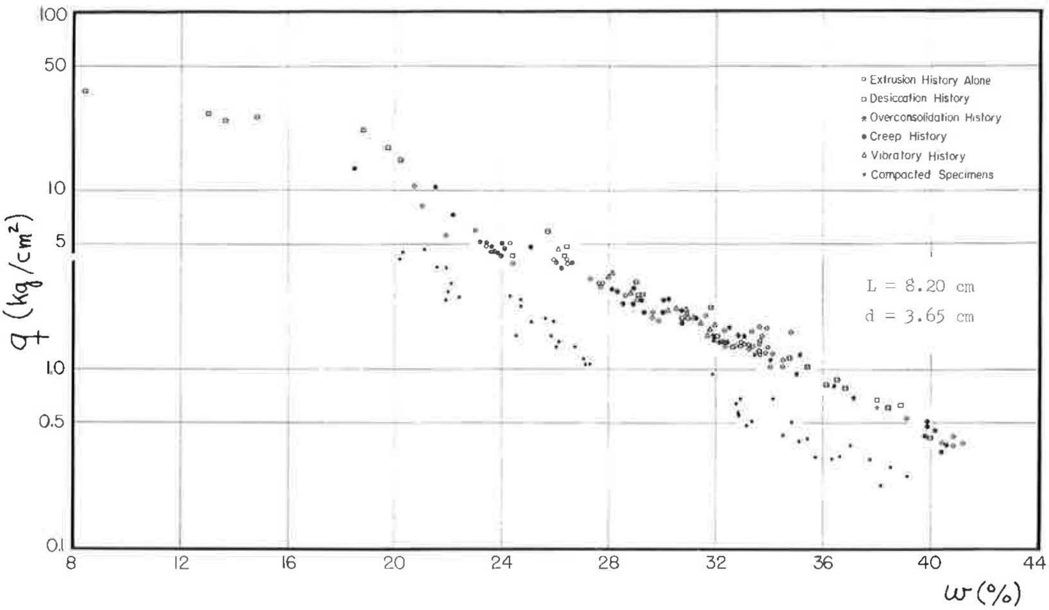

Figure 14. Unconfined compressive strength vs moisture content.

$$\frac{\sigma}{q} = \frac{\frac{\epsilon}{\epsilon_f}}{0.24 + 0.74 \frac{\epsilon}{\epsilon_f}} \tag{4}$$

Both methods of specimen preparation, extrusion and compaction, yield a similar qualitative analytic form, but the different preparation processes do result in different quantitative values for the respective coefficients. Because all data assume a relatively simple analytic representation in terms of the consistency parameters, q and ϵ_f, the stress-strain response of a specimen can be determined if the history and consistency relationships are known.

Consistency Relationships

The consistency indices employed are the compressive strength of the soil and the associated strain at failure. Because the current test program utilizes only the constant-strain-rate unconfined compression test, compressive strength is determined by the maximum axial stress (based on a constant-volume area correction) applied to the specimen. It must be emphasized that the strength so obtained is not an absolute measurement of the true strength of the soil but is only, in itself, an index thereof. Nonhomogeneous strain distributions throughout the specimen (especially as failure becomes incipient) necessarily cast doubt on any exact strength value obtained by use of the simplified constant-volume area correction, and the selection of a soil compressive strength becomes somewhat subjective. With this caution in mind, compressive strengths were obtained from more than 200 tests on specimens with moisture contents from approximately 8.4 to 41.2 percent (Fig. 14). Aside from the close correlation of all extruded specimens, regardless of subsequent history, the most striking point of Figure 14 is the reduction in the strengths of the compacted specimens to approximately one-half those of the extruded ones. For example, an extruded specimen with a moisture content of 22.2 percent and a void ratio of 0.650 had a strength of 7.69 kg per sq

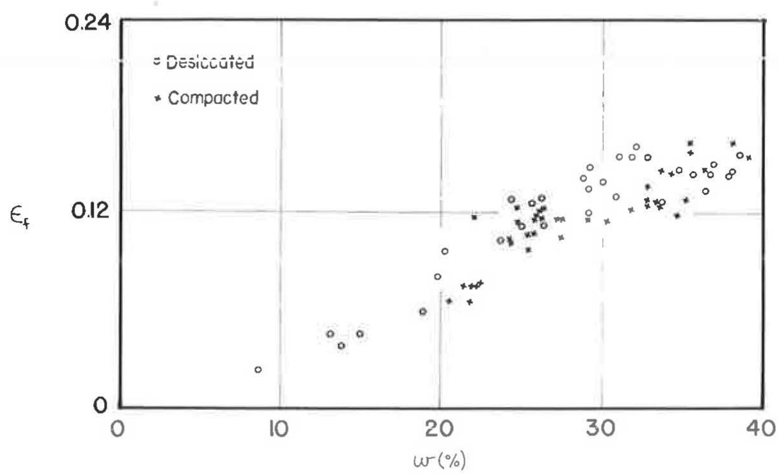

Figure 15. Strain at failure vs moisture content: compacted and desiccated specimens.

cm, whereas a compacted specimen with a moisture content of 22.4 percent and a void ratio of 0.651 had a strength of only 3.02 kg per sq cm. Such radical variations may be due to soil structure and/or the development of pore pressures during compaction and testing. The extrusion process imparts a spiral orientation to a specimen, whereas the compaction process probably results in a more random structure. Possibly overconsolidation stresses have been applied in varying degrees by both processes.

The strain at failure associated with the compressive strength is a more subjective parameter than the compressive strength itself. Its determination becomes extremely difficult because of the flat nature of the stress-strain curve in the region of failure. For this reason, one logical approach is to select such a value by statistical methods. However, in this experimental program the strain at failure is taken to be that strain existing in the specimen (based on the initial length) when the maximum deviator stress is attained. For a small portion of the tests (about 10 percent) in which the stress-strain curve in the failure region is extremely flat, appropriate failure strains consistent with the trend of the majority were determined from that region of the stress-strain curve beyond the point where the stress was 95 percent of its ultimate value. Such failure-strain values are shown in Figure 15 for the compacted and desiccated specimens in which the moisture content range is sufficiently large to indicate a trend. For the vibrated, overconsolidated and extruded specimens in which no trend could be established with moisture content, results are shown in bar graph form in Figure 16. For specimens with creep histories, the failure strain as obtained from a conventional unconfined compression test is a function of the creep strain imposed. Creep strain, in turn, is a function of the applied static load, time, and moisture content. Although failure strain as obtained from an unconfined test was quite variable, ranging from approximately 2 to 18 percent, for these creep history specimens, failure (that is, the point of maximum deviator stress) occurred at a relatively constant value, 16 ± 4 percent, of total strain as obtained from the sum of previously imposed creep strain and uniaxial compression strain from the unconfined test. Such a result is consistent with a maximum strain type of failure theory; however, any definite conclusion regarding this point is purely speculative and certainly premature at this time.

ILLUSTRATIVE EXAMPLES

Strain Rate Effects

To demonstrate a more general application of the preceding technique, data reported by Osterberg and Perloff (7) for variable strain rate tests on an oxidized and weathered glacial till have been analyzed. A typical set of tests corresponds to a moisture content of

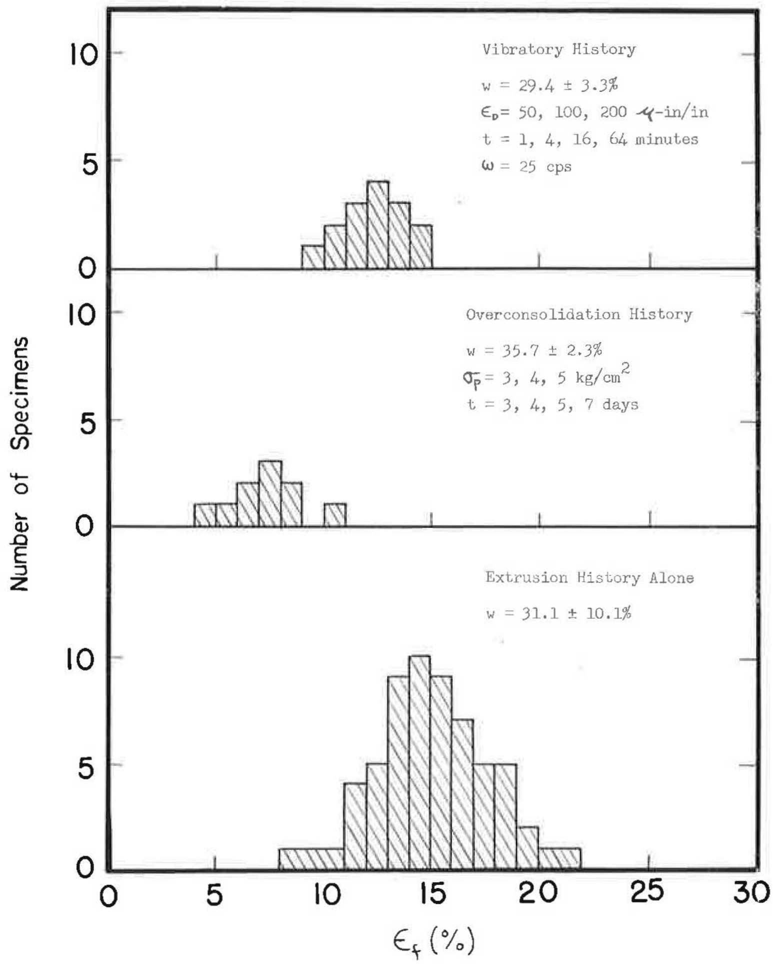

Figure 16. Bar graph representation of strain at failure: vibrated, overconsolidated and extruded specimens.

23.1 ± 0.2 percent and seven different strain rates varying between 5.37×10^{-5} and 1.79×10^{-2} in. per in. per min. Stress-strain data obtained from the reported curves have been recomputed in terms of the stress-strength and strain-failure parameters, and results are shown in transformed hyperbolic form in Figure 17. The data may be approximated by an analytic expression of the form given by Eq. 2. These consistency indices are plotted as a function of strain rate in Figure 18. Hence, strain rate effects on constitutive response are included in the consistency indices, q and ϵ_f.

Triaxial Test Data

Data from approximately 35 triaxial compression tests on the embankment material of the Hybla Valley test track near Alexandria, Va., have been made available through the courtesy of E. S. Barber. A detailed description of this cooperative study conducted by the U. S. Bureau of Public Roads, the Asphalt Institute and the Highway Research Board may be found in a report by Benkelman and Williams (8). The triaxial tests were conducted with a lateral confining pressure of 1 kip per sq ft, moisture contents ranged from approximately 20 to 32 percent, and wet densities varied from approximately 118 to 128 pcf. Stress-strain response is normalized in terms of the maximum deviator

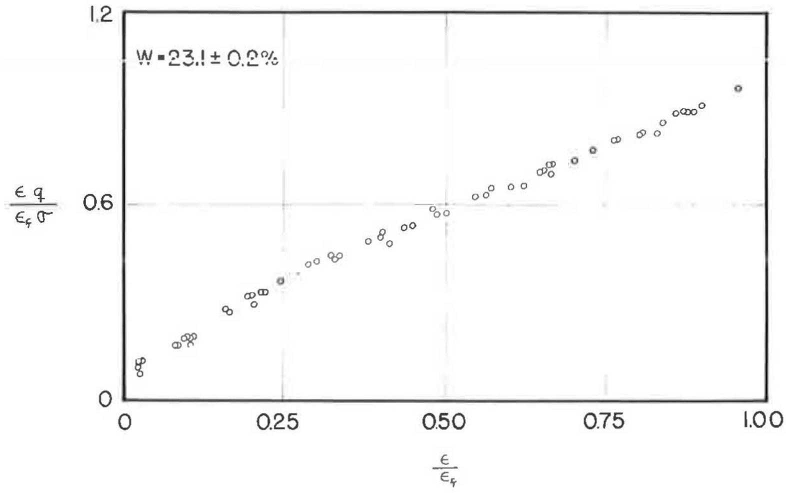

Figure 17. Transformed hyperbolic stress-strain response: different strain rate.

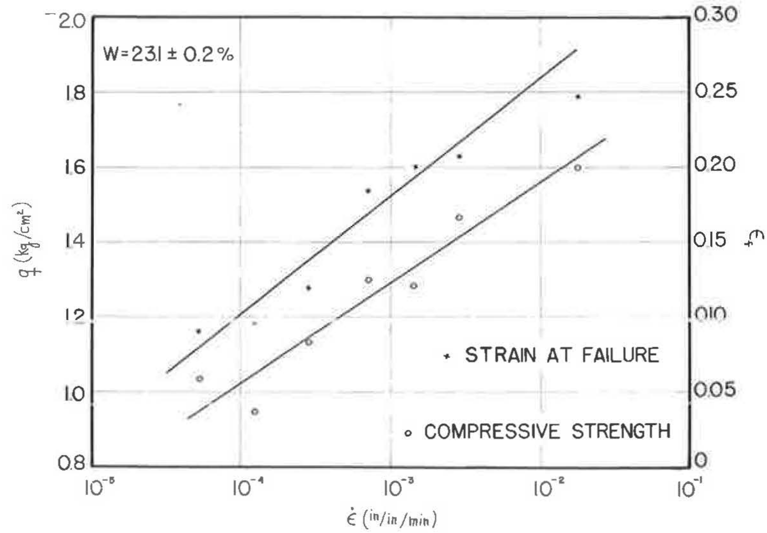

Figure 18. Unconfined compressive strength and strain at failure vs strain rate.

stress and failure strain and the results are shown in transformed hyperbolic form in Figure 19. For these tests, a form of Eq. 2, in which σ is replaced by $(\sigma_1 - \sigma_3)$, again provides a reasonable approximation for constitutive behavior. Compressive strength (maximum deviator stress) and strain at failure varied from approximately 2.9 to 6.7 kips per sq ft and 0.05 to 0.18 in. per in., respectively.

Vibratory Response

An extensive series of vibratory tests on Jordan Buff clay has been reported by Kondner, Krizek and Haas (9). Variations in moisture content have been handled by expressing dynamic stress-strain response in terms of a dynamic stress-strength parameter vs dynamic strain. The unconfined compressive strength was employed as the consistency index, and it apparently accounted for moisture content variations by

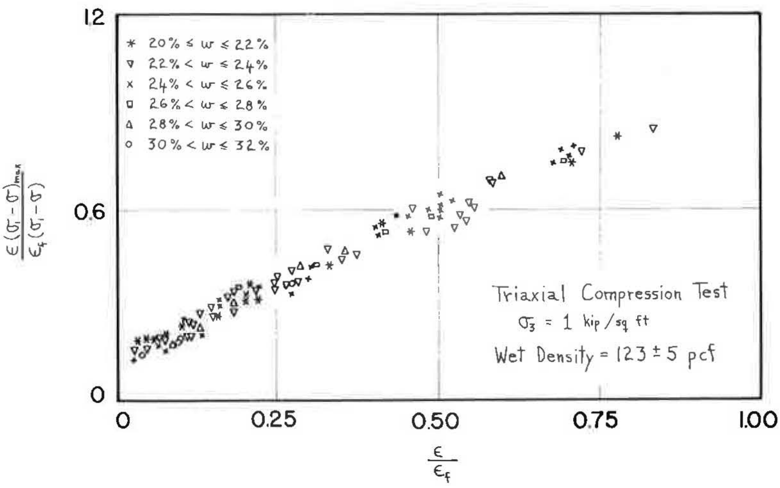

Figure 19. Transformed hyperbolic stress-strain response: triaxial test data.

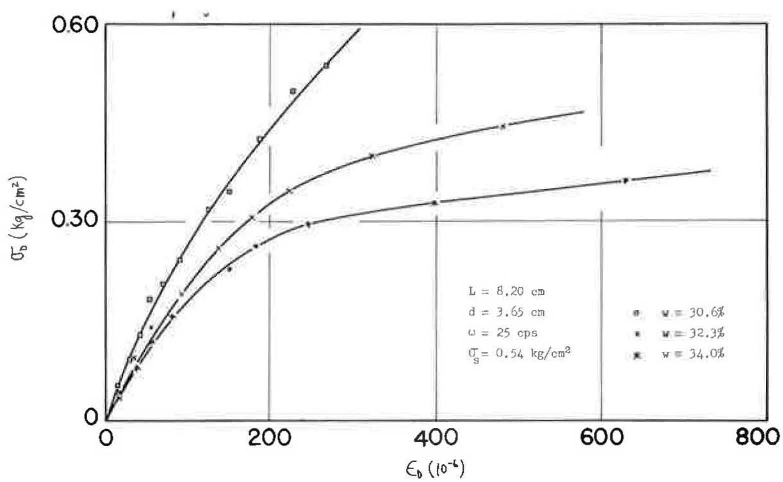

Figure 20. Dynamic stress amplitude vs dynamic strain amplitude: different moisture content.

transforming such vibratory data into a single curve within reasonable limits of experimental error. The usefulness of the dynamic stress-strength parameter may be seen by observing that the dynamic stress-strain data (Fig. 20) are significantly affected by a variation in moisture content within the range 30.6 to 34.0 percent, whereas the same data in terms of the dynamic stress-strength parameter (Fig. 21) seem to center around a single curve. Because most specimens actually failed in the vibratory test, compressive strengths were obtained from the moisture content of the specimen and Figure 14. Additional tests indicate that such a stress-strength technique based on the consistency index is applicable up to moisture contents of approximately 41 percent.

Creep Response

The consistency index, q, is very useful in facilitating a more unified presentation of experimental creep data. For example, 35 specimens with moisture contents between 23.2 and 40.6 percent, examined from the viewpoint of unconfined compression

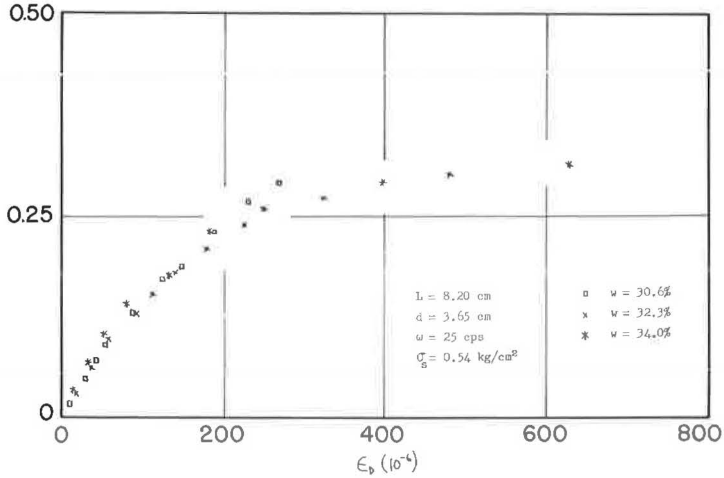

Figure 21. Dynamic stress-strength parameter vs dynamic strain amplitude: different moisture content.

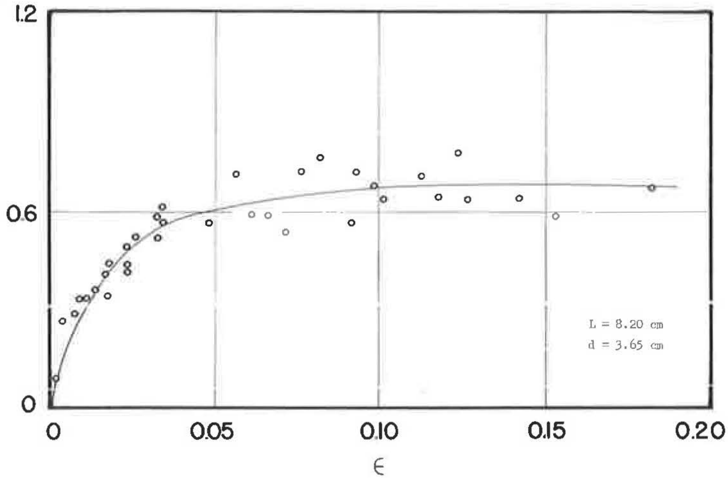

Figure 22. Stress-strength parameter vs strain: creep response.

stress-strain response on a material with creep history, were also analyzed for creep stress-strain response.

Figure 22 shows a typical example of such creep response associated with a particular time (10,000 min). The stress is taken as the applied load divided by the cross-sectional area (based on a constant-volume area correction) and the creep strain is the deformation divided by the initial length of the specimen. The compressive strength is determined by an unconfined compression test conducted on the specimen following the creep test. The tendency of all data points in Figure 22 to form the locus of a single curve over the large moisture content range indicates the usefulness of such a stress-strength parameter, based on the consistency index, q.

Field Determination of Consistency Indices

Since the preceding presentation centers strongly on the role of the consistency indices, q and ϵ_f, in facilitating a unified presentation of stress-strain response in control and testing of materials, the study assumes added significance in light of the possibility of determining these indices by relatively simple field tests. Examples of such tests are penetrometer, plate bearing, cone bearing, and CBR. It is important to note that all influencing variables, such as moisture content, density, void ratio, strain rate, and saturation, are taken to be implicit in the consistency indices of the material.

SUMMARY

The investigation reported in this paper has demonstrated the usefulness of the compressive strength, q, and failure strain, ϵ_f, as consistency indices in developing an analytic expression for the stress-strain response of a remolded, plastic clay at various moisture contents under various loading histories. The compressive strength and failure strain are obtained from uniaxial constant-strain-rate tests. The effects of soil structure, moisture content, density, void ratio, and saturation are taken to be implicit in these consistency indices.

Extrusion and compaction techniques were used for sample preparation, and specimens were subjected to various histories including creep, vibration (repeated load applications), overconsolidation, and desiccation. Consistency relationships are given for the various cases. The consistency indices were affected very little by the imposed history, but the preparation process had a strong influence on the compressive strength of the soil. Extruded specimens had compressive strengths on the order of twice that of compacted ones, all other variables, such as moisture content, void ratio, density, and saturation, being nearly the same. Preparation processes also affected the empirical constants in the analytic stress-strain relations.

Data from the literature indicate that the effects of strain rate and lateral confining pressure (triaxial test) may also be included in the consistency indices, and stress-strain response may be expressed by a similar analytic equation in each case. The consistency index, q, is utilized to form a stress-strength parameter shown to be helpful in unifying experimental response from vibratory and creep testing methods.

The potential for employing relatively simple existing field test techniques, such as penetrometer, plate bearing, cone bearing, and CBR, to determine the soil consistency indices gives added significance to the usefulness of this concept in control and testing of soil materials.

ACKNOWLEDGMENTS

The authors are indebted to Messrs. Ho, Zelasko, Haas, Hasan, Yamamoto, Cheng, Mahoney and Schwartz for their help in conducting various phases of the experimental program analyzed in this paper.

Grateful appreciation is extended the Northwestern University Computing Center for the extensive aid provided in regard to the multitude of routine calculations.

REFERENCES

1. Schmertmann, J. H., and Osterberg, J. O., "An Experimental Study of the Development of Cohesion and Friction with Axial Strain in Saturated Cohesive Soil." Proc. ASCE, Res. Conf. on Shear Strength of Cohesive Soils (1960).
2. Matlock, H., Jr., Fenske, C. W., and Dawson, R. F., "De-aired Extruded Soil Specimens for Research and for Evaluation of Test Procedures." ASTM Bull. 177, pp. 51-55 (Oct. 1951).
3. Kondner, R. L., and Krizek, R. J., "A Vibratory Unixial Compression Device for Cohesive Soils." Northwestern Univ., Evanston, Ill., Tech. Rep. (1963).
4. Kondner, R. L., and Krizek, R. J., "Correlation of Load Bearing Tests on Soils." Proc. HRB, 41:557-590 (1962).
5. Kondner, R. L., "Hyperbolic Stress-Strain Response: Cohesive Soils." Proc. ASCE, 89:SM 1, 115-143 (Feb. 1963).
6. Kondner, R. L., "Friction Pile Groups in Cohesive Soil." Proc. ASCE, 88:SM 3, 117-149 (June 1962).
7. Osterberg, J. O., and Perloff, W. H., "Stress-Strain Characteristics of Compacted Clay Under Varied Rates of Strain." Proc. HRB, 39:605-618 (1960).

8. Benkelman, A. C., and Williams, S., "A Cooperative Study of Structural Design of Nonrigid Pavements." HRB Spec. Rep. 46 (1959).
9. Kondner, R. L., Krizek, R. J., and Haas, H. J., "Dynamic Clay Properties by Vibratory Compression." Presented at ASCE Symposium on Dynamic Response of Materials and Structures, San Francisco (Oct. 1963).

Evaluation of the Laboratory Vane Shear Test

R. D. GOUGHNOUR and J. R. SALLBERG
Materials Research Division, Bureau of Public Roads

A comparison was made between the laboratory vane strength and the unconfined compression strength of several remolded soils. It was found that a constant ratio of unconfined compressive shear strength to the vane shear strength resulted for each soil and this ratio varied from 0.6 to 1.4 for the soils tested. A relationship between the ratio and the plasticity index of the soils was noted. Soils with a low plasticity index generally had a low ratio. The ratio increased and then became relatively constant with increasing plasticity indices.

The effect of vane size, rate of shear, and aging of the remolded samples before testing was studied. Pocket penetrometer tests were also made on each of the samples tested.

•WITH THE PRESENT expansion of the highway construction program, the highway engineer is frequently required to locate and build highways and, particularly, interchanges over poor, submarginal lands and sometimes even swamplands. One problem in designing interchange embankments over soft soils is the determination of the initial shear strength of the foundation soil. This shear strength may be estimated from results of the standard penetration test, obtained during subsurface investigations, or measured directly by the field vane test. In general, however, the initial shear strength of the foundation soil is based upon laboratory unconfined compression tests of undisturbed samples. In cases where the undisturbed samples are very sensitive, or so weak they fail under their own weight, another type of test is needed.

The Materials Research Division of the Bureau of Public Roads purchased a laboratory vane shear device (Fig. 1) for testing very soft soils directly in the sampling tubes. The test is made by inserting the vane into the sample, measuring the resistance to rotation, and from this, calculating the shear strength. This device was evaluated by comparing the shear strength obtained with that obtained using the unconfined compression test.

Initial tests indicated that the laboratory vane shear test and the unconfined compression shear test did not yield the same shear strengths for identical remolded specimens of soil. In an attempt to explain this difference, additional tests were run on both undisturbed and remolded soils. The effects of aging of the samples before testing, the rate of shear, and the vane size were studied for the remolded soils.

A few researchers have compared the shear strength obtained with the field vane, the laboratory vane (undisturbed sample left in the tube when tested), and the undisturbed, unconfined compression tests (1, 2). Generally, the field vane test gives the greatest strength, the unconfined compression test the least, with the results of the laboratory vane test falling in between. Gray (1) believed that for the sensitive clays he tested, the difference was due to disturbance in obtaining the samples and in preparing the unconfined compression test specimens. Fenski (2) found that consolidated undrained triaxial shear tests gave results close to the field vane test. For this reason he concluded that the difference between the field vane and the unconfined compression test was largely due to the different stress conditions created by removing the soil from the ground.

Paper sponsored by Committee on Stress Distribution in Earth Masses.

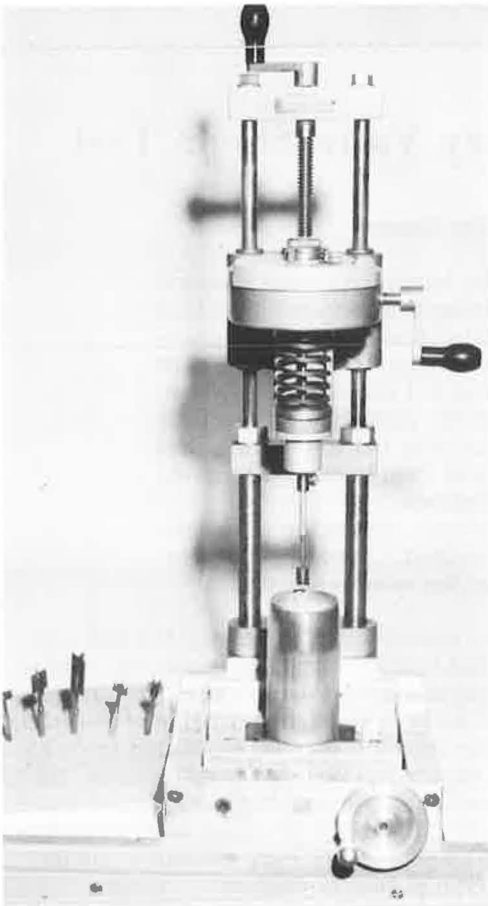

Figure 1. Laboratory vane shear apparatus.

VANE SHEAR APPARATUS

The vane shear apparatus used for this study (Fig. 1) is equipped to measure both torque and rotation of the vane in degrees. Torque is applied to the vane through a calibrated spring by rotating the crack handle. The base of the apparatus was replaced by a clamp to hold the sampling tubes. The vane normally used consists of four blades, each ½ in. high and ¼ in. wide.

CALCULATION OF SHEAR STRESS

The surface of rupture and the possibility of progressive failure for the vane test have been studied for sand and clay by Swedish researchers (3). Their study was conducted by placing wetted tissue paper, with a pattern marked on it, on the surfaces of the samples. The distortion of the pattern was observed as the vane test progressed. It was concluded that for the sand and clay tested, the surface of rupture was a circular cylinder, with the diameter, D, equaling that of the vane, and that any progressive character of failure was slight and did not appreciably affect the test results.

In calculating the vane shear strength, S, in the present study, it was assumed that the failure surface was the circular cylinder of revolution created by rotating the vane. The shear stress was assumed to be constant along the vertical surface and to have a linear distribution on the ends varying from zero at the center to maximum at the edge. The resulting formula for the shearing strength is

$$S = \frac{2\,T_{max}}{\pi D^2 (H + D/4)} \tag{1}$$

in which T_{max} is maximum torque, D is diameter or overall width of the vane, and H is height of the vane.

The unconfined compressive shear strength was computed using the conventional expression

$$S = \frac{Q_u}{2} \tag{2}$$

in which Q_u is the unconfined compressive strength, defined as the maximum applied load divided by the average cross-section of the specimen.

SOIL PREPARATION AND INITIAL TESTING

The soils tested in this study consisted of four clays, two silty clay loams, a clay loam, a loam and two sandy loams. A summary of the tests performed and the mechanical properties of the soils are given in Table 1.

The soil to be used for the remolded tests was air dried, pulverized to break up clay lumps and generally sieved through No. 10 sieve to remove coarse particles. One exception, a silty clay loam, was sieved through No. 4 sieve. Water was then added and thoroughly mixed with the soil to bring it to the selected moisture content. The mixture was stored in a moist cabinet at least 24 hr before molding and testing.

The remolded specimens were prepared in a mold 2 in. in diameter by 5 in. long. The soil was added to the mold in small increments and manually tamped with a $\frac{3}{4}$-in. diameter wooden rod. The density of duplicate specimens could be reproduced within a range of 1.0 pcf by this method. The vane shear tests were generally performed on these specimens while still in the mold. The vane was inserted into the soil until the top of the vane was approximately $\frac{1}{2}$ in. below the top of the specimen. After the vane test, the specimens were pushed from the mold and trimmed to a 4-in. length for the unconfined compression test. The tests listed under Group A in Table 1 were made by this procedure. It was found that for each soil molded into test specimens at moisture contents approximately between the plastic and liquid limits, the ratio of the vane shear strength to one-half the unconfined compression strength (UC) was constant; this ratio, however, varied from soil to soil between 0.6 and 1.4 (Table 1). Typical test results for one soil, showing this constant ratio, are plotted in Figure 2. Duplicate tests were made on this soil to evaluate different vane designs and resulted in seemingly excessive replication at each of the three moisture contents at which specimens were molded.

Four possible causes for the different shear strengths measured by the vane and unconfined compression tests are: (a) nonuniformity of soil structure, that is, particle arrangement and moisture distribution within the specimen; (b) variations in pore pressure developments during shear; (c) progressive failure in the vane test; and (d) effects of testing procedures. To investigate the effects of these factors, additional tests were made.

Structure

Any nonuniformity of structure or strength within the test specimen would be reflected in the vane-UC ratio. This ratio would be greater than one because the vane shears the soil specimen along a fixed surface, whereas the unconfined compression test allows the soil specimen to shear along the weakest surface. Shearing along a fixed surface tends to give an average shear strength, whereas shearing through the weakest part gives the minimum strength.

It was hypothesized that a remolded test specimen has a less uniform structure than an undisturbed test specimen. If this were so, the vane-UC ratio for the specimens of remolded soil would be greater than that for the specimens of undisturbed soil. This hypothesis was investigated using samples of an undisturbed silty clay (Test 10a of Group B) that were obtained from a 12-ft excavation by means of 3- and 6-in. sampling tubes. Vane shear tests were run on this material while still in the tubes. Unconfined compression specimens, 2 in. in diameter by 4 in. long, were trimmed and tested. The vane-UC ratio for this undisturbed soil was found to be about 0.90. This material was then thoroughly remolded and tested (Test 10b). The resultant ratio was about 1.2. This larger vane-UC ratio for the remolded soil appears to support the hypothesis that remolded samples are less uniform than undisturbed samples.

As a further check of the effect of structure uniformity on the vane-UC ratio, the effect of age of the specimen after molding was studied. A remolded sample possibly will become more uniform with age, thereby increasing in unconfined compressive strength and lowering the vane-UC ratio. This was investigated for specimens of clay loam and clay, which were molded at one time, immediately pushed out of the mold, wrapped in aluminum foil, and stored in a moist cabinet until they were tested.

Figures 3a and 4a show strength as a function of curing time and Figures 3b and 4b show the corresponding changes in the vane-UC ratio. Both the vane and the unconfined

TABLE 1

SUMMARY OF SOIL TESTS AND PROPERTIES

Group	Type of Test	Test No.	Ratio of Vane Shear to ½ Unconfined Compressive Strength	Ratio of Pocket Penetrometer Shear to ½ Unconfined Compressive Strength	No. Samples Tested	Moisture Content, w (%)	Dry Density (pcf)	Basic Soil Properties							
								Liquid Limit	Plastic Limit	Plasticity Index	Clay (< 0.005 mm)	Silt (0.074-0.005 mm)	Sand (2.0-0.074 mm)	Classification	
														AASHO	USDA Texture
A	Determination of vane-UC ratio (remolded soils)	1a	1.0	1.5	54	37.0-44.0	73.5-80.6	51	30	21	44	49	7	A-7-5(15)	Silty clay loam
		2a	1.4	1.5	22	20.3-35.5	83.2-97.9	48	20	28	37	23	40	A-7-6(13)	Clay loam
		3a	0.7	2.3	6	33.6-34.3	79.3-80.6	41	35	6	4	33	63	A-5(1)	Sandy loam
		3b	0.8	2.0	3	33.6-35.1	80.7-82.9	36	28	8	22	34	44	A-4(4)	Loam
		5	1.3	1.6	3	35.9-36.0	89.1-89.8	49	33	16	83	10	7	A-7-6(12)	Clay
		6	1.4	2.1	3	47.8-47.9	71.7-71.8	88	41	47	92	7	1	A-7-5(20)	Clay
		7	1.25	1.5	3	64.0-65.0	59.6-61.1	89	34	55	77	12	11	A-7-5(20)	Clay
		8a	0.6	2.1	8	24.7-24.8	98.0-100.7	30	24	6	15	18	67	A-2-4(0)	Sandy loam
		9a	1.3	1.7	3	33.9-34.0	85.9-87.0	55	25	30	83	13	4	A-7-6(19)	Clay
B	Determination of vane-UC ratio (undisturbed soil)	10a	0.9	1.1	5	46.2-47.9	109.7-112.0	46	24	22	46	52	2	A-7-6(14)	Silty clay loam
		10b	1.2	2.0	7	44.8-46.3	110.4-118.5	46	24	22	46	52	2	A-7-6(14)	Silty clay loam
C	Rate of shear	2f	1.4	—	10	25.0-31.6	89.7-98.7	41	19	22	37	23	40	A-7-6(10)	Clay loam
		8b	0.5-1.0	2.3	8	22.1-22.6	101.9-102.7	30	24	6	15	18	67	A-2-4(0)	Sandy loam
D	Effect of age	2d	1.3-1.4	—	6	26.2-26.7	95.5-96.3	41	19	22	37	23	40	A-7-6(10)	Clay loam
		2e	1.4-1.5	—	9	24.9-25.8	96.9-97.5	41	19	22	37	23	40	A-7-6(10)	Clay loam
		9b	1.2-1.4	—	11	32.0-33.0	87.7-87.9	55	25	30	83	13	4	A-7-6(19)	Clay
E	Effect of vane size	1c	1.1	1.7	18	38.1-38.9	78.2-82.9	51	30	21	44	49	7	A-7-5(8)	Silty clay
		2b	1.3	1.3	54	24.9-34.8	84.3-98.9	41	19	22	37	23	40	A-7-6(10)	Clay loam
F	Effect of testing procedure	2c	1.3-2.7	1.3-2.2	8	19.0-21.4	102.3-107.3	41	19	22	37	23	40	A-7-6(10)	Clay loam

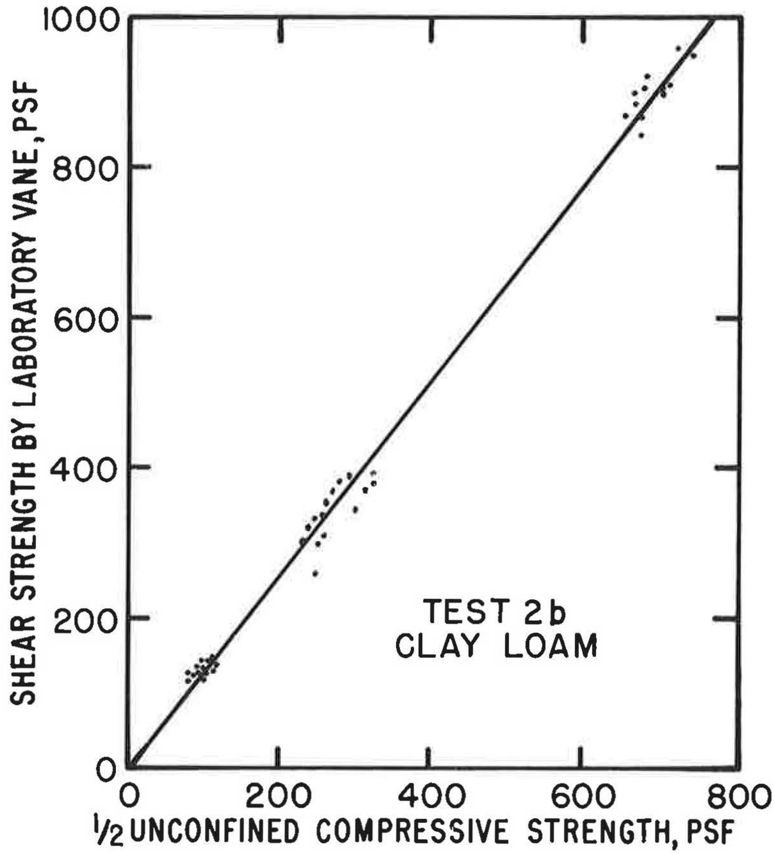

Figure 2. Vane shear vs one-half unconfined compressive strength.

compressive strengths tend to increase with curing time. However, the unconfined compressive strength increases at a more rapid rate, resulting in a decreasing vane-UC ratio. This tendency is more pronounced for the clay loam than for the clay. The strength ratio decreases from about 1.47 at zero time to about 1.33 at 39 days for the clay loam (Test 2e) and from about 1.37 at zero time to about 1.22 at 39 days for the clay (Test 9b). Based on these results, it appears that a remolded soil does gain in uniformity with age and thereby reduces the difference between the shear strengths measured by the two tests.

Pore Pressure

The second factor investigated was the possibility of pore-pressure buildup during shearing. This was investigated indirectly by studying the effect of rate of shear. The rate of shear for the vane test was maintained constant by rotating the crank handle approximately 1 rpm. This resulted in an almost constant rate of stress increase and very little strain as the load increased. As the load approached the shear strength of the soil, a constant rate of strain of approximately 0.2° per sec resulted.

The effect of shear rate was investigated by varying the rate of shear at failure between 0.1° and 1.0° per sec (Group C, Table 1). A clay loam (Test 2f) showed no measurable differences in strength for this range of shear rates. However, Figure 5 shows that a loam (Test 8b) gave a vane-UC ratio of 0.6 at 0.2° per sec and 1.0 at 1.0° per sec. At rates slower than 0.2° per sec, a constant ratio of slightly lower than 0.6 resulted. This apparent constant ratio could be due, in part, to the difficulty

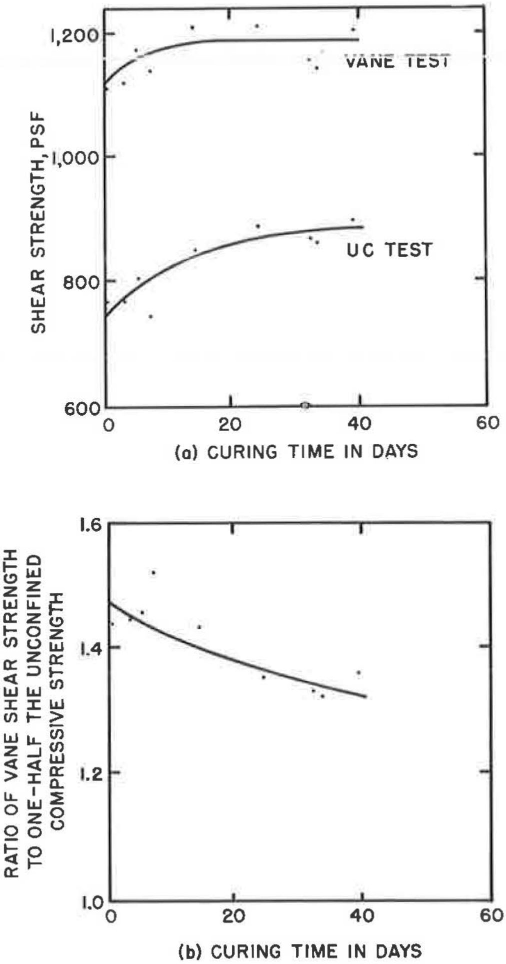

Figure 3. Effect of curing time on shear strength of remolded clay loam specimens (Test 2e).

in manually rotating the crank at a constant rate at these slow speeds, resulting in a variability in readings. Because 0.2° per sec rotation gave the minimum strength, this rate was considered satisfactory for all tests.

Because the loam is a dilatant soil, negative pore stresses may be induced during shear deformation. The negative pore-water stresses would create or increase normal pressure on the rupture surface. This would, in turn, possibly increase an intergranular friction force, resulting in an increased shear strength with increased rate of shear.

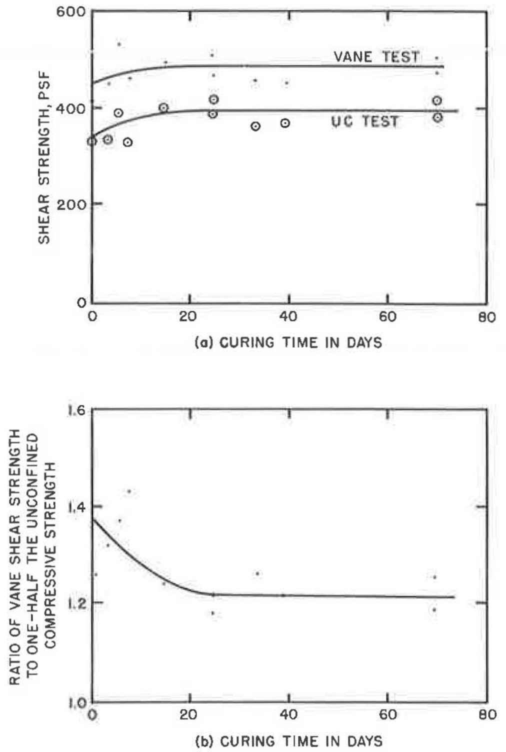

Figure 4. Effect of curing time on shear strength of remolded specimens (Test 9b).

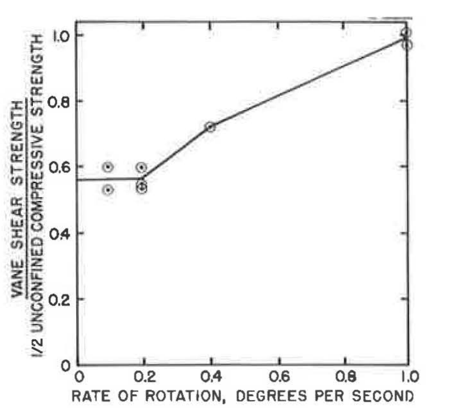

Figure 5. Effect of rate of rotation on vane-UC ratio for sandy loam (Test 8b).

Progressive Failure

The third factor, the possibility of progressive failure in the vane test, was also studied indirectly. If a progressive failure was taking place in the vane test, a six-bladed vane would create a larger shear surface and result in a higher shear strength than a two- or four-bladed vane.

The vane supplied consisted of four blades, each with a height of ½ in. and a width of ¼ in. Two- and six-bladed vanes were also constructed and tested. The six-bladed vane gave average strength values 9 percent greater than the two-bladed vane, whereas the four-bladed vane gave values 2 percent greater. In soft silty soils, the six-bladed vane caused significant compression of the soil during insertion. The effect of this disturbance on the measured strength is unknown. The effect of length of blades was also studied. Vanes with blades 1.0 and 2.0 in. long were built and the strength values were compared with those obtained with the original vane with ½-in. blades. The calculated shear strength values were essentially equal.

Because the six-bladed vane did give strength values slightly greater than the four- and two-bladed vanes, some progressive failure seemed to be taking place.

Effect of Testing Procedure

The fourth factor that possibly affects the shear strength as measured by the vane and the unconfined compression test is the testing procedure used.

Because the vane and the unconfined compression tests both were often run on the same test specimen, there was a possibility that disturbance by the insertion of and testing with the vane would reduce the unconfined compressive strength. To investigate this, duplicate samples not tested by the vane were periodically tested using the unconfined compression test. Strengths obtained by the two methods checked very closely and indicated that the insertion of the vane made no significant difference.

To determine any changes in strength due to removing the soil from the mold, duplicate specimens were tested with the vane in the mold and after removal from the mold. The specimens removed from the mold prior to testing were wrapped in aluminum foil and held by hand while the vane test was run using the normal procedure. No measurable difference in shear strengths was observed for the soils tested inside and outside the mold at moisture contents between the plastic and liquid limits.

Although the vane-UC ratio was constant for each soil within its plastic range, it increased as the moisture content decreased below the plastic limit. This may be due to crumbling of the soil and subsequent reduction of the unconfined compressive strength. When the vane test was conducted on these drier specimens after removal from the mold, the specimens tended to crack, resulting in a reduced vane shear strength. The vane-UC ratio then approached the constant value obtained for the soil at higher moisture contents.

POCKET PENETROMETER TESTS

In conjunction with the laboratory vane test evaluation, shear strength values were obtained using a commercially manufactured "pocket penetrometer." This pocket-size device is used to measure the resistance of a soil mass to the penetration of a 0.245-in. diameter rod at ¼-in. penetration. Pocket penetrometer tests were usually made with each vane shear test. The ratios of the average shear values obtained from the pocket penetrometer to the values obtained from the unconfined compression tests varied from 1.3 to 2.3 (Table 1). The relationship between this ratio and the plasticity index is shown in Figure 6.

MODE OF FAILURE

The wide variation in the vane-UC ratio, from 0.6 to 1.4, indicates that there is a basic difference in the mode of failure between the two tests. Figure 7 shows that the vane-UC ratio is related to the plasticity index. As the plasticity index increases, the vane-UC ratio increases to a value of about 1.4. For a plasticity index of 14, the ratio is 1.0.

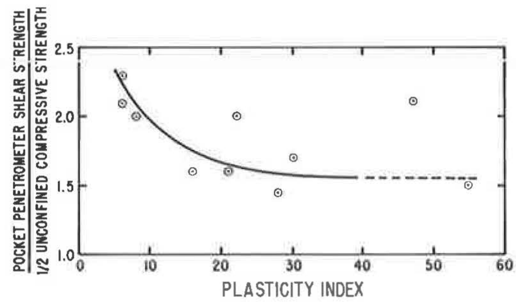

Figure 6. Pocket penetrometer-UC ratio vs plasticity index.

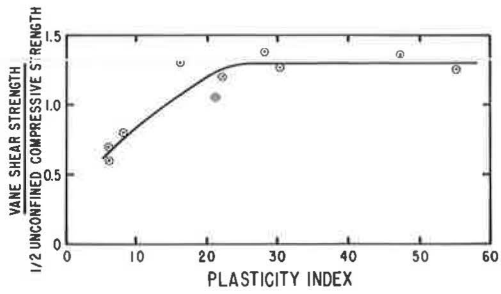

Figure 7. Vane-UC ratio vs plasticity index.

Test specimens with nonuniform structure, water content and density tend to give vane-UC ratios greater than 1.0. It is likely that as the plasticity index of the soil increases, the uniformity of the molded test specimen decreases. For highly plastic soils, the average strength measured by the vane exceeds that measured by the unconfined compression test by 40 percent.

The vane-UC ratios less than 1.0, indicating greater shear strengths by the unconfined compression test, may be due to the inclusion of an intergranular friction component mobilized in the unconfined compression test but not in the vane test. Figures 8a and 8b represent the theoretical mode of failure for the vane and the unconfined compression tests, respectively. In the vane test, if the normal pressure, σ, induced during shear is zero, the shear strength would be a function of cohesion only and would not be affected by intergranular friction. In the unconfined compression test, the shear strength is a function of both cohesion and friction. It is reasonable to expect that as the plasticity index of the soil becomes smaller, the frictional component will increase in significance and result in smaller vane-UC strength ratios.

If the vane measures cohesion only, a useful Mohr diagram can be plotted using results of the vane and the unconfined compression tests. By using the vane-measured strength at a zero normal stress and the Mohr circle determined by the unconfined compression test, the envelope was established as shown in Figure 9.

To check the validity of these envelopes, the resistance to penetration of the penetrometer was compared with that computed using the envelopes. The penetrometer resistance was calculated by Terzaghi's formula (6),

$$F_{Dr} \leq \pi r^2 \; (1.3\, c N_c + 0.6\, \gamma r N_\gamma) \tag{3}$$

in which

F_{Dr} = critical load on a circular footing in lb;
r = radius of footing in ft;
c = cohesion in psf from vane shear test;
N_c, N_γ = bearing capacity factors dependent upon angle of internal friction, ϕ, from unconfined compression test; and
γ = unit weight of soil in pcf.

The theoretical mode of failure for the pocket penetrometer is shown in Figure 8c. A comparison of the computed penetration resistance with the measured forces is given in Table 2. The reasonably good agreement indicates that the Mohr envelopes may be correct.

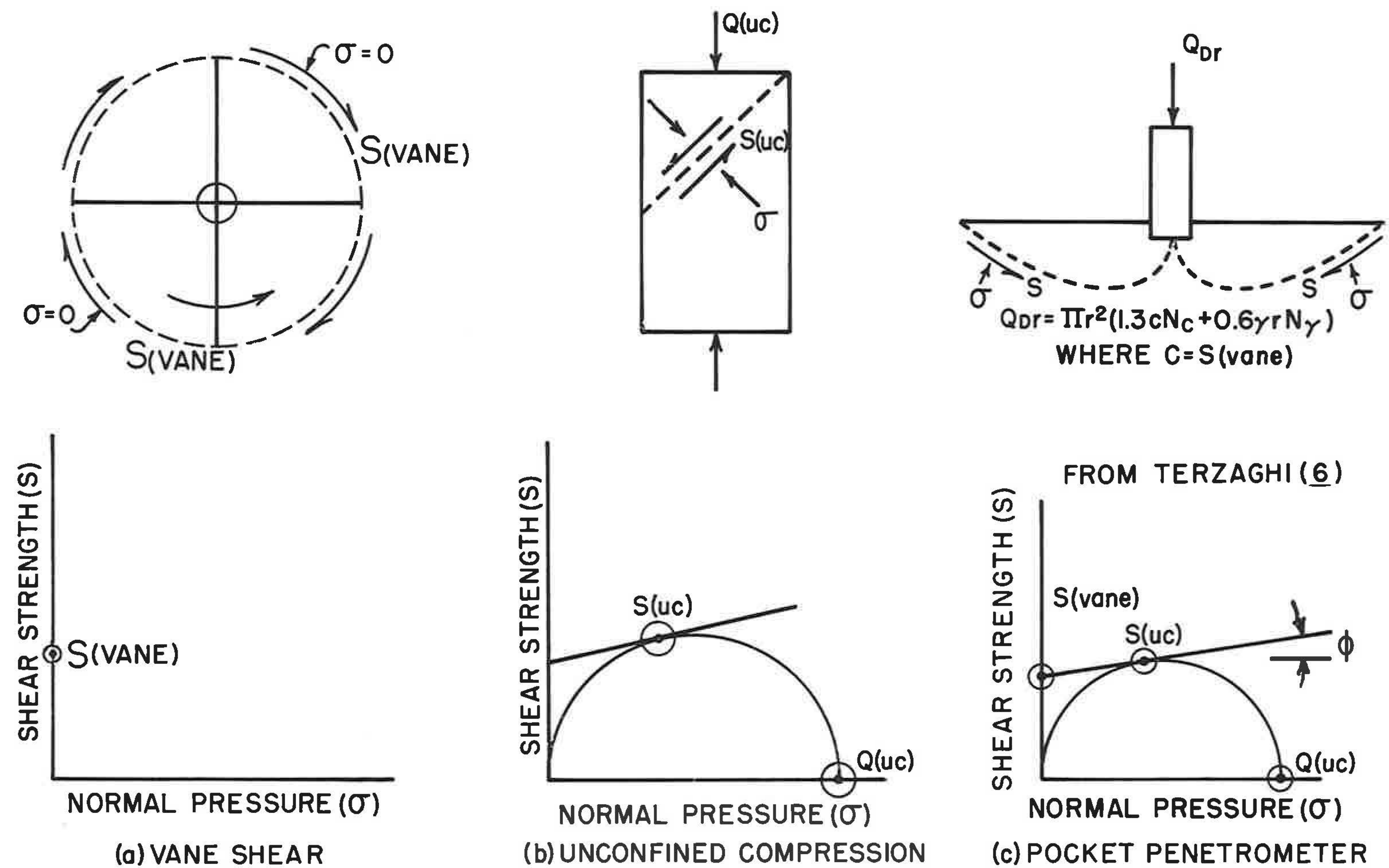

Figure 8. Theoretical modes of failure.

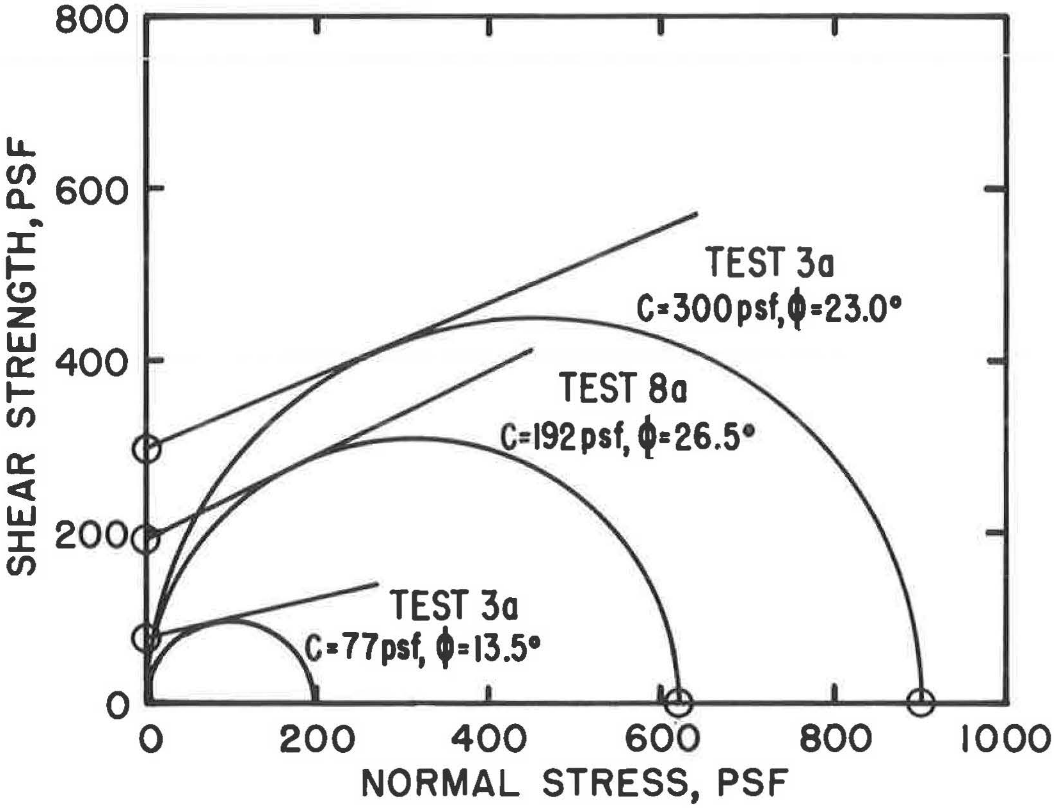

Figure 9. Graphical interpretation of shear strength measured in vane shear and unconfined compression tests.

TABLE 2

MEASURED AND COMPUTED FORCE TO INSERT POCKET PENETROMETER

Soil Test No.	Cohesion, c (psf)	Angle of Inter-granular Friction, φ (deg)	Required Force (lb)	
			Measured	Computed[a]
3a	300	23.0	3.50	3.00
3b	77	13.5	0.62	0.43
8a	192	26.5	2.27	2.24

[a]From Terzaghi's formula.

SUMMARY

Laboratory vane shear and unconfined compression tests on a variety of fine-grained soils, molded into test specimens at moisture contents between the plastic and liquid limits, showed that the ratio of the vane shear strength to one half the unconfined compressive strength for a given soil was constant. This vane-UC ratio varied from soil to soil, ranging from 0.6 to 1.4. Soils with plasticity indices of less than 14 had vane shear strengths less than the unconfined compressive shear strengths, whereas soils with plasticity indices greater than 14 had vane shear strengths greater than the unconfined compressive shear strengths. Possible reasons for this include:

1. A remolded soil with a high plasticity index probably has nonuniform structure. Because the specimen in the vane test fails along a fixed surface and that in the unconfined compression test fails in the weakest area, nonuniformity of structure causes the vane strength to be higher in relation to that of the unconfined compression test. The vane-UC ratios of the undisturbed soil increased from 0.9 before remolding to 1.20 after remolding. The vane-UC ratio also decreased as the age of the specimen increased. The structures of undisturbed specimens and specimens aged after remolding probably were more uniform than those of specimens immediately after remolding, causing the lower vane-UC ratio.
2. A soil with a low plasticity index probably has an intergranular friction force that is mobilized in the unconfined compression test but not in the vane shear test. This results in low vane-UC ratios for such soils.

The buildup of pore-water pressure in the vane test was studied indirectly by the effect of shearing rate on the vane-UC ratio, but the results were inconclusive. However, increasing the rate of rotation of the vane for a soil with a low plasticity index did cause an increase in the shear strength. Because the soil tested was dilatant, negative pore-water stresses were probably induced during the shear deformation. This negative pore-water pressure contributed to the increase in shear strength. No such effect was noted for clays.

The length and the number of blades made little difference on the results of the vane test for the soils tested.

The difference noted by other researchers between the unconfined compressive shear and the vane shear strengths may be due to differences in the modes of failure rather than in the actual shear strength of the soil.

The shear strength values obtained with the laboratory vane shear device appear to be reliable. The ease of testing and the relatively small degree of disturbance to the specimens make this a desirable test, especially for soft, sensitive soils.

REFERENCES

1. Gray, H., "Field Vane Shear Tests on Sensitive Cohesive Soils." ASCE Proc., 81: paper 755 (July 1955).
2. Fenske, C. W., "Deep Vane Tests in the Gulf of Mexico." ASTM Spec. Tech. Publ. 193, Symposium on Vane Shear Testing of Soils (Nov. 1957).
3. Cadling, L., and Odenstad, S., "The Vane Borer, an Apparatus for Determining the Shear Strength of Clay Soil Directly in the Ground." Royal Swedish Geotechnical Inst., Stockholm, Proc., 2 (1950).
4. Darienzo, M., and Vey, E., "Consistency Limits of Clay by the Vane Method." Proc., HRB, 34: 559-566 (1955).
5. Skempton, A. W., "Vane Tests in the Alluvial Plain of the River Forth near Grangemouth." Geotechnique, 1: 2 (Dec. 1948).
6. Terzaghi, K., "Theoretical Soil Mechanics." John Wiley & Sons, New York (1943).

Discussion

NYAL E. WILSON, McMaster University, Canada. —Goughnour and Sallberg proposed two hypotheses regarding the research work on the laboratory vane shear test. These hypotheses are concerned with (a) the influence of pore-water pressures and (b) the effects of progressive failure. Some interesting research work has been conducted on the laboratory vane shear test and the results of this work substantiate the findings of Goughnour and Sallberg.

This research involved using the laboratory vane shear apparatus in dilatant soil; the soil used was a medium-fine silt. The rate of testing was accurately controlled by a variable-speed motor and the vane blade was instrumented so that pore-water pressures could be measured on the shear surface (Fig. 10). The pore-pressure measurements were taken by welding hypodermic tubing to the edge of one of the vane blades; the end of the tubing was slotted and covered by a No. 200 mesh screen.

Influence of Pore-Water Pressures

As in the research by Goughnour and Sallberg, it was found that the torque applied to the vane shaft was dependent on the speed of testing. Figure 11, showing torque vs testing speed for vane tests in silt, indicated that a higher torque was associated with higher testing speeds. The value of the torque was overestimated by about 25 percent when tested at the usual speed in the laboratory. This overestimation was related to the particular torsion spring used in the test. The deformation of the soil was dependent upon the speed of testing, i. e., the angular velocity of the torque dial, was related to the rigidity of the torsion spring, and varied with each apparatus. This is one of the disadvantages of the laboratory vane test that is neither rigorously stress nor strain controlled.

To investigate the influence of pore-water pressure on the torque applied to the vane shaft, a series of tests was conducted in silt (Fig. 12). These tests, conducted at constant speed, also indicated that a change in testing depth from 2 to 3 in. had no significance. The results show that induced pore-water pressures can be in either the neg-

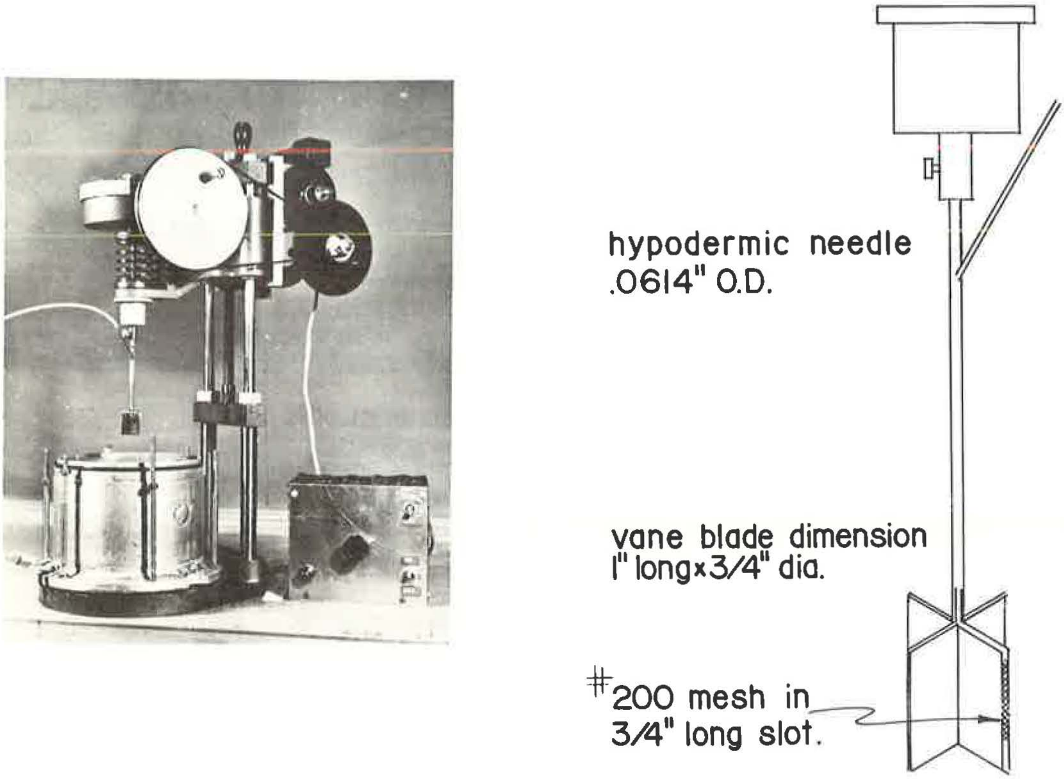

Figure 10. Laboratory vane, with provision for pore-pressure measurements.

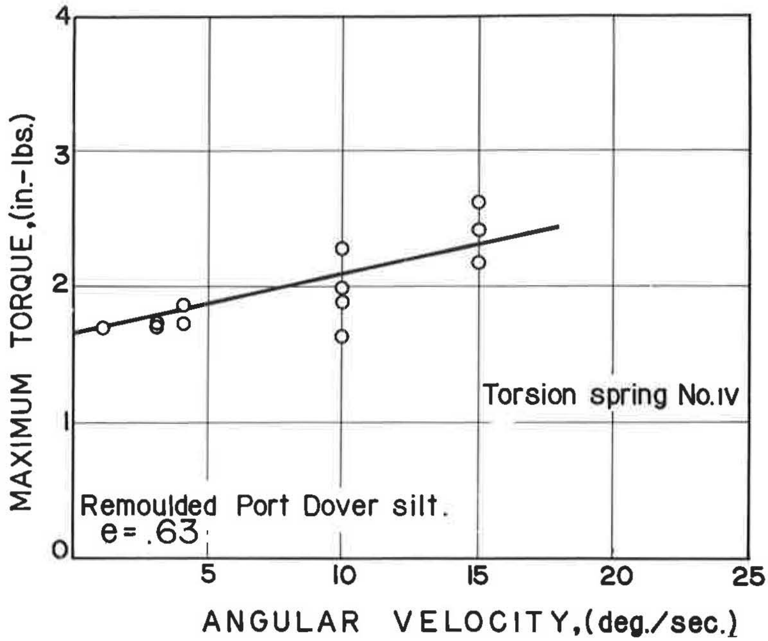

Figure 11. Vane tests in silt—dependence of maximum torque on angular velocity of torque dial.

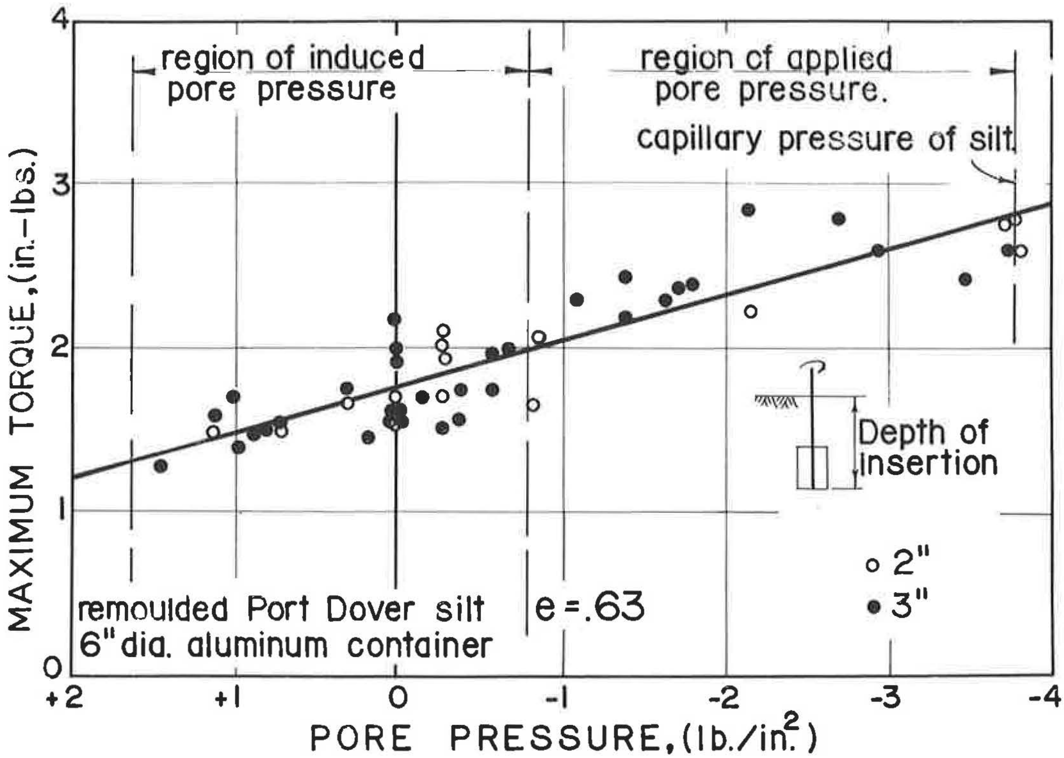

Figure 12. Vane tests in silt—maximum torque vs pore-pressure.

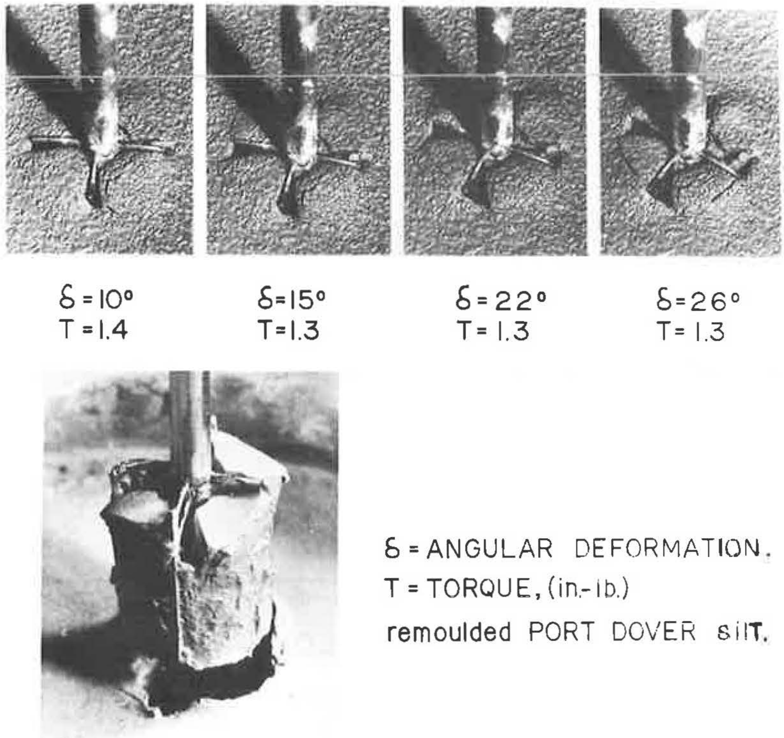

Figure 13. Vane tests in silt—generation of rupture surfaces during test.

ative or positive range, depending on the formation of the meniscus at the start of the test. Negative pore-water pressures were applied to the soil to determine the influence over a greater range. The sloped line indicates that the laboratory vane test, commonly considered as an "undrained" test, acquired the characteristics of a "drained" test in dilatant soils. This anomaly also has been found for triaxial tests on dilatant soils.

Progressive Failure

During the tests progressive failure was investigated. The vane was inserted to the depth of the vane blades and photographed as the torque was applied and as the angular deformation took place (Fig. 13). At a strain of 10°, and when the maximum torque occurred, shear surfaces were generated at the tips of the blades and at right angles to them. At this stage in the test, the shear surface was not cylindrical but almost rectilinear. As the angular strain increased and the torque decreased, the shear surfaces extended until, ultimately, a cylindrical failure surface was formed. During these stages of the test, voids were formed behind the vane blades and the shearing resistance was zero at these voids. Although the ultimate shearing surface was cylindrical, it was not necessary for the shear surface at maximum torque to be cylindrical or the stress distribution on the walls of the cylinder to be uniform. As the stress distribution at the shearing surface and along the vane blades was unknown, it was not possible to use the vane with any accuracy in this type of soil.

References

7. Golder, M. Q., "Techniques of Field Measurement and Sampling." 5th Internat. Conf. on Soil Mechanics and Foundation Eng., Paris (1961).

8. Wilson, N. E., "Techniques of Field Measurement and Sampling." 5th Internat. Conf. on Soil Mechanics and Foundation Eng., Paris (1961).
9. Cadling, L., and Odenstad, S., "The Vane Borer." Royal Swedish Geotechnical Inst. Proc., 2 (1950).
10. Wilson, N. E., "Laboratory Vane Shear Tests and the Influence of Pore-Water Stresses." ASTM Shear Testing Sym. (1963).

R. D. GOUGHNOUR and J. R. SALLBERG, Closure. —The authors are grateful to Prof. Wilson for his interesting and informative discussion. His development of the pore-pressure device results in a welcome contribution. It would be of interest to continue the study of pore-pressure on a variety of soils with a wide range of plasticity indices.

Prof. Wilson refers to the "usual speed" of vane testing, but in Figure 11 shows values up to 15° per sec angular velocity of torque dial. These values appear to be much higher than values of normal testing.

In regard to Prof. Wilson's last sentence, it should be pointed out that the stress distribution is not known for any type of test and, therefore, the vane test could be considered as accurate as any other of the commonly used tests.

Piezoelectric Gages for Dynamic Soil Stress Measurement

E. T. SELIG and E. VEY
Respectively, Research Engineer and Professor of Civil Engineering, IIT Research Institute, Chicago, Illinois

A study was made of the suitability of piezoelectric gages for the measurement of dynamic stresses in soil. A number of variations of thickness-diameter ratio was investigated, as well as several simple methods of sensor encasement. The gages were tested statically and dynamically under fluid pressure and embedded in both confined and constrained specimens of sand.

The disk-shaped piezoelectric sensor from which the gages were constructed was found to have high electrical sensitivity, high stiffness, and to be suitable for miniaturization. It is, however, sensitive to moisture, electromagnetic radiation, temperature, and distortions produced by shearing stresses, bending moments and lateral pressures.

Measurements made with the gages embedded in sand showed that (a) the static and dynamic gage sensitivities are the same; (b) the gage response is influenced by soil density, confining pressure and placement techniques; and (c) the gage output is a nonlinear function of applied stress when the soil stress-strain relationship becomes appreciably nonlinear. It was clear from the study that an elaborate stress gage design is required to isolate the sensing element from all undesirable influences. A more refined gage is currently under development.

•THE MEASUREMENT of stress in soil has long been recognized as a difficult experimental problem. All of the important gage concepts that have been devised and used in the past for measuring stress have involved a transducer whose signal is related to the gage stiffness. The gage functions by using its "built-in" stiffness to resist soil pressure. It is the reaction of the gage to this pressure that is measured, whether the reaction is in the form of a diaphragm deflection, the force required to prevent deflection, or distortion of a crystal as in the case of piezoelectric ceramics. Because the stress-strain characteristics of a particular soil are neither linear nor unique, it is not possible to devise a gage in which the ratio of soil stiffness to gage stiffness can be held constant. Hence, the gage output will not, in general, be a constant function of the soil stress. This is an inherent difficulty in measuring stress in soil.

This paper reports on the results of an investigation of the problem involved in measuring dynamic stresses in soil with miniature gages suitable for embedment in small soil specimens. Ordinary gages are unsuitable for this application because they either are too large, do not have the required shape, or have inadequate high-frequency response. Furthermore, the accuracy of stress measurement with most of these gages has not been clearly established.

Paper sponsored by Committee on Stress Distribution in Earth Masses.

PREVIOUS WORK

Considerable attention has been given to the measurement of stresses in soil. The most important conclusions derived from these studies are:

1. Gages respond differently in different soils.
2. Since the soil stiffness cannot generally be matched by the gage, its stiffness should be high compared to that of the soil.
3. A thickness-diameter ratio of $\frac{1}{10}$ or less is desired because the gage error increases as this ratio increases.
4. Gage placement techniques exert a considerable influence on the accuracy of stress measurements.
5. Accuracies of measurement to within ± 5 percent have been reported, but these appear to have been based upon indirect rather than direct comparison with known stresses.
6. A gage registers stresses higher than those actually existing if its stiffness exceeds that of the soil. This overregistration increases with the ratio of gage stiffness to soil stiffness but apparently reaches a maximum as this ratio becomes very large.
7. The overregistration increases with the ratio of sensitive area to total gage cross-sectional area because of stress concentrations on the perimeter of the gage.
8. In general, all the problems of stress measurement arise because stress gages have stress-strain characteristics different from those of the soil.

GENERAL DESCRIPTION OF GAGES

The gages considered in this study utilized piezoelectric ceramic transducers as sensing elements with a number of variations in the thickness-to-diameter ratio and methods of encasing the gage. The use of a piezoelectric sensing element is not new, but previous piezoelectric gages (7, 13) were not suitable for this application.

The advantages of the piezoelectric transducer are (a) its short response time (microseconds) that makes it especially suitable for shock-type loading, (b) the small crystal size possible, (c) high electrical sensitivity and (d) high stiffness (about the same as aluminum for the gages used in this study). But aside from the inherent difficulties of stress measurement with any type of gage, the use of these transducers introduced other experimental problems. These are, principally, extreme sensitivity to electromagnetic radiation, temperature, and moisture. The piezoelectric ceramics are also sensitive to any impressed distortions resulting from the way in which the stress from the soil is applied to the gage. They are, therefore, sensitive to mounting and method of placement and to the manner in which the sensing element is isolated from the soil. For example, shearing stresses on the face of the transducer, as well as bending moments, produce appreciable signals. The piezoelectric transducer acts as an electrical charge generating device. Because of the resistance-capacitance characteristic of the electrical circuitry (Fig. 1), extremely high circuit resistance is required to measure stresses of greater than a few seconds duration. This required resistance is difficult to obtain.

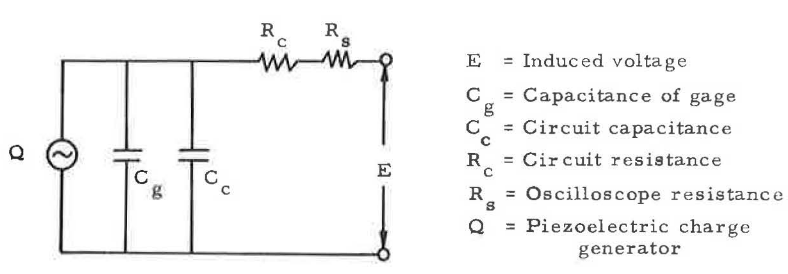

Figure 1. Schematic of piezoelectric circuit.

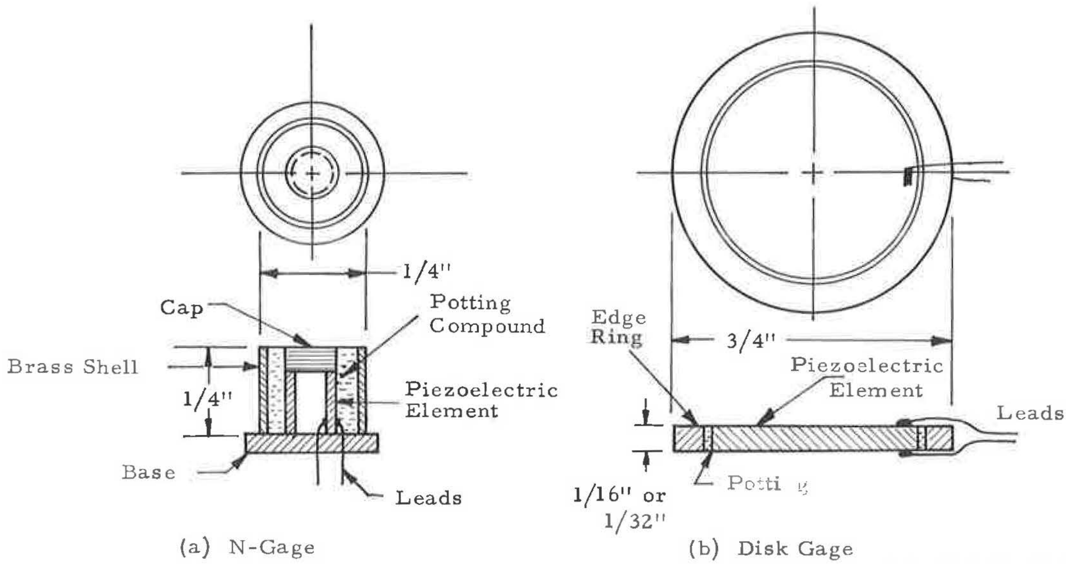

Figure 2. Stress gage configurations.

The gages studied had thickness-diameter, T/D, ratios varying from 1.0 to 0.08 with a maximum gage diameter of 1.0 in. The two basic configurations investigated are shown in Figure 2. Figure 2a shows a cylinder of barium titanate mounted in a small metal cup. This N-gage was designed and constructed by Nagumo of the IIT Research Institute for use in measuring air shock pressures. The other gages, constructed from disk-shaped piezoelectric elements (Fig. 2b), made with and without a metal edge ring to isolate the element from the effects of lateral pressure and with and without a teflon face covering to isolate the effects of friction on the face of the gage. In some cases the unmounted ceramic crystals were coated with moistureproof materials, such as epoxy.

APPARATUS

Several types of tests were used in the gage evaluation: (a) triaxial, or constrained static and dynamic tests; (b) consolidation or confined compression tests; and (c) hydrostatic pressure tests. The soil used was 20 to 40 mesh air-dry Ottawa sand.

The dynamic triaxial tests were performed with a specially designed double pendulum apparatus (Fig. 3). The specimen was horizontally mounted on one pendulum and impacted by a second pendulum. The sand specimens used with this apparatus were 4 in. long and 3 in. in diameter and were enclosed in thin rubber membranes. Stress gages were embedded at several positions within each specimen. The confining pressure was controlled by applying the proper vacuum to the pores through an opening in the reaction pendulum. Initial specimen density was determined by the method of preparation.

The pendulums were constructed of 8-in. long, 3-in. diameter solid steel bars weighing approximately 17 lb each. An accelerometer was mounted on the outside end of each pendulum. In operation, the pendulums were first lined up at the bottom of their swing with the specimen between them. The impact pendulum was pulled back to a predetermined height and then released to impact the specimen. A switch was contacted just prior to impact to trigger the oscilloscopes that recorded the signals from the accelerometers and the embedded stress gages. The accelerations of the two pendulums were recorded throughout the duration of impact. Since the masses of the pendulums were accurately known, the average stress over the ends of the specimen

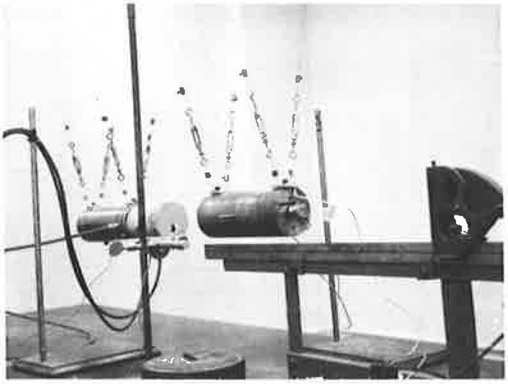

Figure 3. Pendulum apparatus.

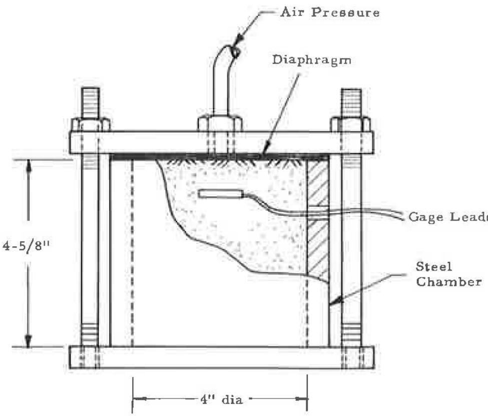

Figure 4. Schematic of confined compression device for gage calibration.

could be computed from the product of the pendulum mass per unit cross-sectional area and its acceleration. The fact that the stress cannot be assumed to be truly uniform over the cross-section is a limitation of this method of calibration.

The confined compression device (Fig. 4) consists of a rigid steel chamber 4 in. in diameter and 4⅝ in. deep covered with a rubber diaphragm and a rigid cap. The gage was embedded approximately 1 in. from the top of the sand surface to minimize wall friction effects and the surface was loaded by applying air pressure through the diaphragm.

For the hydrostatic pressure tests the gage was placed in a closed chamber and pressure was applied and released at controlled rates using either air or water. In this apparatus the pressure could be prevented from acting on the edges of the gages.

CALIBRATION OF N-GAGES

The calibration of the N-gages obtained with air pressure was usually quite linear (Fig. 5), but they were not entirely reproducible. Successive calibrations usually varied less than 5 percent, but over a period of time random variations averaging 13 percent were observed. Perhaps 5 percent of these variations could have derived from the recording system.

Typical records with the pendulum apparatus are shown in Figure 6. The traces are approximately of the general shape expected, but they exhibit a roughness, apparently due to the movement of individual grains of sand. This might be expected because the diameter of the sensing element was only about 6 times the average grain diameter of the sand.

The gages were placed in both the center of the pendulum specimen and approximately ½ in. from the impact end. The initial specimen density and the confining pressure were varied and records were obtained using the maximum gage output voltage and the average maximum stress at the ends of the specimen during impact.

Calibration results for low, high and medium density specimens are given in Figures 7, 8 and 9, respectively. The impact sequence and corresponding impact velocity, v_0, and confining pressures, σ_3, are indicated. The following conclusions were drawn from these results:

1. The sensitivity (defined as ratio of gage output to applied stress) increased significantly with repeated impacts at the same v_0 and σ_3 (see impacts 3, 4, 5, Figs. 7 and 8; and impacts 1, 2, 3, 4, Fig. 9). This effect cannot be explained on the basis of specimen density, but it could have been caused by placement or rearrangement of the sand particles around the gage to form a more stable configuration.

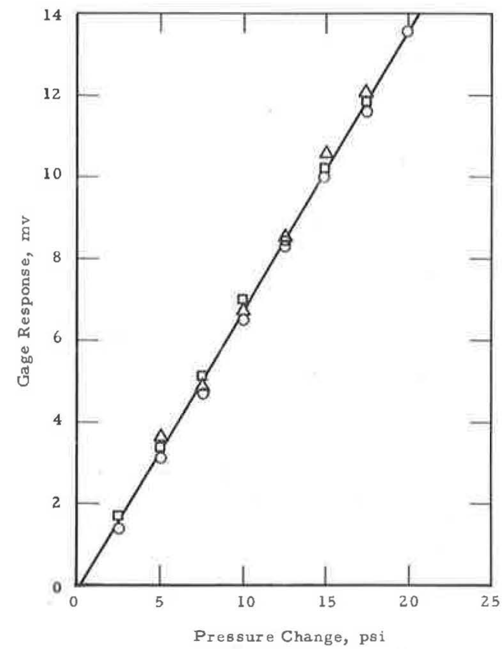

Figure 5. Air calibration results for gage N-11.

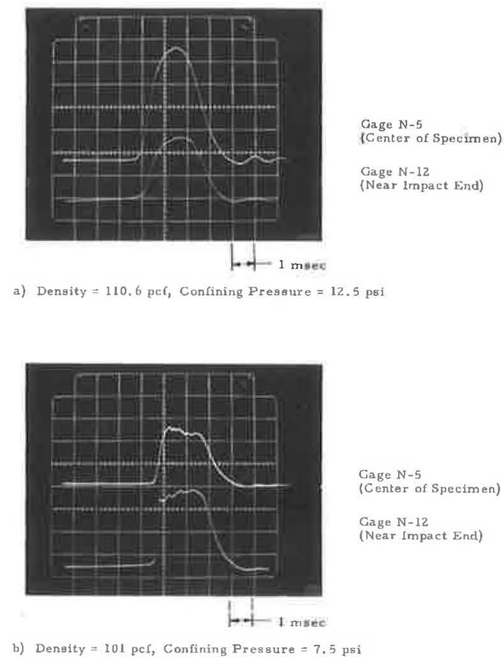

a) Density = 110.6 pcf, Confining Pressure = 12.5 psi

b) Density = 101 pcf, Confining Pressure = 7.5 psi

Figure 6. Typical embedded N-gage stress records.

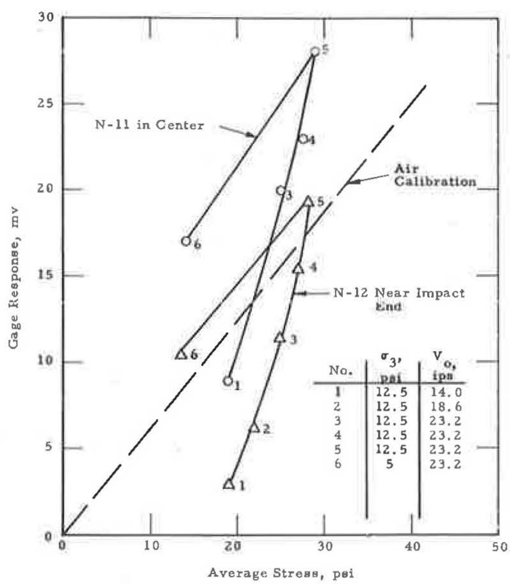

Figure 7. Embedded calibration of N-gages in low density specimen (γ_o = 101.5 pcf).

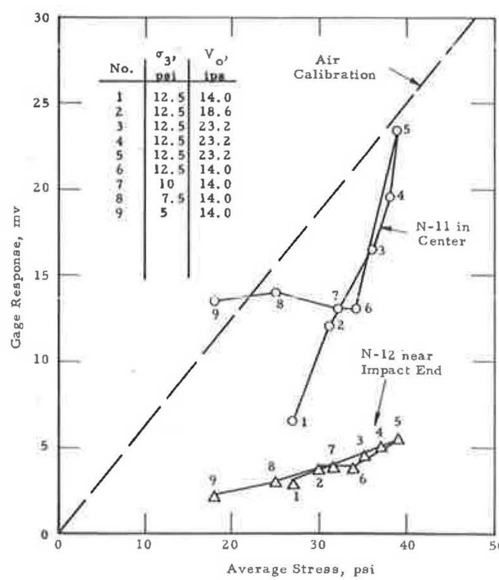

Figure 8. Embedded calibration of N-gages in high density specimen (γ_o = 111.0 pcf).

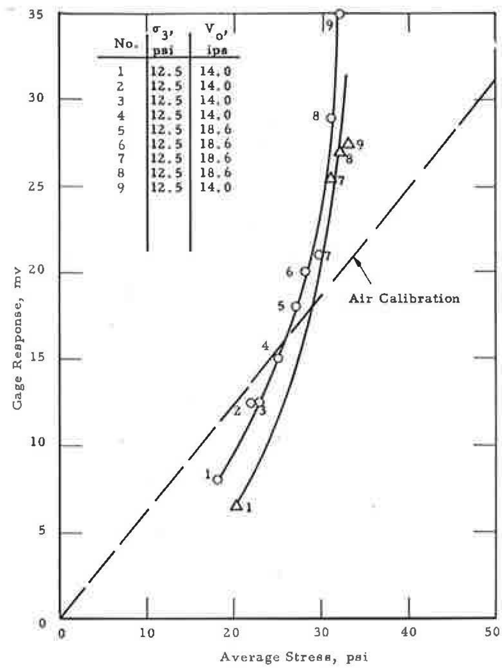

Figure 9. Embedded calibrations of N-12 in center of medium density specimen (γ_0 = 103.6 pcf) showing reproducibility.

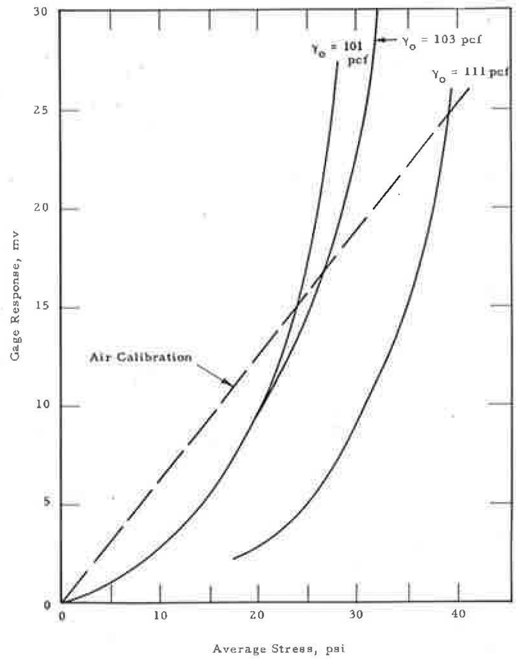

Figure 10. Effect of density on embedded calibration of N-gage in center of specimen at 12.5 psi confining pressure.

2. The sensitivity increased significantly with a decrease in confining pressure (see impacts 6, 7, 8, 9, Fig. 8). This could be predicted because the stiffness of the specimen decreases with a decrease in σ_3. Because the effect of successive impact also is included, it is not possible to say which is the greater effect.

3. Both N-11 and N-12 have similar embedded calibration curves; however, the output of the gage in the center of the specimen is much greater than that near the impact end. Because both gages have approximately equal sensitivities in air, the presence of the rigid boundary at the end may prevent arching over one side of the gage. The difference in output of the gages in the two positions was much greater for the high density than for the low density specimen.

4. The sensitivity of both gages for the first few impacts was less than that for a corresponding air pressure, i.e., underregistration occurred. For a gage in which the over-all stiffness is greater than that of the specimen, this behavior would not be expected. It appears that, although the gage case acts as a stiff unit and picks up load from the soil, because of the way the sensing element is mounted in the case the soil stress arches across the sensing element. Under successive impact this arch breaks down through rearrangement of the sand, thus increasing the gage signal.

5. For the first several impacts, the trace of the gage in the center of the specimen returned to a point above the initial zero, indicating a residual compressive stress. For the last several impacts, the trace ended below its original zero, indicating a tension, relative to σ_3. This appears to be an interaction phenomenon caused by a difference in soil stiffness between stress increase and decrease.

6. The calibration records with the gage in the center of the specimen for the three densities at a constant confining pressure are compared in Figure 10. The gage sensitivity increased with a decrease in density as would be expected because soil stiffness increases with density.

7. In general, the embedded gage sensitivities did not appear to be unique functions of any of the important variables. The observed behavior probably was greatly influenced by details of the particular gage design, in addition to the shape.

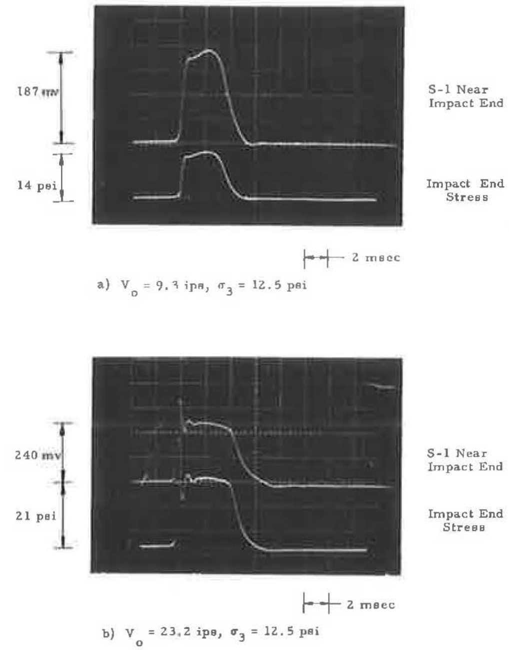

Figure 11. Comparison of embedded disk gage records with applied stress for low density specimen.

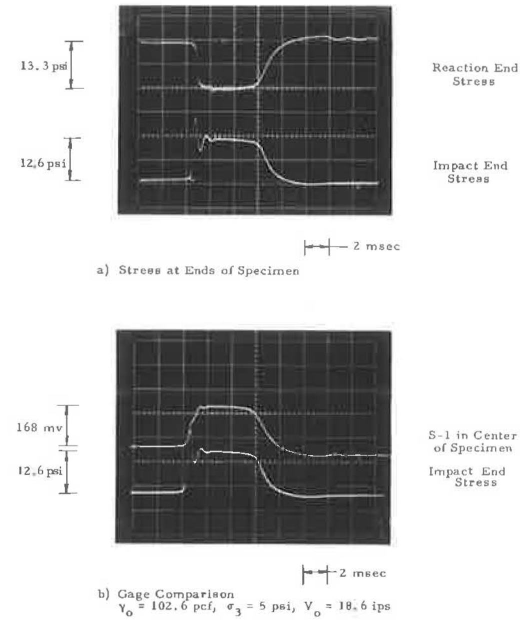

Figure 12. Typical records from pendulum tests with disk gage in center of specimen.

INITIAL STUDIES OF DISK GAGES

To improve stress measurements, disk-shaped gages were considered. The first of these gages were simply piezoelectric disks with silvered surfaces and leads attached, i.e., Figure 2b without the edge ring.

The fluid pressure calibrations showed that the signals generated by the piezolectric material were significantly affected by method of support or clamping, edge pressures, temperature change, moisture and electromagnetic radiation. Any change in clamping or support conditions affected the distortions under pressure of the ceramic crystal. The gage response was an order of magnitude less with the pressure acting all around the disk than it was with pressure acting only on the faces. For one typical gage the temperature sensitivity was 4.5 mv/° F compared to a pressure sensitivity of 0.5 mv/psi. Intrusion of moisture caused a decrease in circuit resistance, thereby decreasing the time constant.

The response of the embedded plain disk gages was also evaluated with the pendulum apparatus. A variety of piezoelectric disks was used, ranging in diameter from ½ to 1 in. and in T/D ratios from 0.026 to 0.12. Figure 11 compares the specimen impact end stress records with the response records of one of these gages (S-1 with a diameter of 1 in. and T/D ratio of 0.12) placed about ½ in. from the impact end. The pairs of traces are geometrically identical, therefore, the gage reproduces the shape correctly. Figure 12 compares the response records for the same gage located in the center of the specimen. The shape of the gage record lies between the shapes of the two end stress records.

The calibration curves corresponding to these two gage locations are compared in Figure 13. Both are reasonably linear and indicated the same sensitivity. The

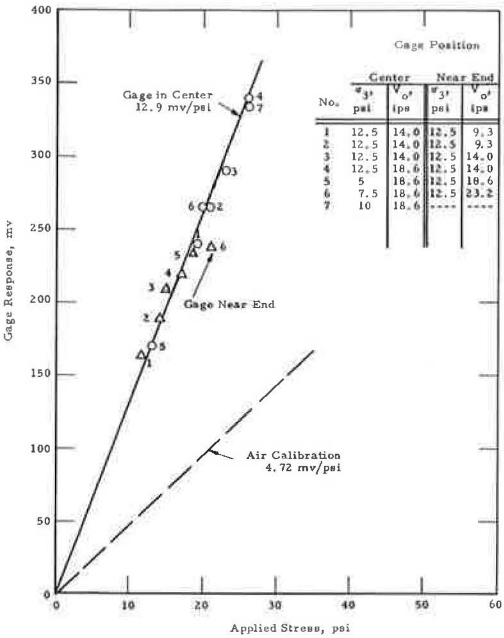

Figure 13. Calibration results for disk gage S-1 in low density specimen (γ_0 = 102.6 pcf).

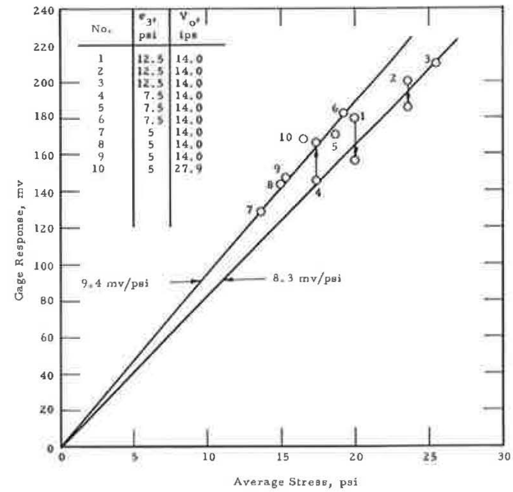

Figure 14. Typical calibration results for disk gage S-21 in high density specimen (γ_0 = 111.7 pcf).

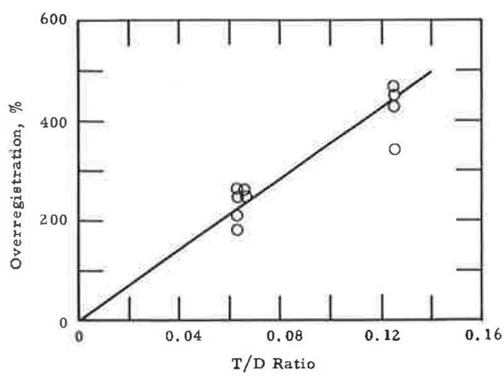

Figure 15. Overregistration of unmounted disk gages for two T/D ratios.

sensitivity was essentially constant for successive impacts. The stress increased at constant v_0 and σ_3, due to a greater deceleration of the pendulum on impacting a stiffer specimen. The sensitivity, however, was about 2.7 times greater than the air calibration value, i.e., overregistration was 170 percent. This high overregistration was largely due to a combination of shearing stress on the face of the gage and reduction of edge pressure resulting from lateral expansion of the soil.

The calibration curves were not always linear and reproducible. The average values varied from test to test and, especially for the high density specimens, the data points were grouped about different values for each σ_3 (Fig. 14). The gage trace did not always return to the inital zero (Fig. 12b). There was generally a positive residual stress indicated for the first impact and a negative residual for the fourth impact, which took place after the confining pressure had been reduced from 12.5 to 7.5 psi. These changes in calibration, indicated by arrows in Figure 14, are caused by a change in the specimen stiffness under each loading cycle.

Two sets of gages were used to evaluate the effect of T/D ratio and density on gage response. The gages were all unmounted piezoelectric disks ½ in. in diameter. One set had a thickness of $^1/_{16}$ in. and the other a thickness of $^1/_{32}$ in.; T/D ratios were 0.125 and 0.062, respectively.

The average variation of the sensitivity of embedded gages in the high density specimens was ± 20 percent and in the low density specimens was ± 16.4 percent. The variation for any one particular test may be taken as roughly half this total variation. Two gages showed an increase in sensitivity with increase in density and three showed a decrease. If density were the most significant factor influencing gage response, all gages would show a decrease.

The average overregistration for the two sets of gages (Fig. 15) appears to be directly proportional to the T/D ratio and ranges from 180 percent to 470 percent. As indicated previously, most of this overregistration was caused by friction on the face of the gage and reduction of pressure on the edge of the gage.

DISK GAGE WITH EDGE RING

The initial studies with the disk gages clearly indicated that the unmounted piezoelectric disks are extremely sensitive to edge pressures. To eliminate this, several gages were ringed with steel, aluminum or plastic with a thin band of rubber latex separating the metal or plastic from the piezoelectric material (Fig. 2).

The embedded calibrations for these gages showed some significant improvements. In general, the trace returned to its initial zero reference; when it did not, the deviation was much less than it had been for the gages without edge rings. The embedded calibration curves were similar in shape for both types of gages (Fig. 14). Gage sensitivities are shown as a function of density in Figure 16. Sensitivity appeared to be independent of density for these gages, but the same variation in average values was found. The metal rings reduced the overregistration by about 100 percent. Part of this reduction may have been due to the decrease in ratio of sensitive area to total face area, but most of it is believed to be attributable to the elimination of edge effects. The plastic rings were not effective, probably because they were not stiff enough to resist the lateral soil pressure.

During the evaluation of the disk gages with edge rings, suitable instrumentation (Kistler Charge Amplifier Model 566, Kistler Instrument Co., N. Tonowanda, N. Y.) became available to permit static measurements with the piezoelectric materials. This capability made possible a more detailed and critical examination of the embedded gage response. A series of static and dynamic tests were performed using gages $^1/_{16}$ in. thick with steel edge rings.

Triaxial soil specimens were used for the first embedded static tests. The specimens were prepared on the reaction pendulum as for the dynamic tests. Load was applied to the specimen with a standard unconfined compression machine. Following the static loading cycle the reaction pendulum was mounted and a series of dynamic tests was performed for comparison.

Typical calibration curves are shown in Figures 17 and 18. In the lower stress range where the stress-strain characteristics of the soil were linear, the gage response was approximately linear. As the soil stiffness decreased under greater stress, the gage sensitivity increased. This increase was observed in some cases to be as much as 100 percent as the failure stresses were approached. The unloading portion of the calibration curves was usually linear or bent slightly downward and, except when the maximum stresses were much lower than failure, there was considerable hysteresis.

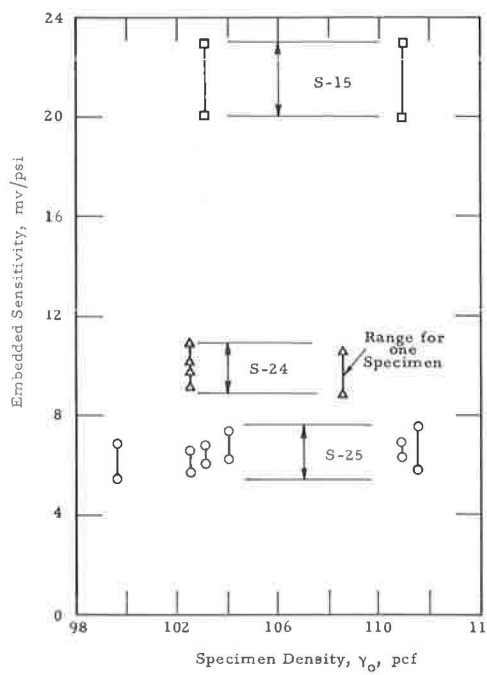

Figure 16. Embedded calibration of disk gages with edge ring as a function of density.

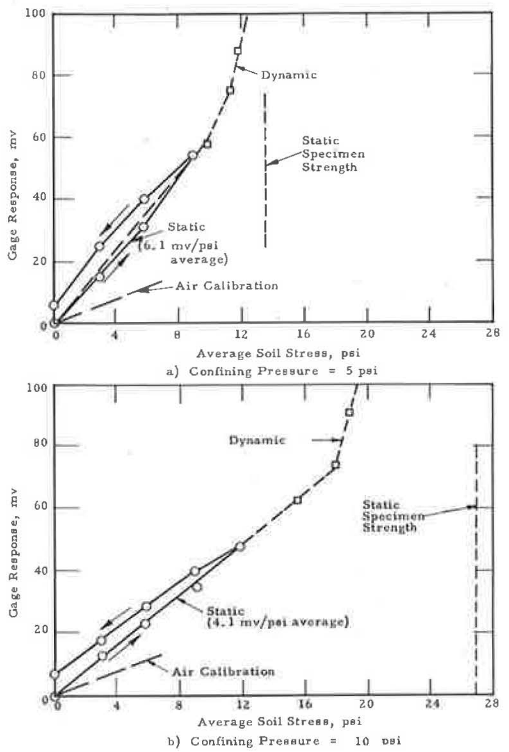

Figure 17. Typical triaxial calibration curves for disk gages with edge ring (maximum stress = below specimen strength, γ_o = 108 pcf).

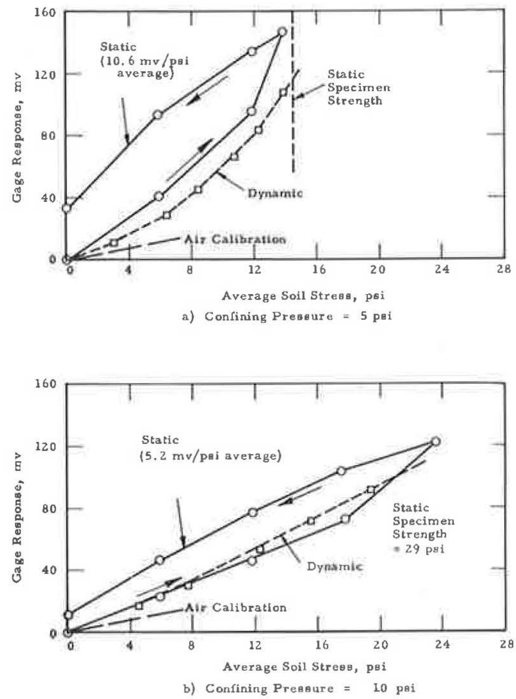

Figure 18. Typical triaxial calibration curves for disk gages with edge ring (maximum stress = specimen strength, γ_o = 110 pcf).

The overregistration for the initial linear portion averaged 100 percent. Some residual charge usually remained after the load was completely removed. This phenomenon was caused partly by electronic drift and partly by soil-gage interaction.

The curves for the dynamic stress coincided approximately with the load portion of the curves for the static tests. Thus, the static and dynamic sensitivities were approximately the same.

A number of the disk gages was embedded in the 3 in. diameter triaxial specimens that were subjected to a series of repeated loadings at stress levels equal to about 50 percent of the specimen strengths. The variation under the repeated load for each placement averaged 20 percent. The variation for four placements of seven gages ranged from 32 to 108 percent and averaged 73 percent (± 36 percent). When the results were separated on the basis of confining pressure the range reduced to ± 26 percent.

DISK GAGE WITH EDGE RING AND TEFLON COVER

Some overregistration was caused by shearing stresses on the face of the gage associated with lateral expansion of the soil specimen. To evaluate this effect, thin flexible teflon sheets were placed over the face of each gage and separated from the gage by a thin coating of silicone grease. Typical results from a series of static and dynamic tests performed with these gages in triaxial specimens of sand are shown in Figure 19.

In general, the amount of hysteresis was less with the teflon cover, and the residual charge did not remain after the soil was unloaded. The static and dynamic results were

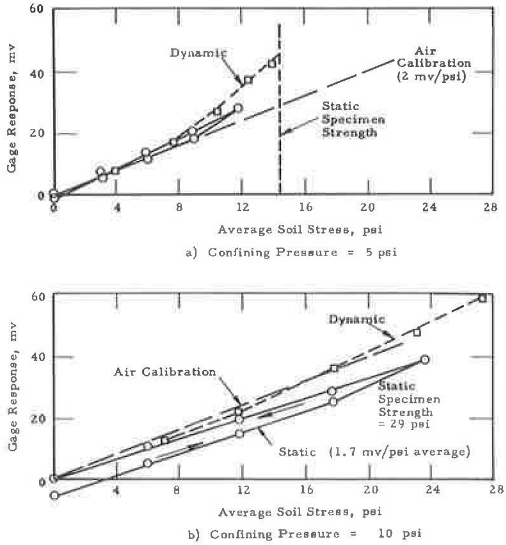

Figure 19. Typical triaxial calibration curves for disk gages with edge ring and teflon cover (maximum stress = specimen strength, γ_o = 110 pcf).

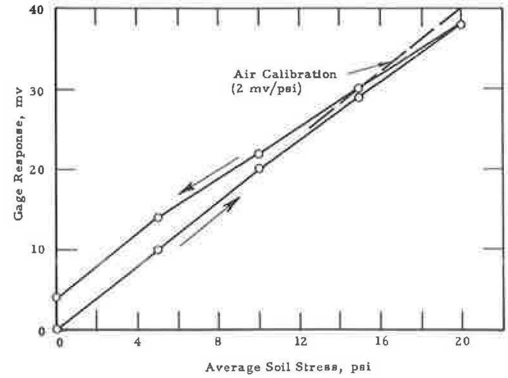

Figure 20. Typical confined calibration curves for disk gages with edge ring and teflon cover.

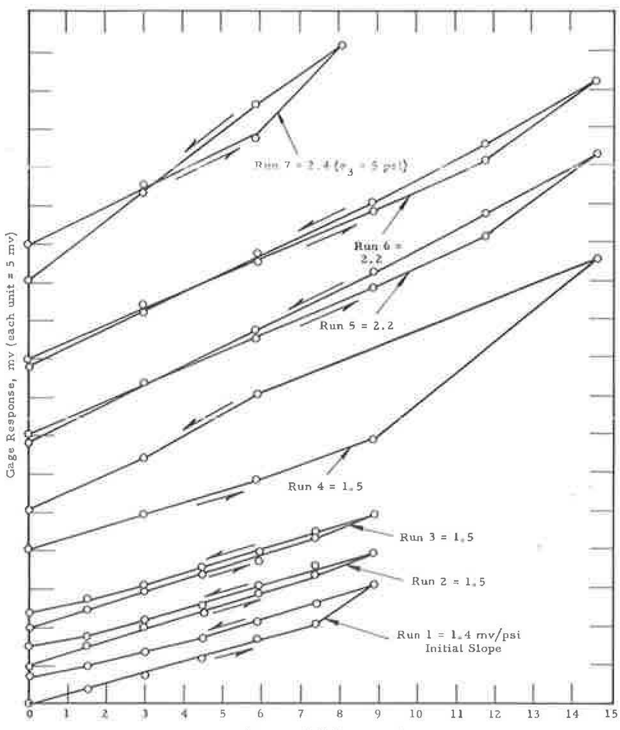

Figure 21. Triaxial calibration curves for gage S-25RT under repeated loading (γ_o = 100 pcf, σ_3 = 12.5 psi).

approximately the same, although the dynamic curve generally bent upward at a lower stress than did the static curve. For a wide range of calibration values the ratio of static to dynamic calibration remained about 1.0 with a variation on the order of ± 10 percent. Sensitivity distinctly tended to decrease with an increase in confining pressure. Gage sensitivity was reduced by approximately 100 percent with the teflon, thus greatly reducing the overregistration.

To further evaluate the factors influencing overregistration, several of these gages were calibrated in the confined compression device (Fig. 4). The resulting calibration curves (Fig. 20) were generally linear on load and unload. The major portion of hysteresis and residual charge may be caused by instrumentation drift.

Previous tests had indicated that gage sensitivities would increase with each consecutive loading cycle. A series of tests was performed to determine this effect under static loading. The test procedure consisted of seven to nine loading cycles. In cycles 1 through 3 the maximum applied stress was approximately

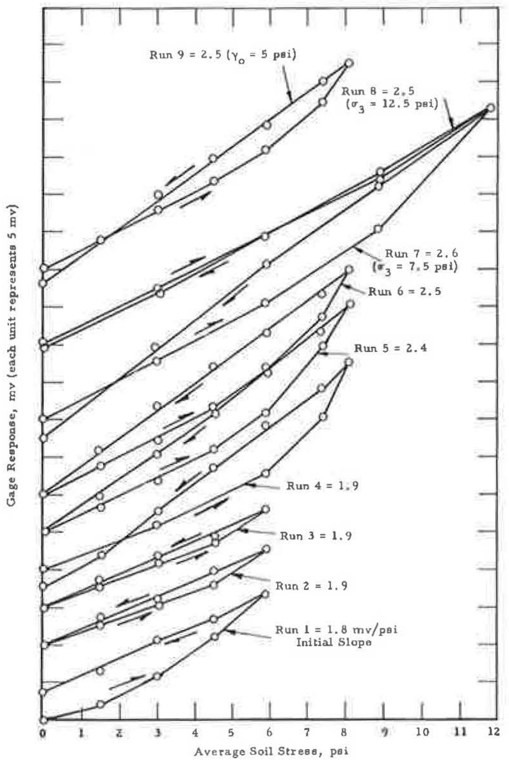

Figure 22. Triaxial calibration curves for gage S-25RT under repeated loading (γ_o = 100 pcf, σ_3 = 5 psi).

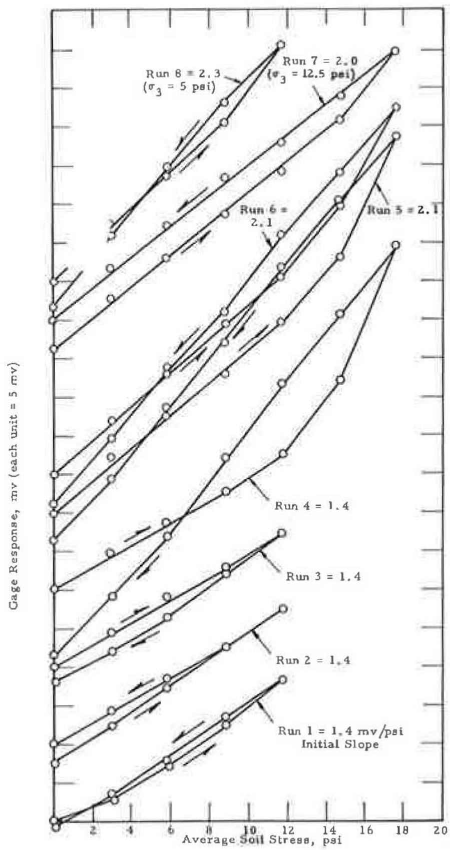

Figure 23. Triaxial calibration curves for gage S-25RT under repeated loading (γ_o = 110 pcf, σ_3 = 7.5 psi).

three-fourths the specimen strength for the existing confining pressure and density. For cycles 4 through 6 the applied stress was increased to failure. The confining pressure was held constant during the first six cycles. In cycles 7 through 9 the specimen was loaded to failure at three different confining pressures.

Results of three such tests are given in Figures 21, 22 and 23. In each example the gage response for the first three cycles was approximately linear and constant. In most cases, however, the slope of the first cycle was different from that of the next two. In general, if all variables, including the peak cycle stress, remained unchanged, the gage response remained unchanged for consecutive loading. As the applied stress was increased toward failure, the gage sensitivity increased, and on unloading and for successive identical cycles remained at this higher value. Increases in confining pressure between cycles reduced the sensitivity on the next cycle and decreases in the confining pressure increased the sensitivity. These changes in sensitivity are summarized in Figure 24.

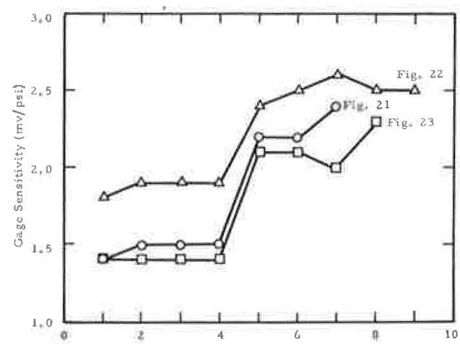

Figure 24. Change of gage sensitivity with repeated loading.

SUMMARY

The cylindrically-shaped N-gage could not satisfactorily measure stress in sand. The embedded gage sensitivity, the calibration factor, varied significantly with specimen confining pressure, sand density, stress level, and repeated loading. The gage was also quite sensitive to placement conditions. As a result the gage could not be calibrated so that its output could be used to reasonably predict the true stress in sand specimens.

The factors contributing to the gage's deficiencies were (a) the stress sensing element was not sufficiently larger than the grain size of the sand, (b) the thickness-diameter ratio was too large, and (c) the location of the electrical leads created placement difficulties. Some of these problems might be less significant in compacted clay specimens.

A disk gage was designed to eliminate the undesirable features of the N-gage. The sensitive area was increased, the thickness-diameter ratio was decreased and the leads were attached to the side of the gage to simplify placement. The sensitivity of the resulting gage was much less influenced by such factors as confining pressure, density, and placement, but these effects were still significant.

An evaluation of overregistration, i.e., ratio of gage sensitivity when embedded to gage sensitivity under uniform hydrostatic pressure, was made using the results from the hydrostatic pressure tests. This evaluation could only be qualitative because of the large variation in values for the embedded calibration. It was observed that for stress levels much lower than specimen failure there was an average of 30 percent overregistration for the embedded gage protected with an edge ring and a teflon covering. Without teflon, the overregistration was about 100 percent, and without either teflon or edge ring the overregistration was about 200 percent. The significant overregistration in the latter two cases was a characteristic of the gage construction because the piezoelectric ceramic was sensitive to friction across its face and pressure on the edges. It is apparent, then, that the largest observed overregistrations can be eliminated by suitable gage design.

The gage calibration curves were linear for stresses well below specimen failure, but the sensitivity increased as the failure stress was approached. The gage response was linear, in general, only when the soil stress-strain relationship was linear. Thus, a change in the soil stiffness had an appreciable effect on the gage response whether it was caused by a change in confining pressure, density or by the normal stress level. This was true even when the gage stiffness itself was very high compared with that of the soil. As a consequence of this effect, the gage calibration curves showed appreciable hysteresis for stresses close to specimen failure. Also as a result the gage performance was much better in confined than in constrained specimens. It is evident that although the gage stiffness was greater by a factor of 200 or more than the soil stiffness, a change in soil stiffness still affected the gage response.

Gage placement was another significant factor affecting gage response and accounting for a significant variation in the response even when all other conditions were constant. Variations due to placement of up to ± 50 percent were observed.

The static and dynamic sensitivities of the disk gages were identical, but showed a ± 10 percent variation when used in specimens having a wide range of confining pressures and densities.

The measurement of stress in soil with embedded gages remains an inherently difficult problem because of the complex nature of the soil stress-strain relationships on which the gage response depends. Gages utilizing the piezoelectric sensing element, however, potentially provide one of the most suitable methods for accomplishing this task. Such gages provide high sensitivity, are simple to construct, and can be made essentially rigid with respect to the soil. Their extremely short response time makes them especially suitable for dynamic measurements. For slowly varying or static stress applications, sensitivity to temperature changes and the instrumentation requirements for maintaining sufficient circuit time constant, present limitations on their use. The reproducibility of the very simple disk gages constructed for the study was not satisfactory for general application. However, the performance was much better than that of miniature diaphragm gages also investigated.

It was clear from this investigation that a more elaborate stress gage design is required to isolate the sensing element from the undesirable influences. The gages used in the study were clearly affected by a complex set of circumstances as a result of their particular design features. This makes generalization of the conclusions to other gage designs subject to some question. The study has indicated the problems involved in stress measurement with piezoelectric sensors. As a result of this information a more elaborate stress gage has been designed which appears to give better performance than the simple versions. Extensive evaluation of the new gage is currently under way.

ACKNOWLEDGMENTS

The research reported in this paper was carried out in the soil mechanics laboratory at the Illinois Institute of Technology under a grant from the National Science Foundation.

The writers wish to acknowledge the contributions of Richard Wetzel, graduate assistant, and Sven Alexander and Al Juskys, undergraduate assistants, in the conduct of the experiments.

REFERENCES

1. Goldbeck, A. T., and Smith, E. B., "An Apparatus for Determining Soil Pressures." Proc. ASTM, 16:2, 310-319 (1916).
2. Benkelman, A. C., and Lancaster, R. J., "Some Important Considerations in the Design and Use of Soil Pressure Cells." Public Roads, 21:12, 235 (Feb. 1941).
3. "Soil Pressure Cell Investigations, Interim Report." U. S. Army Engineer Waterways Exp. Sta. (1944).
4. Taylor, D. W., "Pressure Distribution Theories, Earth Pressure Cell Investigations and Pressure Distribution Data." U. S. Army Engineer Waterways Exp. Sta. (1947).
5. Monfore, G. E., U. S. Dept. of Interior, Bur. Reclamation, Res. and Geol. Div., Res. Lab. Rep. S. P. 26 (1950).
6. "Stress Distribution in a Homogeneous Soil." HRB Res. Rep. 12-F (Jan. 1951).
7. Whiffin, A. C., "The Pressures Generated in Soil by Compaction Equipment." Sym. on Dynamic Testing of Soils, ASTM Spec. Tech. Publ. 156, pp. 186-210 (1954).
8. "Investigations of Pressures and Deflections for Flexible Pavements." Rep. 4, "Homogeneous Sand Test Section." U. S. Army Engineer Waterways Exp. Sta., Tech. Memo. 3-323 (Dec. 1954).
9. Peattie, K. R., and Sparrow, R. W., "The Fundamental Action of Earth Pressure Cells." J. Mech. and Phys. of Solids, 2:141-155 (1954).
10. "Stresses under Moving Vehicles—Wheeled Vehicles in Lean and Fat Clay, 1957." U. S. Army Engineer Waterways Exp. Sta., Tech. Rep. 3-545 (May 1960).
11. Hamilton, J. J., "Earth Pressure Cells—Design, Calibration and Performance." Nat. Res. Council, Canada. Div. of Building Res., Tech. Paper 109 (Nov. 1960).
12. McMahon, T. F., and Yoder, E. J., "Design of a Pressure-Sensitive Cell and Model Studies of Pressures in a Flexible Pavement Subgrade." Proc. HRB, 39:650-683 (1960).
13. Durelli, A. J., and Riley, W. F., "Performance of Embedded Pressure Gages under Static and Dynamic Loadings." Sym. on Soil Dynamics, ASTM Spec. Tech. Publ. 305, pp. 20-37 (1961).
14. Bernhard, R. K., "Biaxial Stress Fields in Noncohesive Soils Subjected to Vibratory Loads." Sym. on Soil Dynamics, ASTM Spec. Tech. Publ. 305, p. 3 (1961).
15. Buck, G. F., "An Interim Report on the Cell Action Studies Connected with Research on Pressure Measurements in Sand." Proc. Midland Soil Mechanics and Foundation Eng. Soc., 4:95-105 (1961).
16. Trollope, D. H., and Lee, I. K., "The Measurement of Soil Pressures." Proc. 5th Internat. Conf. on Soil Mechanics and Foundation Eng., II: 493-499 (1961).

17. "Nuclear Geoplosics, Part Three—Test Sites and Instrumentation." Prepared for Defense Atomic Support Agency by Stanford Research Inst. (Feb. 1962).
18. Selig, E. T., "Detection of Transient Stresses and Strains in Soil." Proc. Sym. on Detection of Underground Objects, Mater. and Prop., Ft. Belvoir, Va., pp. 163-190 (March 1962).
19. Whiffin, A. C., and Morris, S. A. H., "Piezoelectric Gauge for Measuring Dynamic Stresses under Roads." Engineer, pp. 3-7 (April 1962).

Effect of Stress History on Strength of Cohesive Soils

W. H. PERLOFF, JR., and J. O. OSTERBERG
Respectively, Assistant Professor of Civil Engineering, Ohio State University, and Professor of Civil Engineering, Northwestern University

The purpose of this investigation was to determine, on a behavioral basis, the effect of stress history on the undrained triaxial compressive strength of cohesive soils.

A semitheoretical analysis of the variables affecting shear strength indicates that the undrained shear strength of a given cohesive soil tested at a constant strain rate is a function of the over-consolidation ratio. The effective stresses need not be considered because they are functions of the over-consolidation ratio.

Consolidated undrained triaxial compression tests with measured pore water pressures were performed on remolded clay specimens with varied stress histories. By use of curve-fitting procedures an explicit relationship was found between the strength parameter (the maximum stress difference divided by the consolidation pressure) and the over-consolidation ratio. A similar relationship was found between it and the Skempton pore pressure parameter at failure. Published data from several other investigators for undrained triaxial compression tests on remolded and sedimented soils and undrained extension tests on a remolded soil were found to fit the equations developed.

• SINCE COULOMB (4) presented his empirical equation for the shear strength of cohesive soils, research efforts have been directed toward expressing strength in an explicit form, including as many variables as possible. Coulomb's empirical equation was first modified to consider effective stresses (23) and later the effect of stress history (8, 10). The Coulomb-Hvorslev equation has gained general acceptance, and the validity of the Hvorslev parameters has been demonstrated by many investigators (3, 5). However, the applicability of these parameters in practice is limited by the difficulty of obtaining accurate pore pressure measurements in the zone of failure and by the number of tests that must be performed to evaluate them.

The use of effective stress analysis is not necessary if the shear strength can be expressed in terms of parameters to which effective stresses, or pore water pressures, are also related. In the following sections, such parameters are shown to exist.

Notation.—The symbols used herein are defined where they first appear and for convenience are listed alphabetically in the Appendix.

SEMITHEORETICAL ANALYSIS

Limitations

The analysis is subject to the following limitations and applies only to the following cases:

Paper sponsored by Committee on Stress Distribution in Earth Masses.

1. The analysis applies for an individual saturated clay soil. Different soils will give different values of the material constants.

2. The results are valid only for a single type of test, that is, a consolidated undrained triaxial compression test, where failure is induced by increasing the axial stress while the lateral stress is held constant. For other types of tests, where the boundary stress and strain conditions are changed, different results could be expected. These are likely, however, to be susceptible to this same type of analysis.

3. All specimens tested must have the same initial conditions, such as water content and structure.

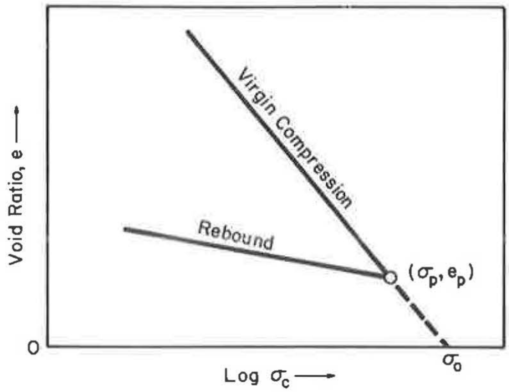

Figure 1. Idealized equilibrium void ratio-pressure relationship.

Assumptions

The assumptions required for the following discussion are:

1. The individual soil particles are incompressible under the magnitude of stresses imposed. This assumption appears reasonable because, according to Skempton and Bishop (21), the cubical compressibility of soil grains is approximately 1×10^{-8} sq cm per kg, whereas that for water is approximately 2.4×10^{-7} sq cm per kg. Thus, water is approximately 24 times more compressible than the soil grains.

2. The compressibility or bulk modulus of water is constant over the range of stresses encountered. Actually, the compressibility of water varies from approximately 2.4×10^{-7} to 2.3×10^{-7} sq cm per kg as the pressure increases from 1 to 10 kg per sq cm. Thus, the compressibility of water varies by about 4 percent over a range of pressures larger than is generally observed in a triaxial compression test on a clay soil.

3. Equilibrium is reached after consolidation under a constant isotropic pressure, and a plot of the equilibrium void ratio, e, vs the consolidation pressure, σ_c, will be a unique curve for a particular soil with given initial conditions. It has been suggested that this assumption will be valid for a great many clays (21, 22, 24). It is not known if soils exhibiting significant secondary compression under isotropic pressures will reach equilibrium. The relative amounts of secondary and primary consolidation in these soils will depend upon the pressure increment ratio, $\Delta P/P_0$ (22, 25). However, Wahls (25) has shown that, for one-dimensional consolidation tests on a soil exhibiting large secondary compression, a unique void ratio-pressure curve can be constructed for the primary consolidation portion and that this curve is independent of $\Delta P/P_0$.

4. The virgin compression curve and the rebound curves on a semilogarithmic plot of void ratio vs pressure can be represented by straight lines (Fig. 1). Furthermore, the slopes of all rebound curves will be the same. Taylor (22) and Terzaghi and Peck (24) suggest that these are reasonable approximations for the majority of cohesive soils. Experimental results from Taylor, Henkel (7), and this paper reinforce this view. Although there is some disagreement about the constancy of the rebound slopes, this assumption appears to be a valid approximation.

FACTORS AFFECTING SHEAR STRENGTH

The Coulomb-Hvorslev equation modified for the triaxial compression test (21) is

$$\frac{\sigma_1 - \sigma_3}{2} = c_e \frac{\cos \varphi_e'}{1 - \sin \varphi_e'} + \sigma_3' \frac{\sin \varphi_e'}{1 - \sin \varphi_e'} \tag{1}$$

in which $\sigma_1 - \sigma_3$ is the principal stress difference at failure, c_e is the effective cohesion, φ_e' is the effective angle of internal friction, and σ_3' is the effective minor principal stress at failure. Gibson (5) and Bjerrum (3) have demonstrated that, for limitations 1, 2, 3, and a constant strain rate, φ_e' is a soil constant, independent of the void ratio.

For a standard consolidated undrained triaxial compression test

$$\sigma_3 = \sigma_c; \; \sigma_3' = \sigma_c - u_f \tag{2}$$

in which u_f is the pore water pressure at failure. Substituting Eq. 2 into Eq. 1 and making use of the fact that at a constant strain rate, φ_e' is a material constant, Eq. 1 becomes

$$\sigma_1 - \sigma_3 = K_1 \, c_e + K_2 \, (\sigma_c - u_f) \tag{3}$$

in which $K_1 = 2 \cos \varphi_e'/(1 - \sin \varphi_e')$ and $K_2 = 2 \sin \varphi_e'/(1 - \sin \varphi_e')$ are soil constants for a constant rate of strain.

Terzaghi (23) and Hvorslev (8, 10) have shown that c_e is a function of the void ratio. Bjerrum and Hvorslev (10) further demonstrated that, for a constant strain rate, there is a linear relationship between the effective cohesion and the equivalent consolidation pressure:

$$c_e = K_3 \, \sigma_e' \tag{4}$$

in which K_3 is the slope of the linear relationship and σ_e' is the equivalent consolidation pressure. This pressure, corresponding to any e, is the consolidation pressure for a point on the virgin branch of the void ratio-pressure curve with the ordinate e.

Figure 1 shows that the void ratio at any point on the virgin branch of the idealized curve is (assumption 4)

$$e = -C_c \log \left(\frac{\sigma_e'}{\sigma_o}\right) \tag{5}$$

in which C_c is the absolute value of the slope of the virgin curve on a semilogarithmic plot ($C_c = |\Delta e/\Delta \log \sigma|$) and σ_o is the theoretical pressure required to produce a void ratio equal to zero. Rearranging Eq. 5 and solving for the logarithm of σ_e' gives

$$\log \sigma_e' = \log \sigma_o - \frac{1}{C_c} e \tag{6}$$

Substituting Eq. 6 into the logarithm of Eq. 4 yields

$$\log c_e = \log c_z - \frac{1}{C_c} e \tag{7}$$

in which $c_z = K_3 \, \sigma_o$ is the theoretical effective cohesion at zero void ratio. For limitations 1, 2, 3 and a constant strain rate, c_z will be a material constant (3, 10).

Referring again to the idealized void-ratio pressure relationships (Fig. 1), the void ratio on any portion of the curve can be expressed as (assumption 4)

$$e = -C_c \log \left(\frac{\sigma_p}{\sigma_o}\right) + C_e \log \left(\frac{\sigma_p}{\sigma_c}\right) \tag{8}$$

in which C_e is the absolute value of the slope of the rebound curve on a semilogarithmic plot ($C_e = |\Delta e/\Delta \log \sigma|$), σ_p is the maximum pressure to which the soil has been subjected, and σ_c is the present consolidation pressure producing e. For a normally consolidated specimen, $\sigma_c = \sigma_p$ and the term involving C_e becomes zero (Eq. 5). Eqs. 5 and 8 pertain to equilibrium conditions of the consolidation process and are not related to the rate at which the strength is tested.

Substituting Eq. 8 into Eq. 7 gives

$$\log c_e = \log c_z + \log \left(\frac{\sigma_p}{\sigma_o}\right) + K_4 \log \left(\frac{\sigma_p}{\sigma_c}\right) \tag{9}$$

in which $K_4 = -C_e/C_c$. As a consequence of assumptions 3 and 4, σ_o and K_4 are material constants. Eq. 9 can be rewritten

$$c_e = \frac{c_z}{\sigma_o} \sigma_p \left(\frac{\sigma_p}{\sigma_c}\right) K_4 \tag{10}$$

Substituting Eq. 10 into Eq. 3 leads to

$$\sigma_1 - \sigma_3 = K_5 \sigma_p \left(\frac{\sigma_p}{\sigma_c}\right) K_4 + K_2 (\sigma_c - u_f) \tag{11}$$

in which $K_5 = K_1 c_z/\sigma_o$, $K_1 = 2 \cos \varphi_e'/(1 - \sin \varphi_e')$, and $K_2 - 2 \sin \varphi_e'/(1 - \sin \varphi_e')$. K_5 and K_2 are material constants when strength is tested at a constant strain rate and $K_4 = -C_e/C_c$ is a material constant independent of the rate of strain.

Eq. 11 shows that, for a constant strain rate, the shearing resistance is a function of several variables, including the pore water pressure at failure, u_f, and, therefore, it is necessary to determine the variables affecting u_f.

Factors Affecting Pore Water Pressure

The development in the following section is a modification of that presented by Skempton and Bishop (21).

If a saturated clay specimen is not permitted to drain, a change in principal stresses of $\Delta\sigma_1$, $\Delta\sigma_2$, $\Delta\sigma_3$ will cause a change in the volume of the specimen. As a consequence of assumption 1, this will be due entirely to a change in volume of the pore spaces. Resistance will come from both phases of the soil-water system: the soil skeleton and the water in the pore spaces.

Resistance Due to Pore Water.—The volume compressibility or bulk modulus of the pore water is defined as

$$C_w = -\frac{1}{V_w} \frac{\Delta V_w}{\Delta u} \tag{12}$$

in which V_w is the initial volume and ΔV_w the change in volume of the water, and Δu is the change in pore water pressure (compression positive). Hence, the pore water pressure is related to the undrained volume change of the specimen in the following way (assumption 1):

$$\Delta V = -V \frac{e}{1 + e} C_w \Delta u \tag{13}$$

in which ΔV is the change of volume of the specimen, V is the total volume of the specimen, $Ve/(1 + e)$ is the volume of the pore water, and C_w is the compressibility of the pore water. The relationship between ΔV and Δu is independent of the stress history or the rate at which the strength is tested (assumptions 2 and 3).

Resistance Due to Soil Skeleton.—To consider the resistance offered to volume change by the soil skeleton, certain quantities involved in this process must be defined: the effective stresses, the compressibility of the soil skeleton, and the "A" factor.

For a triaxial compression test, the changes in the effective principal stresses induced in the soil skeleton are

$$\left.\begin{aligned} \Delta\sigma_1' &= \Delta\sigma_1 - \Delta u \\ \Delta\sigma_2' &= \Delta\sigma_3' - \Delta\sigma_3 - \Delta u \end{aligned}\right\} \tag{14}$$

in which $\Delta\sigma_1'$, $\Delta\sigma_2'$, and $\Delta\sigma_3'$ are, respectively, the changes in the effective major, intermediate, and minor principal stresses and $\Delta\sigma_1$ and $\Delta\sigma_3$ are, respectively, the changes in the total major and minor principal stresses.

The volume compressibility of the soil skeleton under an isotropic pressure is

$$C_s = -\frac{1}{V} \frac{\Delta V'}{\Delta\sigma_a'} \tag{15}$$

in which V is the volume of the specimen, $\Delta V'$ is the change in the volume of the specimen, and $\Delta\sigma_a'$ is the change in effective isotropic stress ($\Delta\sigma_a' = \Delta\sigma_1' = \Delta\sigma_3'$, compression positive).

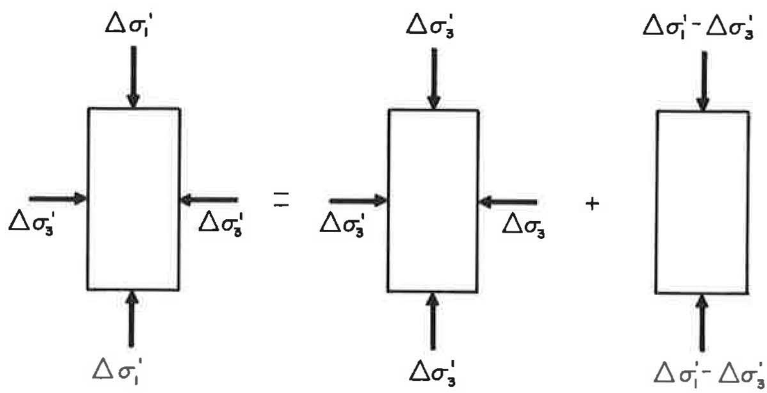

Figure 2. Resolution of general effective stress change into isotropic and uniaxial components.

When dealing with volume change characteristics of the soil skeleton in relation to nonisotropic stress conditions, the role of dilatancy must be considered. Dilatancy is defined as the property of volume change as a consequence of shear distortion. Purely elastic and plastic materials are generally considered to be nondilatant; that is, volume change occurs only as a result of isotropic stresses and shear stresses produce only distortion. These materials do exhibit some dilatancy, but it is a second order effect and can be neglected when strains are small (18).

Soils, in general, do exhibit significant dilatant properties (18, 21, 24). In attempting to express this effect explicity, it is most convenient to think in terms of a uniaxial stress change, rather than a change in the shear stresses (21), because it is the uniaxial stress change that is usually measured in the triaxial compression test.

A general change in effective stresses, $\Delta\sigma_1'$ and $\Delta\sigma_3'$ can be resolved into an isotropic stress change, $\Delta\sigma_3'$, and a uniaxial stress change, $\Delta\sigma_1' - \Delta\sigma_3'$ (Fig. 2). Application of $\Delta\sigma_1' - \Delta\sigma_3'$ will produce a volume change, $\Delta V''$, which can, in principle, be measured. The value of $\Delta V''$ may depend on the magnitude of $\Delta\sigma_1' - \Delta\sigma_3'$ or the manner in which it is applied. There will be some isotropic stress, $\Delta\sigma_m'$, which, if applied in place of $\Delta\sigma_1' - \Delta\sigma_3'$, will produce the same $\Delta V''$. These two stresses can be related in the following way:

$$\Delta\sigma_m' = A\,(\Delta\sigma_1' - \Delta\sigma_3') \qquad (16)$$

in which $\Delta\sigma_1' - \Delta\sigma_3'$ is a change in uniaxial stress, $\Delta\sigma_m'$ is the change in isotropic stress that will produce the same volume change as $\Delta\sigma_1' - \Delta\sigma_3'$, and A is a dimensionless parameter representing the relationship between the compressibility of the soil skeleton under a uniaxial stress change and the compressibility under an isotropic stress change. Because $\Delta V''$ may depend upon the value of $\Delta\sigma_1' - \Delta\sigma_3'$ and the manner in which it is applied, A may also depend upon these factors. For an elastic material where strains are small (nondilatant), $A = \frac{1}{3}$. For soils, A varies from approximately +1 to -1, depending upon soil type and certain other variables.

With these definitions it is now possible to formulate the relationship between the volume change, ΔV, and the changes in effective stresses, $\Delta\sigma_1' - \Delta\sigma_3'$. Referring to Eq. 15 and Figure 2, the relationship between the isotropic component of stress increase, $\Delta\sigma_3'$, and the volume change connected to it, $\Delta V'$, is

$$\Delta V' = V C_S \Delta\sigma_3' \qquad (17)$$

Referring to Eq. 16 and Figure 2, the relationship between the uniaxial component of stress increase, $\Delta\sigma_1' - \Delta\sigma_3'$, and the volume change connected to it, $\Delta V''$ is

$$\Delta V'' = -V C_S A\,(\Delta\sigma_1' - \Delta\sigma_3') \qquad (18)$$

The total change in volume, ΔV, will be the sum of that due to the change in isotropic pressure, $\Delta V'$, and that due to the change in uniaxial stress, $\Delta V''$ (assumption 1). Thus:

$$\Delta V = \Delta V' + \Delta V'' \tag{19}$$

or

$$\Delta V = -V\, C_s \left[\Delta\sigma_3' + A\,(\Delta\sigma_2' - \Delta\sigma_3') \right] \tag{20}$$

Combined resistance.—As a consequence of assumption 1, the change in volume of the pore water (Eq. 13) must be equal to the change in volume inclosed by the soil skeleton (Eq. 20) or

$$\frac{e}{1+e} C_w\, \Delta u = C_s \left[\Delta\sigma_3 - \Delta u + A\,(\Delta\sigma_1 - \Delta\sigma_3) \right] \tag{21}$$

in which $\Delta\sigma_3 - \Delta u = \Delta\sigma_3'$ and $\Delta\sigma_1 - \Delta\sigma_3' = \Delta\sigma_1' - \Delta\sigma_3'$ (Eq. 14). Rearranging Eq. 21 to solve for Δu yields

$$\Delta u = \frac{1}{1 + \frac{e}{1+e}\left(\frac{C_w}{C_s}\right)} \left[\Delta\sigma_3 + A\,(\Delta\sigma_1 - \Delta\sigma_3) \right] \tag{22}$$

There are few published data indicating values for C_s for different soils. However, Skempton and Bishop (21) have shown that C_s is of the same order of magnitude for isotropic as for one-dimensional consolidation, where it is usually denoted by m_v. An examination was made of results from Taylor (22) and unpublished data at Northwestern University for consolidation tests on many soils to determine a probable minimum value for C_s. The minimum value found was between 10 and 1 kg per sq cm pressure on the rebound curve of a Milwaukee clayey silt specimen from 70 ft below ground surface, where C_s and m_v are 0.001 sq cm per kg. Thus, the order of magnitude of C_w/C_s is likely less than $(2.4 \times 10^{-7})/10^{-3}$ or 2.4×10^{-4} (assumption 2). Therefore, to a very close approximation

$$\frac{1}{1 + \frac{e}{1+e}\left(\frac{C_w}{C_s}\right)} = 1 \tag{23}$$

and Eq. 22 becomes

$$\Delta u = \Delta\sigma_3 + A\,(\Delta\sigma_1 - \Delta\sigma_3) \tag{24}$$

Eqs. 22 and 24 are two forms of the well-known pore pressure equation for saturated soils (20).

Expressed in terms of the conditions at failure for a consolidated undrained triaxial compression test ($\Delta\sigma_3 = 0$), Eq. 24 becomes

$$u_f = A_f\,(\sigma_1 - \sigma_3) \tag{25}$$

in which A_f is A at failure. For a constant strain rate A_f varies from approximately +1 to -1, depending on the soil type and stress history (2, 21).

Elimination of Pore Pressure from Strength Determination

Substituting Eq. 25 into Eq. 11 gives

$$\sigma_1 - \sigma_3 = K_5\, \sigma_p \left(\frac{\sigma_p}{\sigma_c}\right) K_4 + K_2 \left[\sigma_c - A_f\,(\sigma_1 - \sigma_3) \right] \tag{26}$$

Rearranging Eq. 26 and solving for $\sigma_1 - \sigma_3$ yields

$$\sigma_1 - \sigma_3 = \frac{K_5}{1 + K_2 A_f}\, \sigma_p \left(\frac{\sigma_p}{\sigma_c}\right) K_4 + K_2\, \sigma_c \tag{27}$$

Expressing a relationship such as Eq. 27 in dimensionless form, considering each dimensionless ratio as a single variable, permits consideration of a fewer number of variables and simplifies analysis of experimental results. Such a form is obtained by dividing Eq. 27 by σ_c.

$$\frac{\sigma_1 - \sigma_3}{\sigma_c} = \frac{K_5}{1 + K_2 A_f}\left(\frac{\sigma_p}{\sigma_c}\right)(1 + K_4) + K_2 \tag{28}$$

in which $(\sigma_1 - \sigma_3)/\sigma_c$ is called the shear strength parameter, $K_2 = 2 \sin \varphi_e'/(1 - \sin \varphi_e')$, $K_4 = -C_e/C_c$, σ_p/σ_c is the over-consolidation ratio, and $K_5 = 2\, c_z \cos \varphi_e'/\sigma_o (1 - \sin \varphi_e')$. K_2 and K_5 are material constants when the strength is tested at a constant strain rate, and K_4 is a material constant independent of strain rate.

Eq. 28 shows that, for a given soil tested at a particular strain rate, and for the other limitations and assumptions stated above

$$\frac{\sigma_1 - \sigma_3}{\sigma_c} = F_1\left(\frac{\sigma_p}{\sigma_c}, A_f\right) \tag{29}$$

There is no presently available way to determine theoretical relationships for A_f in terms of the variables affecting it because of the definition of A_f. The A factor is, in part, a function of the dilatancy of the soil skeleton. This property, related to the structural arrangement of the clay particles, is not yet well understood, because quantitative description of the changes in structural arrangement in response to stress changes is still lacking. Attempts have been made in this direction (9, 10, 14, 16, 17), but the available information is still quite general. However, it has been shown experimentally (2, 7, 16) that, for Limitations 1, 2, 3 and a constant strain rate, A_f depends only on σ_p/σ_c. Thus, from these investigations, for a constant strain rate

$$A_f = F_2\left(\frac{\sigma_p}{\sigma_c}\right) \tag{30}$$

Substituting Eq. 30 into Eq. 29 gives

$$\frac{\sigma_1 - \sigma_3}{\sigma_c} = F_3\left(\frac{\sigma_p}{\sigma_c}\right) \tag{31}$$

Eq. 31 shows that for the assumptions and limitations stated above, and a constant strain rate, the shear strength parameter for a cohesive soil is a function of the over-consolidation ratio. The strength can be related to these variables without reference to the effective stresses because, as shown by Eq. 30, A_f and, therefore, the effective stresses, are themselves functions of these same variables.

In the following sections experimental results will be used to determine explicit forms for the functional relationships given in Eqs. 30 and 31.

EXPERIMENTAL ANALYSIS

Laboratory experiments were performed to determine the interrelationship between strength and stress history. These experiments consisted of consolidated undrained triaxial compression tests, at several rates of strain, on a saturated clay soil that had been subjected to various stress histories.

Description of Soil Used

The soil used in this investigation has as its chief constituent the clay mineral illite. It is found in the Goose Lake area of Grundy County, Ill., and is sold under the trade name of "Grundite" by the Illinois Clay Products Company. The origin and properties of this soil have been discussed in some detail (6). The clay is upper Pennsylvanian in age and has been exposed, at the site where it is mined, by erosion of the sediments immediately overlying it. Grim and Bradley have said, "The source of this clay, like that of the other underclays of the Pennsylvanian, is believed to be somewhat weathered surface material from the area enclosing the region of accumulation (6). The classification properties are given in Table 1.

TABLE 1

CLASSIFICATION PROPERTIES OF GRUNDITE

w_L (%)	w_P (%)	I_p (%)	G	Clay Fraction (%) (<2 μ)
54.5	26.0	28.5	2.74	85

TABLE 2

SPECIMEN DIMENSIONS AND PROPERTIES

Length (cm)	Diameter (cm)	Initial Wt. (gm)	w (%)	Void Ratio
7.60	3.54	134.29 ± 0.57	43.2 ± 0.4	1.183 ± 0.012

Specimen Preparation

The Grundite was received from the Illinois Clay Products Company in dry, powdered form. It was mixed, as received, with distilled water to a water content of approximately 43 percent, which was as close to the liquid limit as the soil could be molded. The moist clay was thoroughly mixed by hand and by a mechanical mixer. It was then passed through a "Vac-Aire" sample extruder several times to insure uniform moisture distribution. This equipment, designed for the extrusion of clay specimens, has been described by Matlock et al. (13). On the third time through the extruder, specimens approximately 4 in. long were cut and immediately covered with six coats of a flexible wax. Waxed specimens were placed on a shelf inside a sealed jar with water in the bottom to maintain 100 percent humidity. The jar was then placed in a humid room. The specimens were cured for approximately 6 wk. During that time, at periodic intervals, specimens were removed and tested in unconfined compression to determine if thixotropic hardening was taking place. No evidence of this was found, because the unconfined strengths of all the specimens tested during the 6-wk period after extrusion were the same within ± 1.5 percent.

Testing Procedure

When the soil was ready for triaxial compression testing, each specimen was stripped of its wax cover, which was sufficiently strong to be easily peeled from the specimen. The specimen was then placed in a miter box with an inside diameter exactly equal to that of the specimen. The specimen was trimmed with a wire saw to the proper length and immediately weighed. Specimen dimensions and properties are given in Table 2. After weighing, the specimen was surrounded by drainage strips (2, pp. 81-82), to facilitate consolidation. The specimen was placed inside a 0.005-in. latex membrane which was then painted with Dow-Corning DC 200 silicone fluid to prevent passage of moisture from the soil or glycerine from the chamber into the soil. A second membrane was placed around the first one. The specimen was then mounted in the triaxial compression chamber on a saturated porous stone connected to a pipette open to the atmosphere outside the chamber. The membranes were sealed to the pedestal and loading cap with a layer of Dow-Corning silicone grease and held in place by rubber bands.

The triaxial chamber was filled with glycerine, and the desired consolidation pressure was applied to the glycerine by air pressure. Readings of the water level in the pipette indicated the degree to which consolidation had progressed. One hundred percent consolidation was found to occur in approximately 24 hr when filter strips were

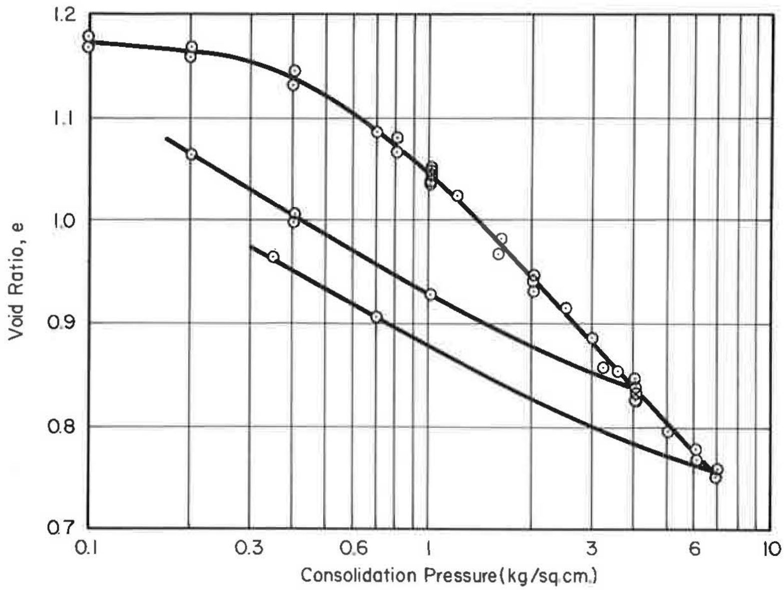

Figure 3. Triaxial consolidation results for Grundite.

used. Wahls (25) showed the importance of the pressure increment ratio, $\Delta P/P_0$, in one-dimensional consolidation tests on a soil exhibiting large secondary compression. However, Grundite exhibited no such secondary compression in triaxial consolidation and, therefore, various pressure increment ratios were chosen by convenience.

A specific over-consolidation ratio, σ_p/σ_c, was obtained by consolidating a specimen under a pressure, σ_p, higher than the preconsolidation pressure induced by the extrusion process (approximately 0.6 kg per sq cm) and then rebounding the specimen under a pressure, σ_c, which gave the desired σ_p/σ_c. Results of these consolidation tests (Fig. 3) represent tests on 23 specimens. Some of the tests consisted of a single load increment, some of several increments. There were too many tests to indicate each with a separate symbol, and to avoid confusion, only two of the rebound curves are shown.

When consolidation was completed, the drainage line was closed, pressure was removed from the triaxial chamber, and the glycerine was drained. The specimen was then taken out of the chamber and the rubber membranes and filter strips were removed. The specimen was immediately recovered by either one or two membranes with a layer of silicone fluid between them, depending on the duration of test to be performed. A solid base and cap were placed on the ends of the specimen. A small hole, approximately $\frac{1}{4}$ in. in diameter, was cut in the membrane at mid-height of the specimen and a pore pressure measuring needle (Fig. 4) filled with distilled water was inserted into the specimen. The needle consisted of a brass tube, $\frac{5}{64}$ in. in diameter and about $1\frac{1}{4}$ in. long, with a wall thickness of $\frac{1}{64}$ in. Two holes, approximately $\frac{3}{8}$ in. in length, were filed in the tube wall in the positions shown in Figure 4. The inside of the tube was filled with a rolled 200 mesh screen to prevent clay from entering the holes. The tube was inserted into $\frac{1}{8}$-in. saran tubing and sealed to the tubing with Chrysler epoxy resin. The tubing was connected to a water-filled copper line leading to a null-balance pore pressure measuring device. This particular device was designed at the Norwegian Geotechnical Institute and constructed by Geonor A/S, Oslo, Norway. The design and operation of this device are described in detail by Andresen et al. (1).

After insertion of the pore pressure needle, the specimen was mounted on the testing frame and the hole in the membrane around the needle was sealed with a liquid rubber compound. The triaxial chamber was placed over the specimen, glycerine was introduced to fill the chamber, and the desired chamber pressure was applied. The solid

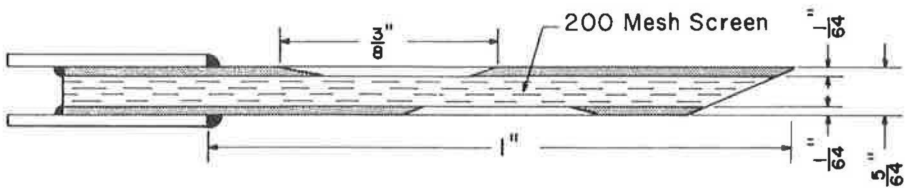

Figure 4. Sketch of pore pressure needle.

lucite cap and base of the specimen permitted no drainage. In general, a chamber pressure of 2 kg per sq cm higher than the consolidation pressure for the specimen was used, to induce a back pressure in the pore water and insure that there were no air bubbles in the soil or measuring system. When pore pressure equilibrium had been reached, the test was begun.

The load on the specimen was measured with a steel proving ring. The pore water pressure was measured with a Bourdon gage connected to the pore pressure apparatus. Deflections of the specimen were measured with a standard dial gage with 0.001-in. divisions.

Four series of tests were performed, each at a different rate of strain. Only one of these series is discussed in this paper. The strain rate for this series was 100 percent per hr. Six specimens each at a different over-consolidation ratio were tested at this strain rate.

The manner in which a specimen failed appeared to depend on the chamber pressure. Under low chamber pressures, 3 kg per sq cm and less, failure occurred along a well-defined shear plane. Little or no bulging was apparent. Under high chamber pressures, 5 kg per sq cm and more, specimens failed by bulging. There was no shear plane evident, although the load on the specimen decreased after reaching a maximum. Between 3 and 5 kg per sq cm chamber pressure, failure appeared to be a combination of both types, although the shear plane was not always very distinct. Sometimes, in this intermediate chamber pressure zone, there were many shear planes apparent and all were parallel. When a shear plane occurred, it was generally parallel to the pore pressure needle and tangent to it. This was very likely because the pore pressure needle created stress concentrations in the specimen. All shear planes were inclined at an angle of approximately 52° to the horizontal. The test results did not appear to be influenced by the mode of failure.

RESULTS

Figure 5 shows the results of the series of tests performed at a strain rate of 100 percent per hr. This figure shows the ratio of the principal stress difference at failure to the consolidation pressure immediately prior to testing $(\sigma_1 - \sigma_3)/\sigma_c$ and the pore pressure parameter at failure $A_f = u_f/(\sigma_1 - \sigma_3)$ as a function of the over-consolidation ratio σ_p/σ_c. In the following discussion, the quantities $(\sigma_1 - \sigma_3)/\sigma_c$ and A_f will always refer to the conditions at failure.

The experimental curves shown in Figure 5 have the appearance of power functions of the form

$$\frac{\sigma_1 - \sigma_3}{\sigma_c} = r\left(\frac{\sigma_p}{\sigma_c}\right)^{s} + t \tag{32a}$$

and

$$A_f = m\left(\frac{\sigma_p}{\sigma_c}\right)^{-n} + p \tag{32b}$$

where r, s, t and m, n, p are constants for a constant strain rate.

To determine if the experimental data can actually be represented by such equations, curve fitting techniques must be applied.

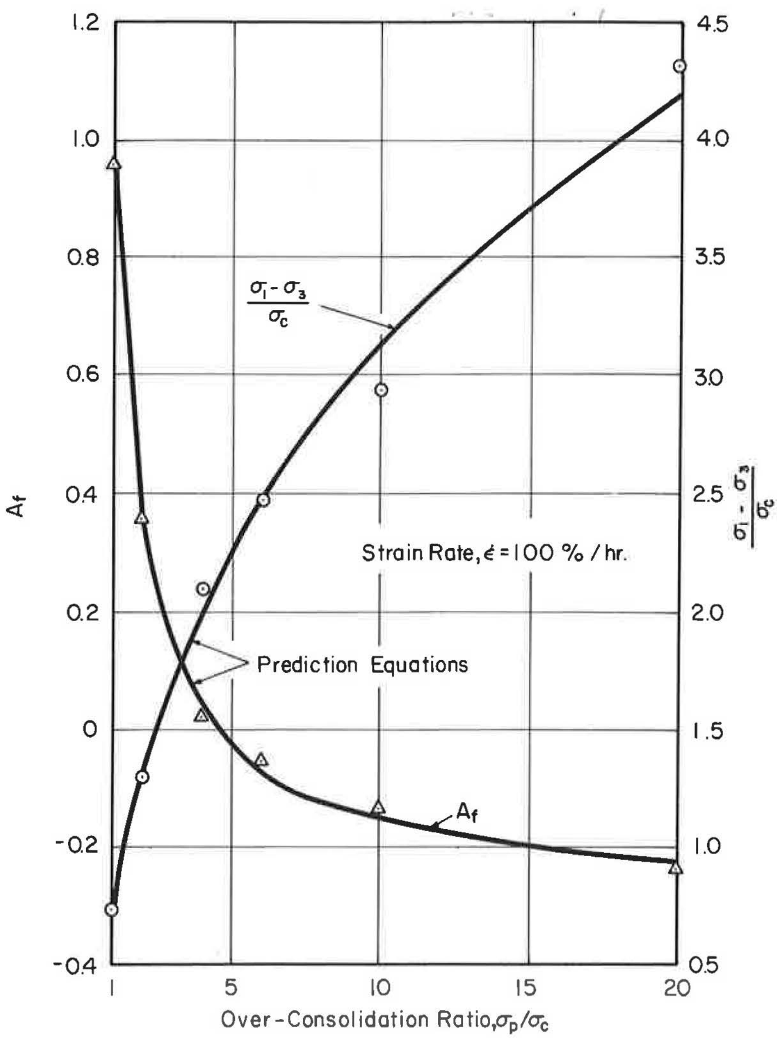

Figure 5. Effect of over-consolidation ratio on failure conditions for Grundite.

Technique and Results of Curve Fitting

If experimental curves are of the form of Eqs. 32a and 32b, then

$$\log\left(\frac{\sigma_1 - \sigma_3}{\sigma_c} - t\right) = \log r + s \log\left(\frac{\sigma_p}{\sigma_c}\right) \tag{33a}$$

and

$$\log\left(A_f - p\right) = \log m - n \log\left(\frac{\sigma_p}{\sigma_c}\right) \tag{33b}$$

Eqs. 33a and 33b are equations of straight lines. Thus, if the experimental data can be described by Eqs. 32a and 32b, they must appear as straight lines when plotted in the form of Eqs. 33a and 33b. Eqs. 33a and 33b are, therefore, test plots of the validity of representing the experimental results by Eqs. 32a and 32b.

However, in order to make the test plots, the constants t and p must be evaluated. Johnson (11, p. 117) suggests a method for calculating mathematically the value of the

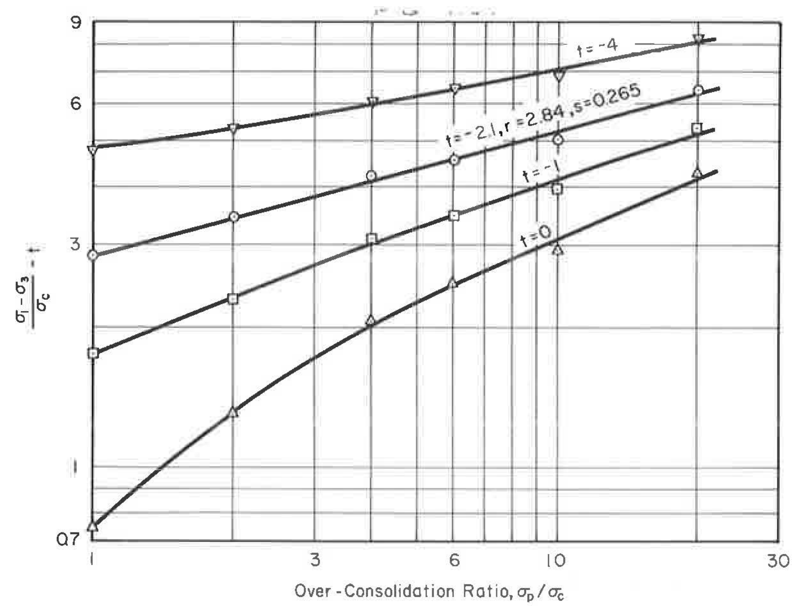

Figure 6. Test plots of strength equation for Grundite clay, ϵ = 100 percent per hr.

required constants. But because his method involves the use of several actual data points and a certain amount of scatter in the data is common, several trials are generally necessary before the correct values of t and p are found. Therefore, straight trial-and-error procedure is much simpler. Figure 6 illustrates this procedure for the test plot of Eq. 33a with the results of tests at a strain rate of 100 percent per hr. The lowest curve in this figure is a plot of the raw data, t = 0. Because the points do not lie on a straight line on the logarithmic plot, t = 0 will not yield an equation to fit the experimental data. Above this curve, the data are plotted for t = -1.00. This curve is not a straight line, but it is distinctly flatter than the lower curve. The uppermost curve, with t = -4.00, has reversed its curvature, indicating that the absolute value of t is too large. The set of points below this, where t = -2.10, adheres to a straight line. This indicates that the experimental data can be fairly represented by Eq. 33a and, therefore, by Eq. 32a, for t = -2.10. The best straight line through the experimental points on the logarithmic plot was determined by the method of least squares.

The constants r and s are found by substitution in Eq. 32a. When σ_p/σ_c = 1, log (σ_p/σ_c) = 0 and r = $(\sigma_1 - \sigma_3)/\sigma_c$ - t. The constant s is the slope of the straight line on the logarithmic plot. Thus, s is equal to the logarithm of the ratio between two values of $(\sigma_1 - \sigma_3)/\sigma_c$ - t, which are one cycle apart. Application of these procedures to the straight line curve in Figure 6 for t = -2.10 yields r = 2.84 and s = 0.265.

Figure 7 is a test plot of Eq. 32b for the pore pressure parameter data for the test series discussed previously. Again, it can be seen that the points lie along straight lines, indicating that the experimental data can be represented by Eq. 32b. The numerical values of the constants m, n, p are shown on the test plot. The close fit of Eqs. 32a and 32b to the experimental data can also be seen in Figure 5. The "experimental curves" for $(\sigma_1 - \sigma_3)/\sigma_c$ and A_f vs σ_p/σ_c are, in fact, plots of Eqs. 32a and 32b with the appropriate constants found from Figures 6 and 7.

RESULTS FROM OTHER INVESTIGATIONS

Jurgenson (12) and Rutledge (19) investigated the shear strength of cohesive soils in terms of external variables for the simplest case, that is, normally consolidated soil, in which the strain rate was held constant. They both found that $(\sigma_1 - \sigma_3)/\sigma_c$

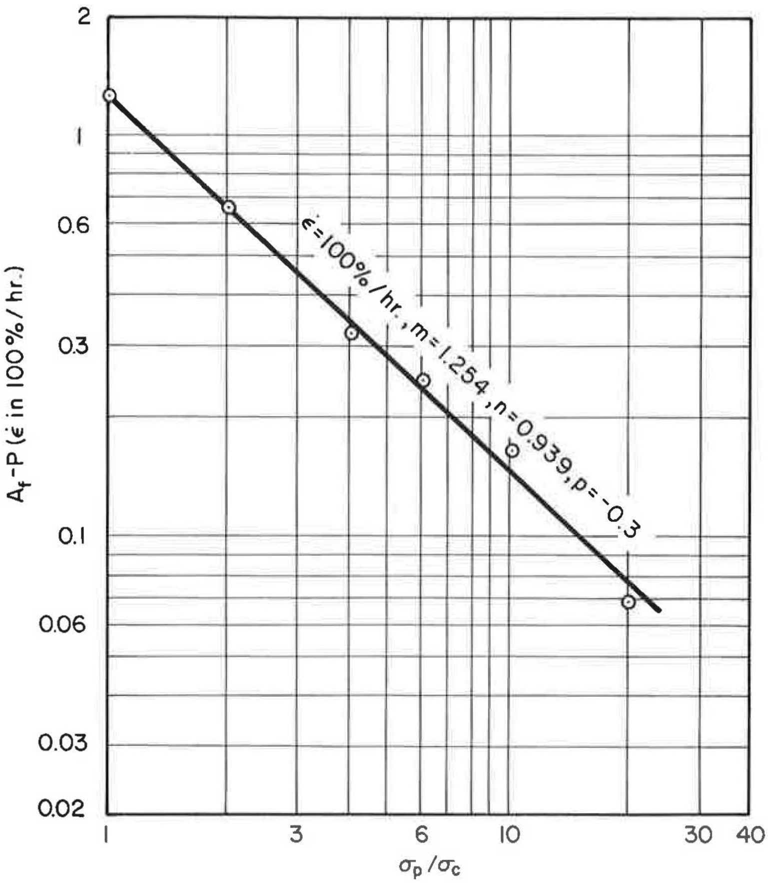

Figure 7. Test plot of pore pressure parameter equation for Grundite.

equaled a constant. Their work is verified by Eq. 32a which, for a normally consolidated soil ($\sigma_p/\sigma_c = 1$) reduces to

$$\frac{\sigma_1 - \sigma_3}{\sigma_c} r + t = \text{constant} \tag{34}$$

They were able to circumvent the use of effective stresses because Eq. 32b and, therefore, the pore pressure, exhibits a similar relationship:

$$A_f = m + p = \text{constant} \tag{35}$$

for $\sigma_p/\sigma_c = 1$.

Henkel (7) and Parry (16) performed series of consolidated drained and undrained triaxial compression and extension tests at a constant strain rate on remolded Weald clay, and consolidated drained and undrained triaxial compression tests on remolded London clay varying the stress history. The tests discussed in the following were consolidated undrained triaxial compression tests in which failure was induced by increasing the axial stress at a constant rate of strain as the lateral stress was held constant. Pore water pressures were measured at the base of the specimens and filter strips were used on the sides of the specimen to reduce pore pressure gradients. The classification properties of the two clays are given in Table 3 (16).

The results of these tests are replotted to arithmetic scales in Figures 8 and 9. The resultant experimental curves, again, have the general shape of power functions of the form of Eqs. 32a and 32b. The data were tested by the method previously outlined to

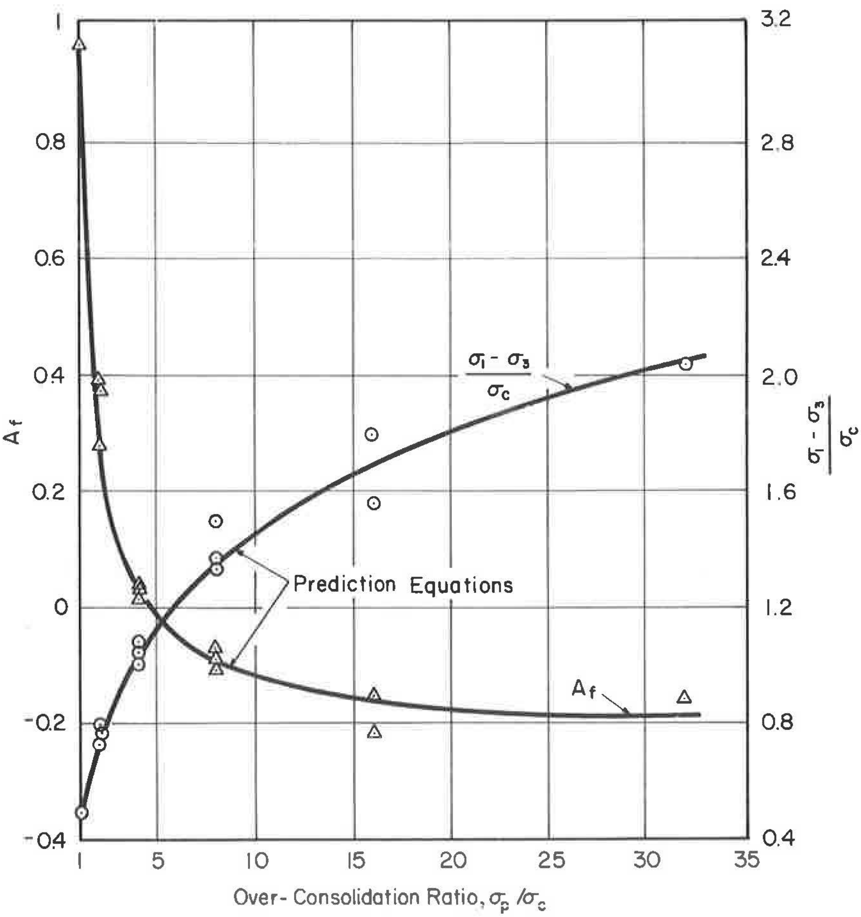

Figure 8. Effect of over-consolidation ratio on failure conditions for London clay (7).

determine if they could be represented by these equations. The test plots are shown in Figures 10 and 11. It is evident from these figures that Eqs. 32a and 32b fairly represent the experimental results. This is further verified in Figures 8 and 9, where the "experimental curves" are, in fact, plots of these equations with the appropriate constants determined in Figures 10 and 11.

TABLE 3

CLASSIFICATION PROPERTIES OF WEALD CLAY AND LONDON CLAY

Type	w_L (%)	w_P (%)	I_p (%)	Clay Fraction (%)
Weald Clay	43	18	25	40
London Clay	78	26	52	50

Olson (15) performed consolidated undrained triaxial compression tests on sedimented and remolded specimens of a calcium illite, varying the stress history. Classification properties of the calcium illite are given in Table 4. These data have been used to plot Figures 12 and 13, which show the effect of over-consolidation on $(\sigma_1 - \sigma_3)/\sigma_c$ and A_f for both sedimented and remolded specimens of calcium illite. The test plots of Eqs. 33a and 33b are shown in Figures 14 and 15. Again, the test plots indicate the validity of Eqs. 32a and 32b for this soil. The "experimental curves" in Figures 12 and 13 are, as before, plots of Eqs. 32a and 32b with the

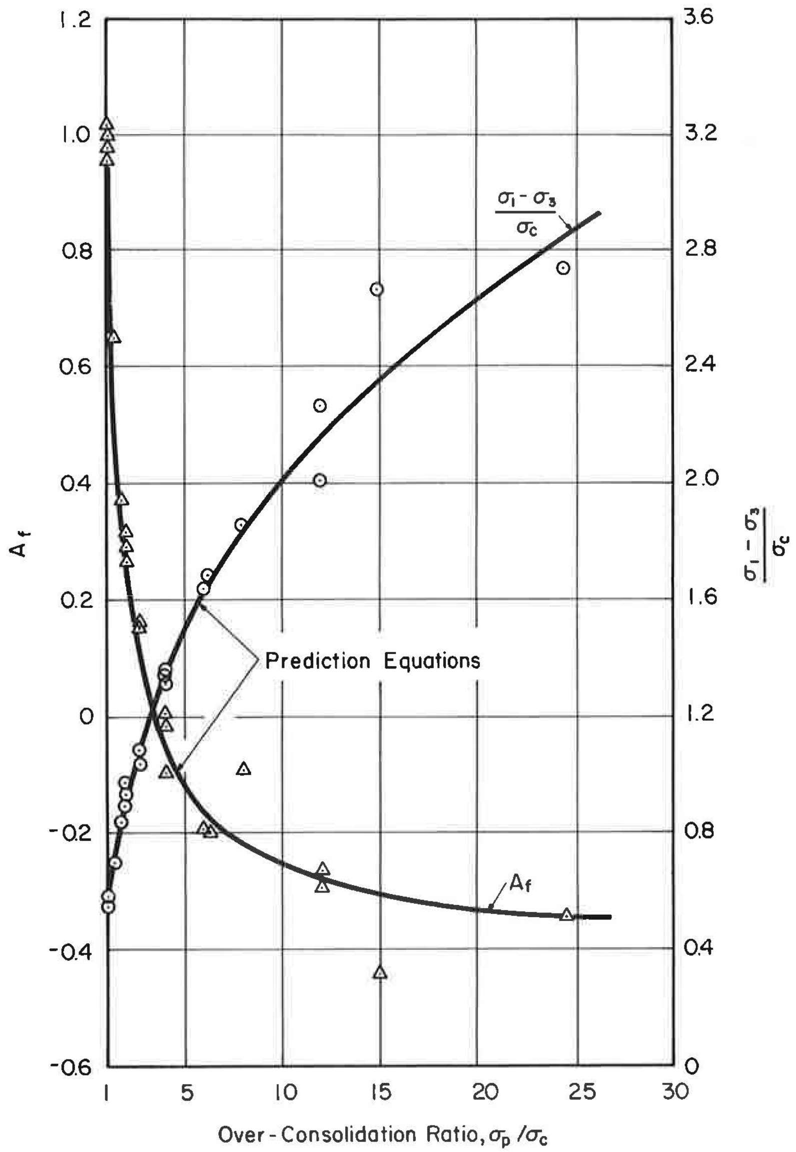

Figure 9. Effect of over-consolidation ratio on failure conditions for Weald clay (16).

constants determined from Figures 14 and 15.

The results of the consolidated undrained extension tests from Parry (16) can also be described by Eqs. 32a and 32b. These results are shown in Figure 16, with the test plots shown in Figures 17 and 18.

TABLE 4

CLASSIFICATION PROPERTIES OF CALCIUM ILLITE

w_L (%)	w_P (%)	I_p (%)	Clay Fraction (%)
85	37	48	100

DISCUSSION OF RESULTS

The relationship of the "constants" previously discussed to the physical properties of soils is not immediately obvious. Although Eq. 32a appears to be of the same form

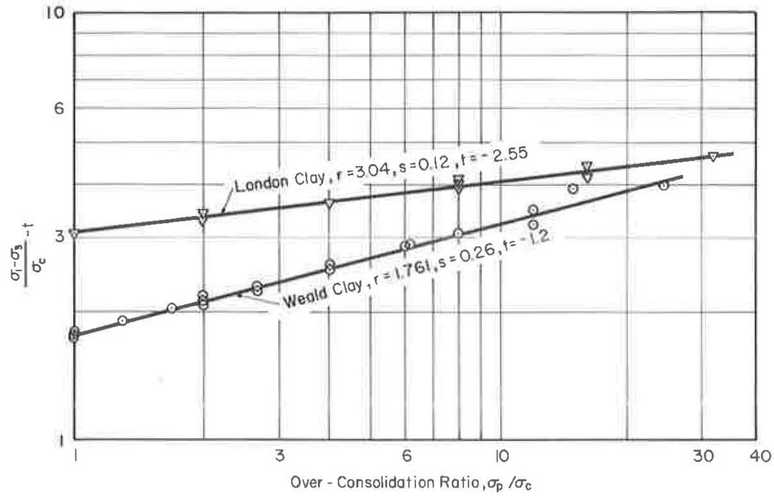

Figure 10. Test plots of strength equation for Weald clay (16) and London clay (7).

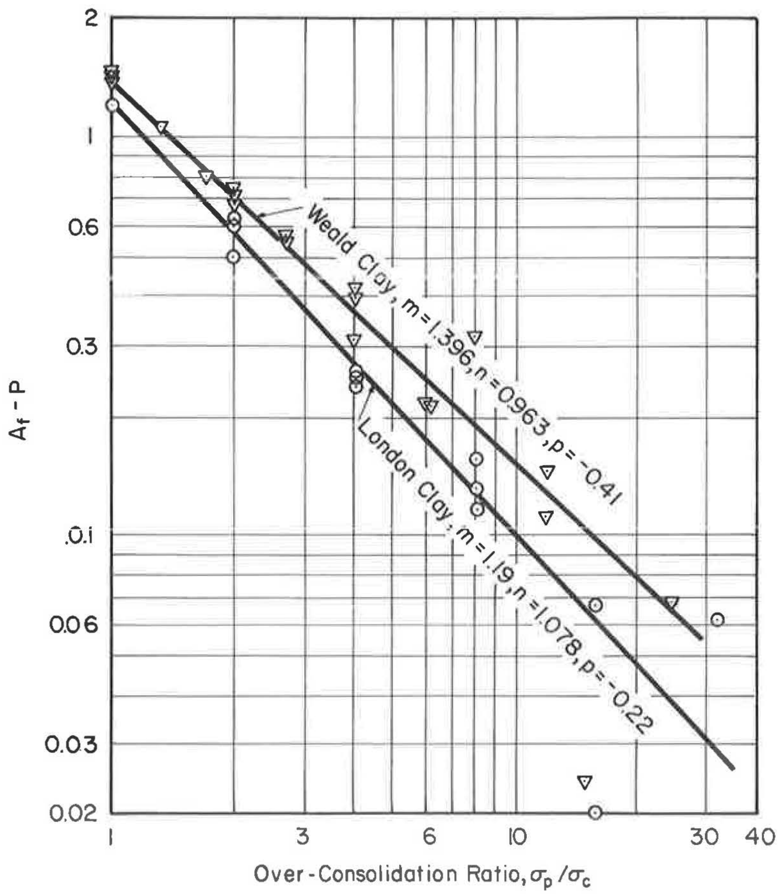

Figure 11. Test plots of pore pressure parameter equation for Weald clay (16) and London clay (7).

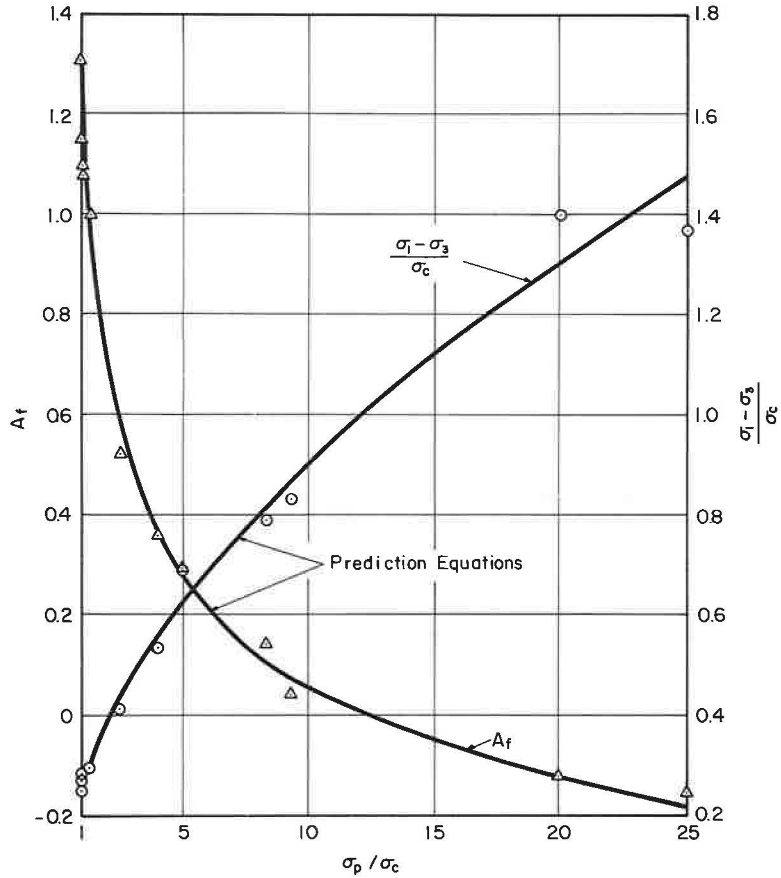

Figure 12. Effect of over-consolidation ratio on failure conditions for sedimented calcium illite (15).

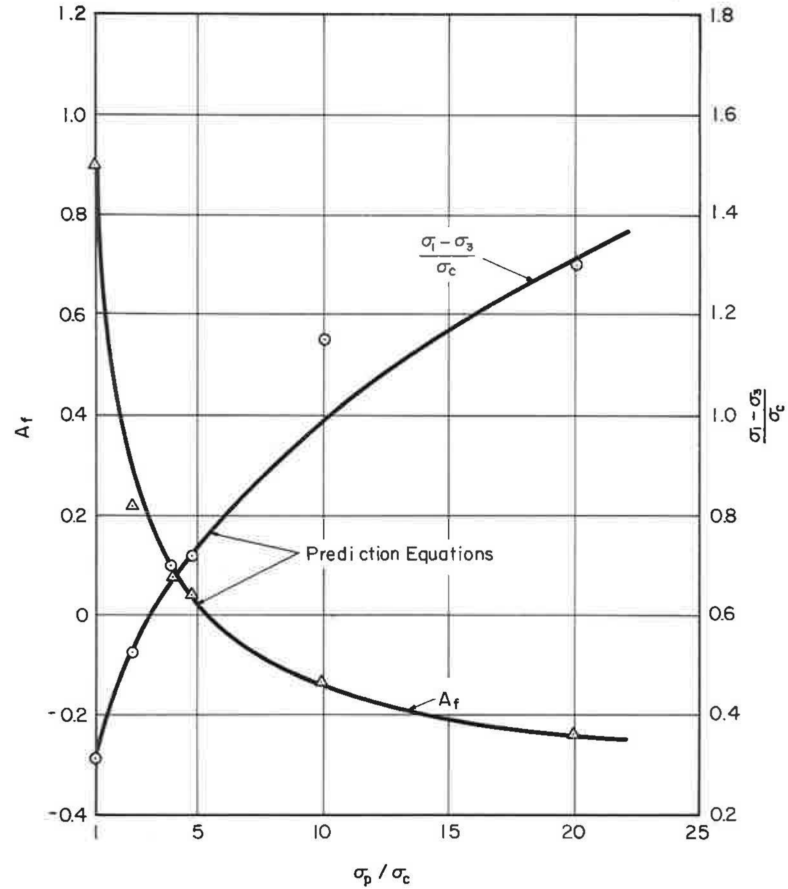

Figure 13. Effect of over-consolidation ratio on failure conditions for remolded calcium illite (15).

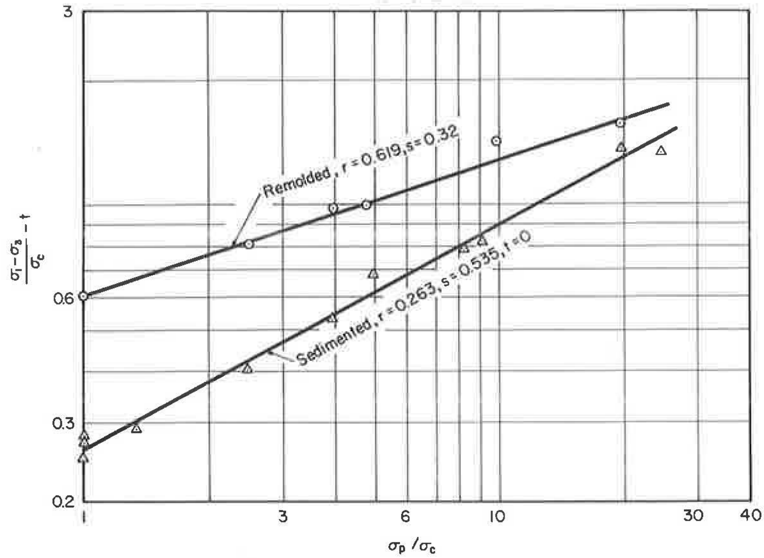

Figure 14. Test plot of strength equation for calcium illite (15).

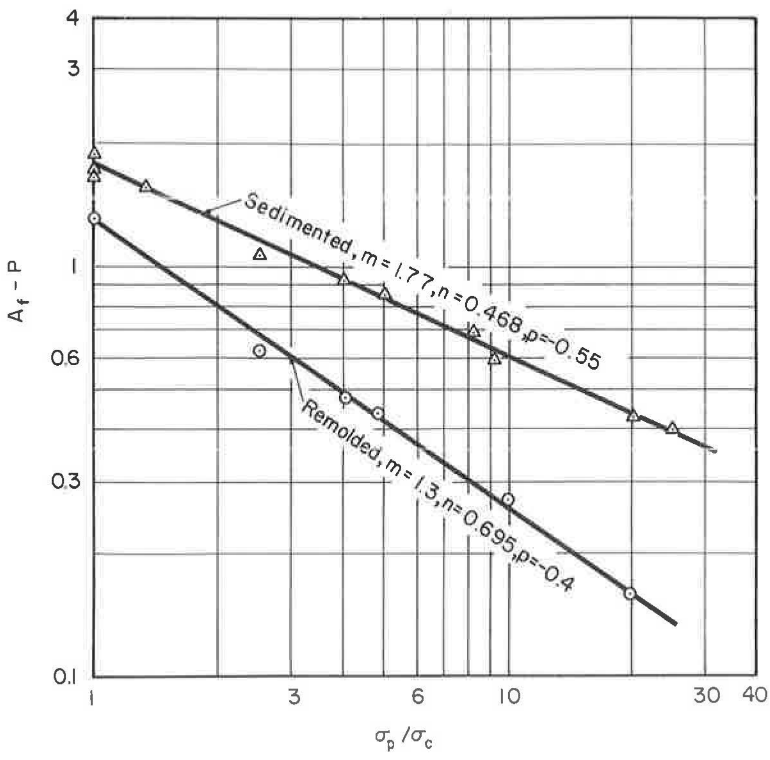

Figure 15. Test plots of pore pressure parameter equation for calcium illite (15).

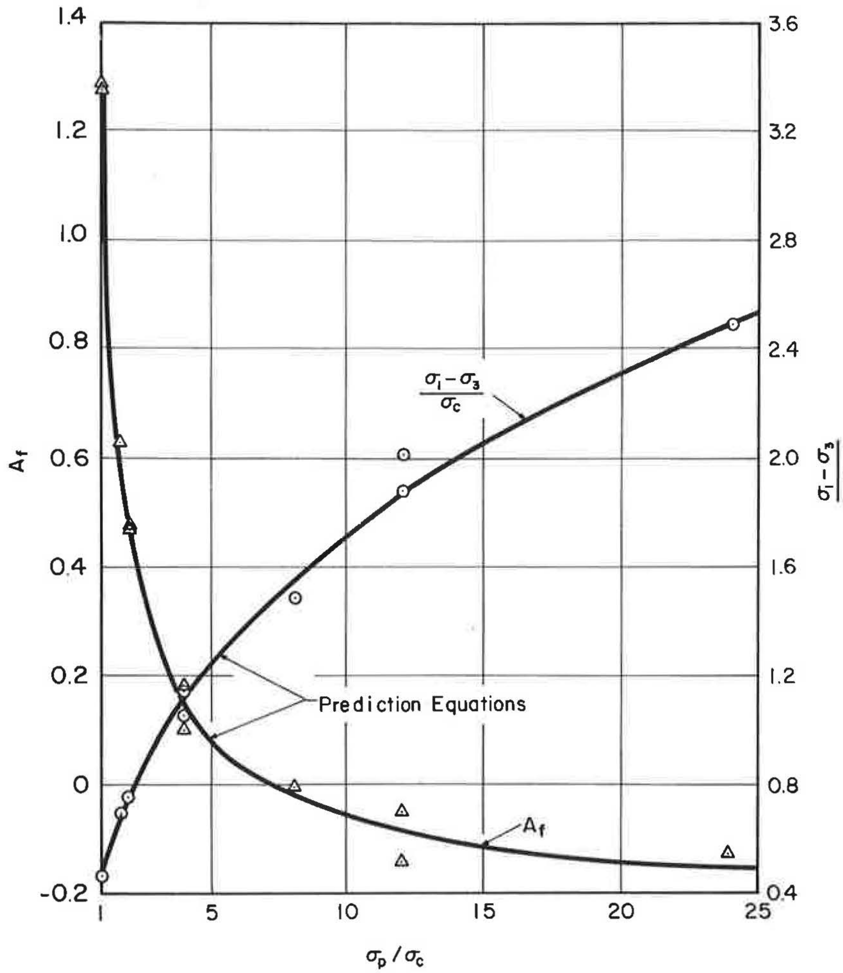

Figure 16. Effect of over-consolidation ratio on failure conditions for extension tests on Weald clay (16).

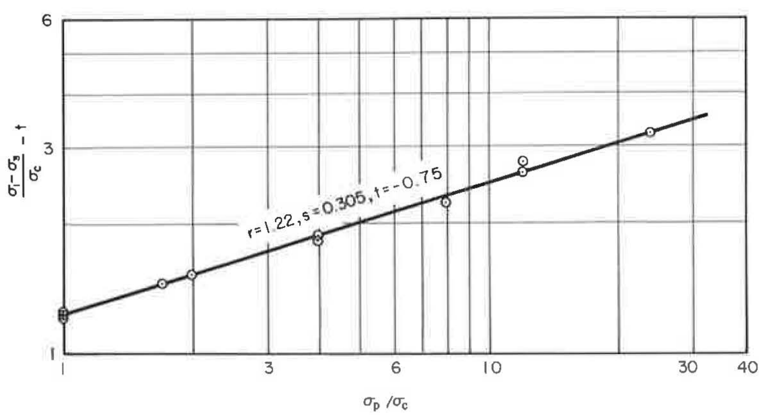

Figure 17. Test plot of strength equation for extension tests on Weald clay (16).

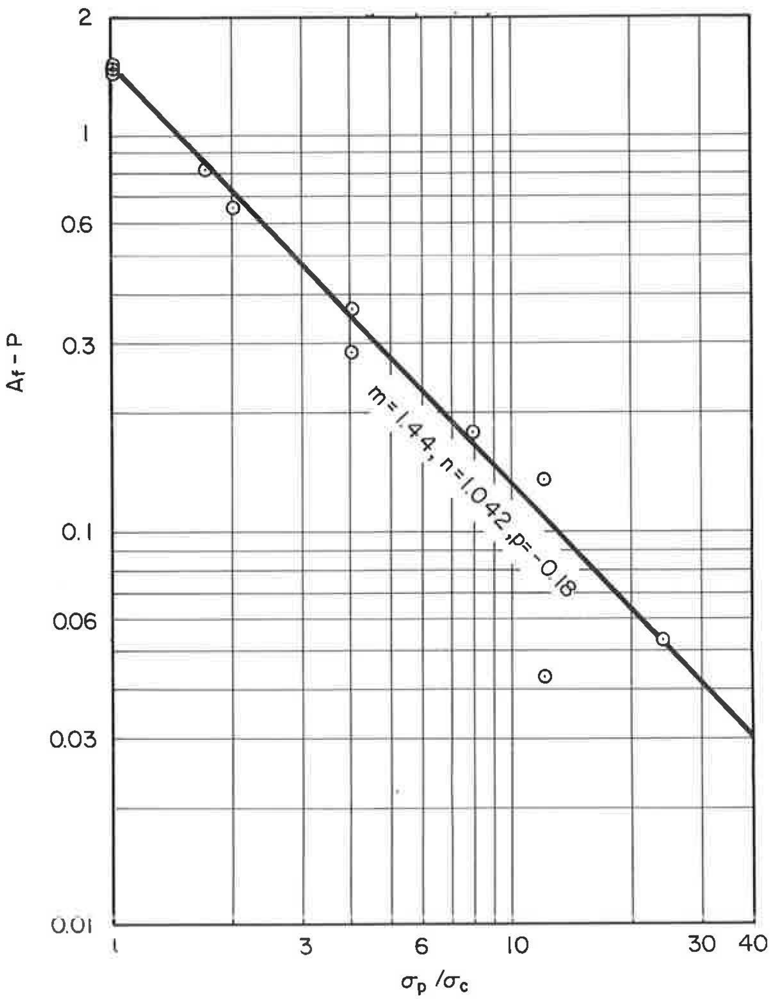

Figure 18. Test plot of pore pressure parameter equation for extension tests on Weald clay (16).

as Eq. 28, this similarity is misleading. Because Eq. 28 contains A_f in the denominator of the first term, A_f may influence the form of a theoretical expression containing A_f as a function of σ_p/σ_c. Thus Eqs. 32a and 28 are not directly comparable. Substitution of Eq. 32b into Eq. 28 to eliminate A_f yields an expression much more complex than Eq. 32a. This is not surprising, because Eqs. 32a and 32b are empirical relationships. The variables involved have been determined on a semitheoretical basis, but the power function form is only suggested by theoretical considerations. Some other function, such as a Fourier series, might be manipulated to produce the same empirical curve. The stress history constant t in Eq. 32a represents the theoretical value of $(\sigma_1 - \sigma_3)/\sigma_c$ when $\sigma_p/\sigma_c = 0$. In practice, of course, it is not possible to test a specimen with an over-consolidation ratio equal to zero, just as it is difficult to conceive of a negative $(\sigma_1 - \sigma_3)/\sigma_c$.

The stress history constant p in Eq. 32b can be shown to have a physical interpretation. As σ_p/σ_c approaches infinity, in Eq. 32b, A_f approaches p. Thus p is the limiting value of A_f as the over-consolidation ratio approaches infinity. In order to verify this experimentally, one test was performed on a specimen consolidated under 2 kg per sq cm and rebounded under zero stress. Thus σ_p/σ_c was equal to infinity. The measured value of A_f was -0.328, which compared favorably to the value of p = -0.300 found in Figure 7.

These results clearly indicate the applicability of Eqs. 32a and 32b to a variety of soils, tested, undrained, under a variety of stress conditions. The undrained shear strength of these soils at any degree of over-consolidation can be predicted without the use of effective stresses, because for a given soil and a given type of test, the strength and pore pressure parameters at failure are both uniquely related to the over-consolidation ratio.

CONCLUSIONS

Based on the results of this investigation, the following conclusions can be drawn.

1. For the several cohesive soils examined, both remolded and sedimented, when tested in consolidated undrained triaxial compression, an explicit empirical equation can be written relating the shear strength parameter, $(\sigma_1 - \sigma_3)/\sigma_c$, to the over-consolidation ratio, without the use of effective stress analysis. The use of these variables can be justified semitheoretically.
2. The use of effective stress analysis is not necessary because the Skempton pore pressure parameter at failure, and therefore, the effective stresses are also a function of the over-consolidation ratio.
3. Published results from another investigation indicate that the preceding conclusions are also valid for consolidated undrained extension tests on a remolded soil.

ACKNOWLEDGMENT

This research was made possible by a grant from the Advanced Research Projects Agency of the United States Department of Defense administered by the Materials Research Center of Northwestern University.

REFERENCES

1. Andresen, A., Bjerrum, L., Di Biago, E., and Kjaernsli, B., "Triaxial Equipment Developed at the Norwegian Geotechnical Institute." Norwegian Geotechnical Publ. 21 (1957).
2. Bishop, A. W., and Henkel, D. J., "The Measurement of Soil Properties in the Triaxial Test." Edward Arnold, Ltd., London, England (1957).
3. Bjerrum, L., "Theoretical and Experimental Investigations on the Shear Strength of Soils." Norwegian Geotechnical Publ. 5 (1954).
4. Coulomb, C. A., "Essai sur une Application des Regles de Maximis et Minimis à Quelques Problemes de Statique, Relatifs a l' Architecture." Mem. Acad. Sci. (Savants Etrangers), 7:343-382 (1776).
5. Gibson, R. E., "Experimental Determination of the True Cohesion and True Angle of Internal Friction in Clays." Proc. 3rd Internat. Conf. on Soil Mechanics and Foundation Eng., I, pp. 126-130 (1953).
6. Grim, R. E., and Bradley, R. F., "A Unique Clay from the Goose Lake, Illinois Area." Jour. Amer. Ceram. Soc., 22:5 (May, 1939).
7. Henkel, D. J., "Effect of Overconsolidation on Behavior of Clays During Shear." Geotechnique, VI:4 (Dec. 1956).
8. Hvorslev, M. J., "Conditions of Failure for Remolded Cohesive Soil." Proc. 1st Internat. Conf. on Soil Mechanics and Foundation Eng., III:51-53 (1936).
9. Hvorslev, M. J., "The Shearing Resistance of Remolded Cohesive Soils." Proc. U. S. Eng. Dept. Soils and Foundations Conference, Boston (1938).
10. Hvorslev, M. J., "Physical Components of the Shear Strength of Saturated Clays." U. S. Army Engineer Waterways Exp. Sta. Misc. Paper 3-428 (Jan. 1961).
11. Johnson, L. H., "Nomography and Empirical Equations." John Wiley, New York (1952).
12. Jurgenson, L., "The Shearing Resistance of Soils." Jour. Boston Soc. of Civil Eng., XXI:3 (July 1934).
13. Matlock, H., Jr., Fenske, C. W., and Dawson, R. F., "De-aired, Extruded Soil Specimens for Research and for Evaluation of Test Procedures." ASTM Bull. 177 (Oct. 1951).

14. Mitchell, J. K., "The Fabric of Natural Clays and Its Relation to Engineering Properties." Proc. HRB, 35:693-713 (1956).
15. Olson, R. E., "The Shear Strength Properties of Calcium Illite." Geotechnique, XII:1 (March 1962).
16. Parry, R. H. G., "Triaxial Compression and Extension Tests on Remolded Saturated Clay." Geotechnique, X:4 (Dec. 1960).
17. Perloff, W. H., Jr., "The Effect of Stress History and Strain Rate on the Undrained Shear Strength of Cohesive Soils." Ph. D. Dissertation, Northwestern Univ. (June 1962).
18. Reiner, M., "Deformation, Strain and Flow." 2nd Ed., Interscience Publishers, New York (1960).
19. Rutledge, P. C., "Cooperative Triaxial Shear Research Program of the Corps of Engineers." Soil Mechanics Fact Finding Survey, Progr. Rep. U. S. Army Engineer Waterways Exp. Sta. (April 1947).
20. Skempton, A. W., "The Pore Water Coefficients A and B." Geotechnique, IV:4 (Dec. 1954).
21. Skempton, A. W., and Bishop, A. W., "Soils." Chapter X from "Building Materials. Their Elasticity and Inelasticity." Ed., M. Reiner, North Holland Publishing Co., Amsterdam, Holland, pp. 417-482 (1954).
22. Taylor, D. W., "Fundamentals of Soil Mechanics." John Wiley Publishing Co., New York (1948).
23. Terzaghi, K., "The Shearing Resistance of Saturated Soils and the Angle Between the Planes of Shear." Proc. 1st Internat. Conf. on Soil Mechanics and Foundation Eng., I:54-56 (1936).
24. Terzaghi, K., and Peck, R. B., "Soil Mechanics in Engineering Practice." John Wiley Publishing Co., New York (1948).
25. Wahls, H. E., "Primary and Secondary Effects in the Consolidation of Cohesive Soils." Unpubl. Ph. D. Thesis, Northwestern Univ.

Appendix

A = Skempton pore pressure parameter;
A_f = Skempton pore pressure parameter at failure;
C_e = expansion index;
C_c = compression index;
C_s = compressibility of the soil skeleton ($F^{-1}L^2$);
C_w = compressibility of water ($F^{-1}L^2$);
c_e = Hvorslev effective cohesion (FL^{-2});
c_z = theoretical effective cohesion at zero void ratio (FL^{-2});
e = void ratio;
$F_N(x)$ = a function of x;
I_p = plasticity index = $w_L - w_p$;
m = stress history constant for the pore pressure parameter prediction equation;
N = an integer;
n = stress history constant for the pore pressure parameter prediction equation;
p = stress history constant for the pore pressure parameter equation;
$\Delta P/P_o$ = pressure increment ratio for a consolidation test;
r = stress history constant for the strength prediction equation;
s = stress history constant for the strength prediction equation;
t = stress history constant for the strength prediction equation;
Δu = pore pressure change due to a change in principal stresses (FL^{-2});
u_f = pore pressure at failure (FL^{-2});
w = water content;
w_L = liquid limit;
w_P = plastic limit;
ϕ_e' = Hvorslev effective angle of internal friction;
σ_1 = major total principal stress (FL^{-2});
σ_2 = intermediate total principal stress (FL^{-2});

σ_3	=	minor total principal stress (FL^{-2});
σ_1'	=	major effective principal stress (FL^{-2});
σ_2'	=	intermediate effective principal stress (FL^{-2});
σ_3'	=	minor effective principal stress (FL^{-2});
$(\sigma_1 - \sigma_3)$, $(\sigma_1' - \sigma_3')$	=	principal stress difference (FL^{-2});
σ_c	=	consolidation pressure immediately prior to strength test (FL^{-2});
σ_e'	=	Hvorslev equivalent consolidation pressure (FL^{-2});
σ_o	=	theoretical pressure required to produce zero void ratio (FL^{-2});
σ_p	=	maximum preconsolidation pressure (FL^{-2}); and
σ_p/σ_c	=	over-consolidation ratio.

Load-Time Relationships In Direct Shear of Soil

H. C. SAXE, L. D. GRAVES, and B. B. SCHIMMING
Respectively, Professor and Head, Associate Professor, and Assistant Professor, Department of Civil Engineering, University of Notre Dame

Development of a direct shear apparatus capable of failing a soil specimen in a time interval ranging from a few milliseconds to days is described. The apparatus, referred to as DACHSHUND I, utilizes a pneumatic system for the application of both static and dynamic loads. Special design features include impact accelerators and a double triggering system that allows either separate or synchronous application of normal and shear loads. The maximum shear and normal load capability of the pneumatic system is 500 lb. Soil specimens up to 4 in. in diameter and 0.75 in. thick can be accommodated by the shear box.

Preliminary static and dynamic test results conducted on Standard Ottawa Sand and Jordan Buff Clay indicate that the shear strength of dry sand is insensitive to loading rate, whereas the strength of an unsaturated clay increases with increased loading rates.

•THE WORK described in this paper is part of a broad research effort sponsored by the United States Air Force with the ultimate objective of obtaining dynamic shearing and frictional force data on soils for use in the design of protective structures and in the interpretation of laboratory experiments in soil dynamics. The objective of this part of the research effort is to design and build a direct shear-type device with which soils of all types can be forced to fail on a chosen plane by either dynamic or static loadings. In addition, the device should be capable of recording the time history of normal and shearing loads and deformations reasonably close to those on the failure plane. Such a device could be very useful in the highway field, as well as in military construction.

DESIGN CRITERIA

An exhaustive literature search resulting in a sizable annotated bibliography by Woods (6) did not reveal any previous investigations of the dynamic strength of soil using direct shear devices. However, the soil characteristics determined by other methods can be used as guides for choosing the design criteria for a direct shear device. In the following discussion, the static and dynamic soil characteristics found by other investigators are considered in the development of the design criteria.

Specimen Size

The grain size of the soil to be tested determines the minimum size of test specimen because of the need to develop a macroscopic effect across the shear plane. Too thick a specimen may induce progressive shear failure, whereas too thin a specimen may

Paper sponsored by Committee on Stress Distribtuion in Earth Masses.

not be able to accommodate the larger grain sizes. For soil with grain sizes up to fine gravel, a compromise thickness of 0.75 in. and a diameter of 4 in. was chosen.

Shear Deformation Capacity

Previous investigators have found that shear failure occurs in soils at a wide range of deformation values. Stiff shale-like clay was reported by Casagrande and Shannon (2) to reach peak load at about 1 percent strain in triaxial compression tests. The same authors found that a disturbed soft muck, in an unconfined compression test, did not reach peak load before 30 percent strain. Other authors report values between these for various soils. Use of the method suggested by Taylor (4) for calculating the shear strains in compression and direct shear indicates that the direct shear deformation corresponding to Casagrande and Shannon's 30 percent compressive strain would be more than 0.5 in. for a soil specimen 4 in. in diameter and 0.75 in. thick. Thus, in order to accommodate ultimate strains that may be in excess of peak strains, it was decided that the device should be capable of applying maximum shear deformations of 1.25 in.

Load Capacity

An absolute value for the maximum normal and shear force that the device should be capable of applying to the soil specimen is not easily chosen. The wide range in the shearing resistance of soil and the time dependency of the shear strength of a particular soil sample makes it difficult to assign a maximum value. In sands the shearing strength is controlled by the normal pressure on the shearing plane, and the required shearing force should not exceed the normal force. On the other hand, there is no such direct relation for cohesive soil. Whitman (5) has measured dynamic compressive strengths as high as 400 psi for a stiff clay soil. Thus, the shear strength would be 200 psi if the shear strength is one half the compressive strength. A 4-in. diameter sample could be made to fail with a shear force of 2,500 lb. However, by adding filler rings in the shear box, a soil sample 1 in. in diameter could be failed using a force of only 160 lb. With this sort of data in mind, as well as the static strengths of average soils, it was decided that the apparatus should be designed to apply a maximum force of 500 lb normal and parallel to the shear plane. Especially strong soils could then be tested by using filler rings and smaller diameter samples.

Minimum Loading Time

Whitman (5) and Richardson (3) have attempted to obtain minimum loading times of 1 msec; but in doing so with the cylindrical compressive specimens they encountered wave propagation and lateral inertial problems that limited the meaningful rise time to a value of about 10 msec. This type of restriction is less evident in a direct shear test and, therefore, it seemed feasible to attempt to develop a device that could apply the failure load in about 1 msec.

METHOD OF LOAD APPLICATION

Literature review revealed that previous investigators had used testing devices that fell into five general categories as to their manner of load application. Each of these categories was reviewed and considered for the project.

Gravity Testers

Three types of gravity testers have been used. One type simply drops a weight from a preselected height in a guide rail system. Another type accelerated the falling weights by means of elastic cords. The last type, the pendulum, allowed a suspended weight to be raised to a preselected height and released to strike the specimen at maximum velocity. All gravity testers accomplished the rapid loading desired and were simple to operate, but they lacked flexibility and were very bulky.

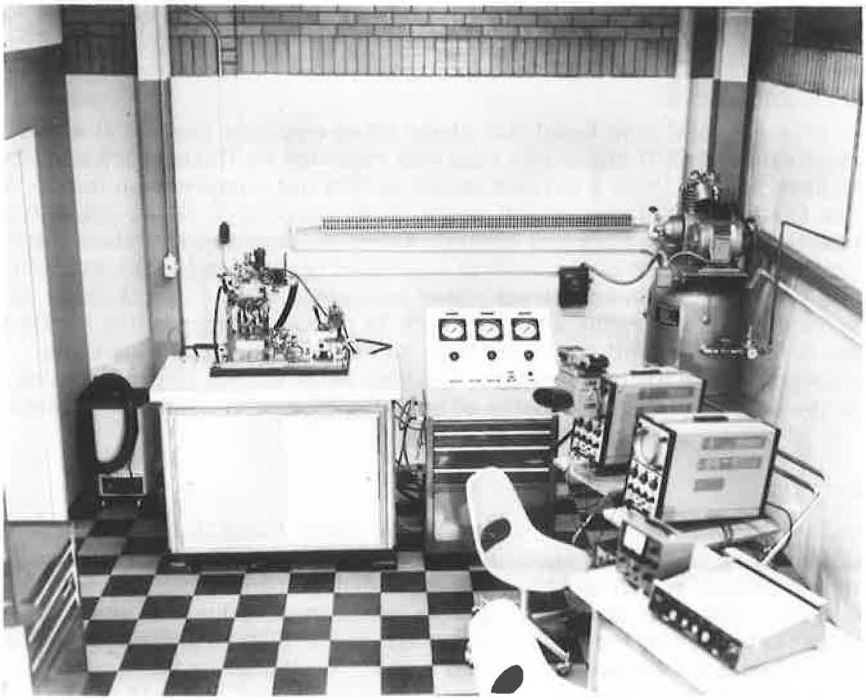

Figure 1. Laboratory facility.

Explosive-Operated Testers

The entire category of explosive-operated devices was discarded from consideration for this project because of their inflexibility and hazardous nature.

Shock Tubes

Whereas shock tubes were suggested as a possible loading type in the early work on the project, further consideration showed that such an apparatus could not be made compact enough for ordinary use and would be difficult to operate in the static range.

Hydraulic Loading Machines

Hydraulic loading machines can be used for all loading speeds desired and meet all other criteria established for the apparatus design. However, the valving and pumping equipment are more complex than for a pneumatic system.

Pneumatic Loading Machines

Pneumatic loading machines also meet all criteria established for the design of the apparatus and seem to offer the possibility of the most compact design.

After considering each of the over-all categories of loading arrangements, it was decided that the apparatus be a pneumatic loading arrangement designed around a standard configuration for the shear box. The developed apparatus has been given the name DACHSHUND I (Dynamically Applied Controlled Horizontal SHear—University of Notre Dame I). A photograph of the complete installation is shown in Figure 1 and a schematic representation of the various parts in Figure 2.

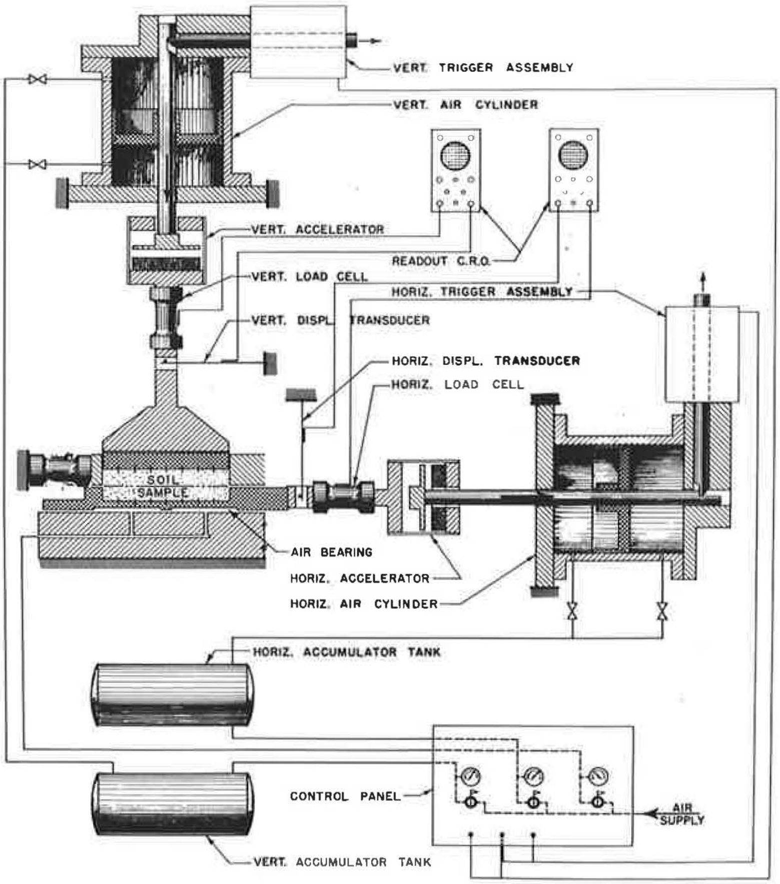

Figure 2. Schematic of apparatus—DACHSHUND I.

APPARATUS

Pneumatic System

The pneumatic system devised for applying loads to the soil sample consists of the following components: air compressor, two accumulator tanks, a vacuum pump, and two air cylinders. These components are supplemented by the necessary valving, piping, pressure regulators, and gages required to transmit and control the air as needed.

When a dynamic test is made, air is fed to the accumulator tanks from the air compressor through the pressure regulators. After the air pressure in the accumulator tanks has reached a predetermined value, the cylinders are locked in position by their triggering devices and air from the tanks is let into the rear of the cylinders and into the air bearing. The shear test is started by actuating the solenoids that cause the triggering device to release the pistons. The pistons are made to move rapidly by the expanding air and the soil is sheared off in a few milliseconds. The air pressure behind the moving piston is quickly reduced as the specially contoured skirts of the piston first cover the air inlet port and then uncover the outlet port in each cylinder. The air pressure is thus dissipated and the piston stops. Compression of air on the forward side of the piston can be used to help stop the piston, or a vacuum can be created to speed the forward motion. In either case, a rubber bumper at the end of the cylinder stops the piston at the end of its travel. The air gap in the vertical and horizontal accelerator is used to synchronize the application of normal and shearing loads or permit the pistons to gain speed before load application.

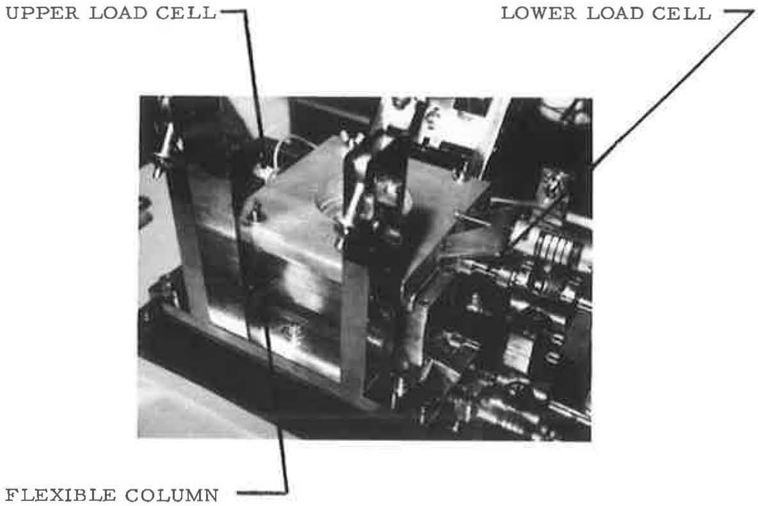

Figure 3. Shear box assembly.

When a slow shear test is to be made, the pistons are not locked in position and their motion is controlled by gradually increasing the air pressure in the accumulator tanks, cylinder and air bearing as desired to run a test in a predetermined time.

Shear Box

In a direct shear device, shearing action takes place between a fixed and a movable shear box. Because a high shear rate is sought, the lower shear box (Fig. 3) should be the movable member. This box is made of No. 43 casting aluminum, selected because of its high strength-weight ratio and its resistance to the corrosive action of moist soils. The moving shear box rests on a cushion of air provided by an air bearing, thus minimizing frictional resistance. Eccentric loads are resisted by four small ball bearings mounted in cages, recessed into the brass support plate at a depth allowing approximately a 0.002-in. clearance between the shear box and the plate under load. Four hardened stainless steel strips are inlayed into the bottom surface of the shear box for contact with the ball bearings.

Although the movable shear box slides on a relatively frictionless interface, significant inertial forces may distort the measured value of soil resistance. Therefore, the fixed or upper shear box was supported vertically by mounting it on four thin flexible columns and was restrained in a horizontal direction by fastening it to a load cell. Thus, shear loads can be measured on both the upper and lower shear boxes to evaluate inertial and friction forces and the shearing force on the soil.

Load Measuring Devices

Measurement of the normal and shearing forces applied to the soil sample involves two measuring systems. These are:

1. Bourdon Tube Pressure Gages. —For static load measurements, visual readout of Bourdon Tube pressure gages is made by the operator to ascertain the pressures corresponding to the normal and shearing forces being applied to the test sample, as well as the air bearing. Fine adjustments in these applied pressures may be obtained by manual adjustments of needle valve controlled pressure regulators. However, the pressures recorded on the gages include piston friction, which is not a constant.
2. Electronic Load Transducers. --Because the pressure gage readings are not a true measure of the force on the soil, an electronic load transducer near the soil is used for both static and dynamic tests. The load cell designed for the measurement of the normal and shearing forces applied to the test specimen (Fig. 3) consists of a thin-

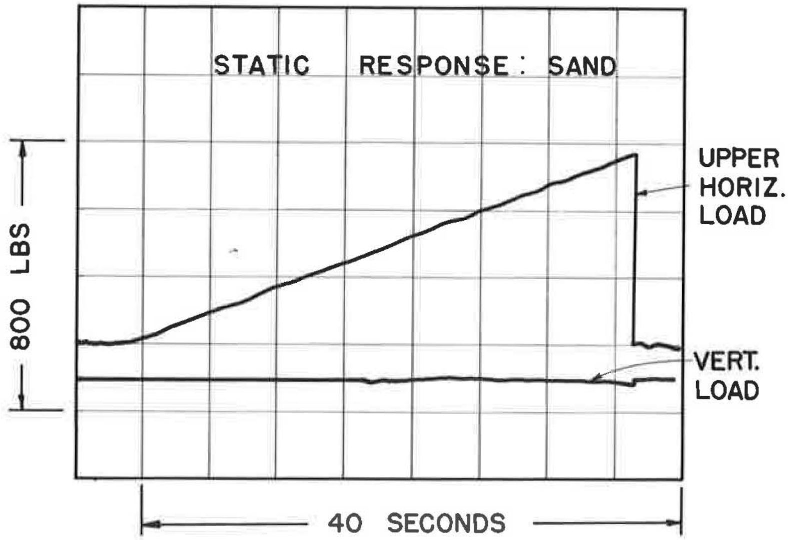

Figure 4. Static response: sand.

walled spool-shaped cylinder provided with enlarged threaded ends for the in-line connection to the piston rods. The transducing elements of the load cells consist of four wire resistance strain gages, cemented to the walls of the hollow cylindrical spool and connected to form a Wheatstone bridge circuit. The specific type of wire resistance strain gages used was SR-4, type CD-7. The output of the load cells is displayed on an oscilloscope and recorded with a camera during dynamic tests or on an X-Y recorder during static tests.

Displacement Measuring Devices

Both vertical and horizontal motions are measured just outside the shear box by linear varying potentiometers. For dynamic shear tests the output is shown on an oscilloscope and recorded with a camera, whereas for slow shear tests the output is recorded on an X-Y recorder.

EXPERIMENTAL RESULTS

A series of preliminary tests has been conducted on both a cohesionless and cohesive soil. The cohesionless soil is a Standard Ottawa Sand (20 to 30 sieves). Two relative densities have been studied. The cohesive soil is a Jordan Buff Clay sold commercially by the United Clay Mines, Trenton, N. J. The characteristics of this clay are: liquid limit, 54 %; plastic limit, 26 %; shrinkage limit, 22 %; plasticity index, 28 %; and specific gravity, 2.74. The clay was purchased in powder form, mixed with distilled water to a moisture content of approximately 31 % and compacted to a wet density of 114 pcf.

To compare the behavior of DACHSHUND I with conventional direct shear machines, a series of static calibration tests was run. Figures 4 and 5 indicate a typical set of results on the Ottawa Sand for a test duration of approximately 40 sec. The shear load was increased manually at approximately a linear rate.

The failure envelopes obtained from a series of such static tests on the Ottawa Sand in both loose and dense conditions are shown in Figure 6. The resulting friction angles are compared with those previously reported by Burmister (1) (Table 1).

Despite the unique features of DACHSHUND I, it is capable of imposing essentially the same force system on a soil specimen as the more conventional direct shear devices.

Figures 7 and 8 show a typical set of traces recording the dynamic response on the same Ottawa Sand. Pressure was developed in the horizontal cylinder while the piston was restrained by the triggering system. On release of the trigger, a shear load was

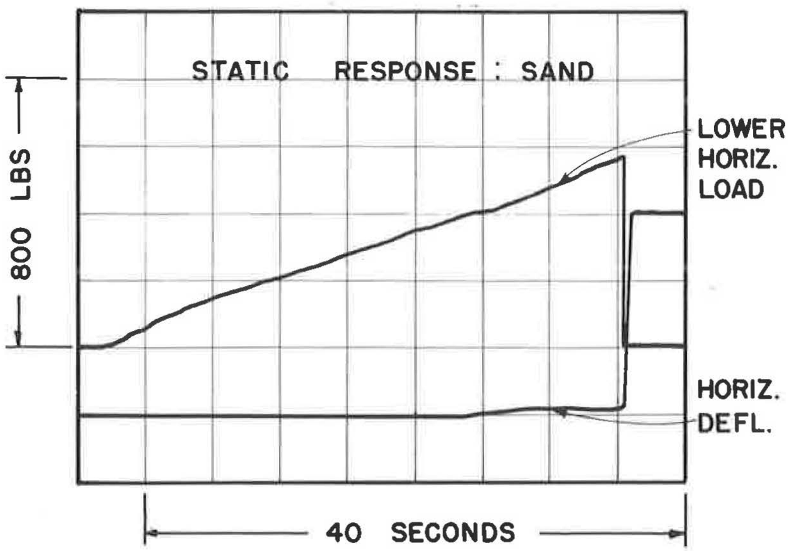

Figure 5. Static response: sand.

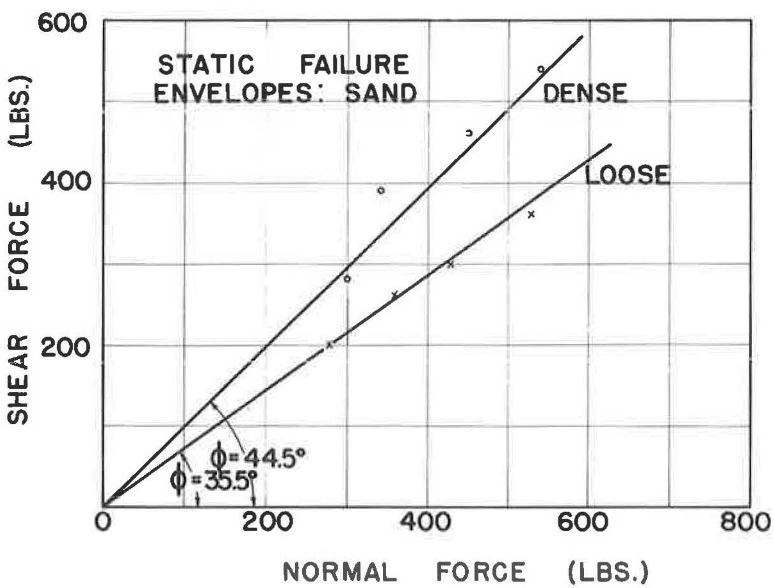

Figure 6. Static failure envelopes: sand.

TABLE 1

STATIC TEST RESULTS AT VARYING DENSITIES

Soil	Rel. Density	Friction Angles, ϕ (deg)	
		DACHSHUND I	BURMISTER
Ottawa Sand	90%	44.5	43
Ottawa Sand	33%	35.5	37

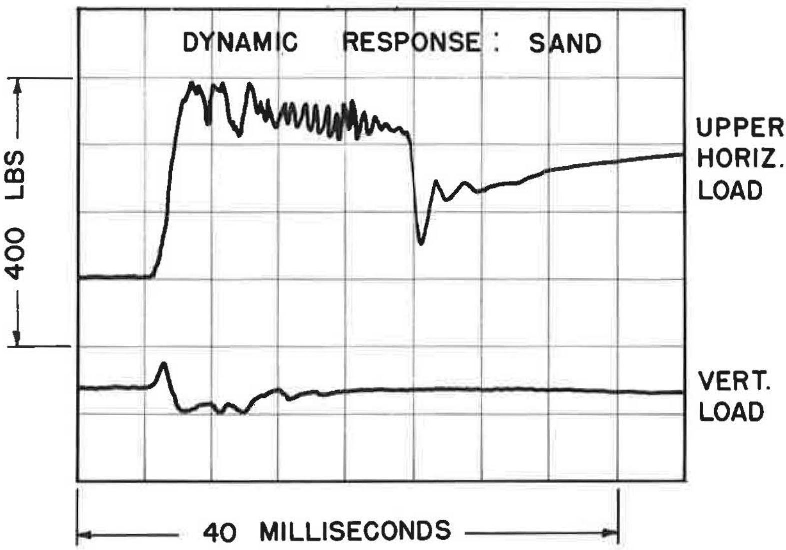

Figure 7. Dynamic response: sand.

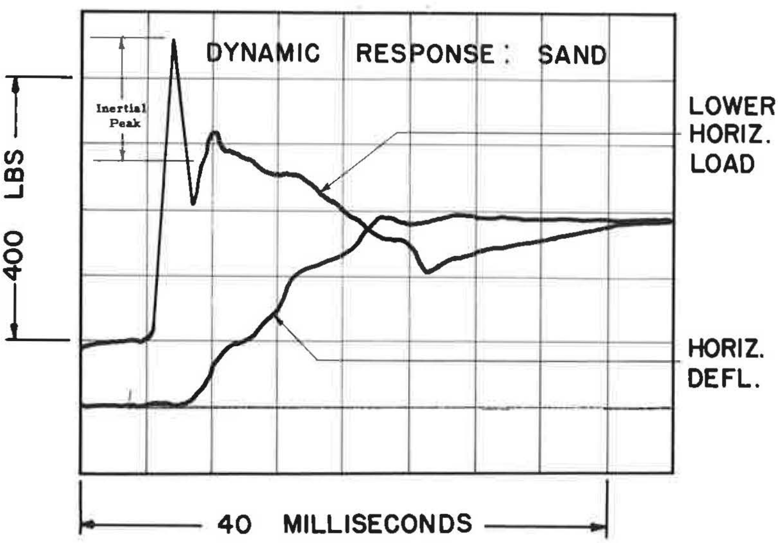

Figure 8. Dynamic response: sand.

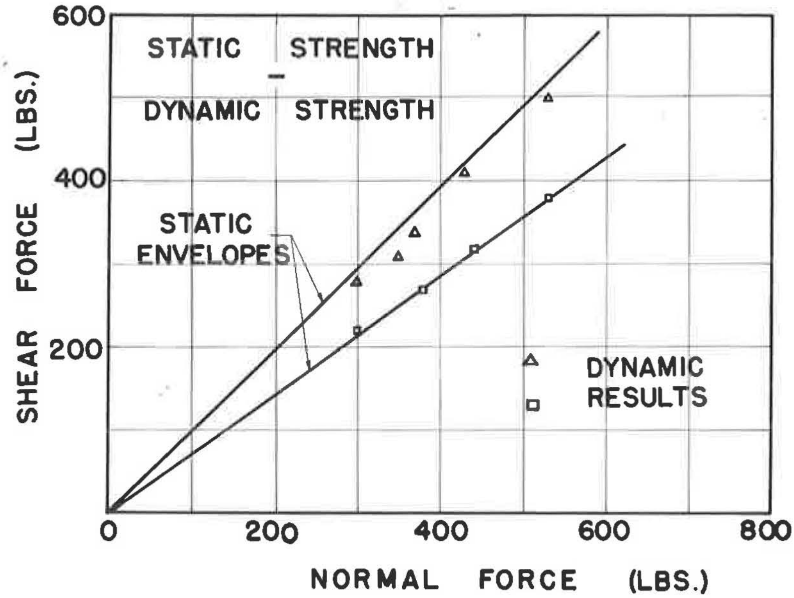

Figure 9. Comparison of dynamic strength and static envelopes: sand.

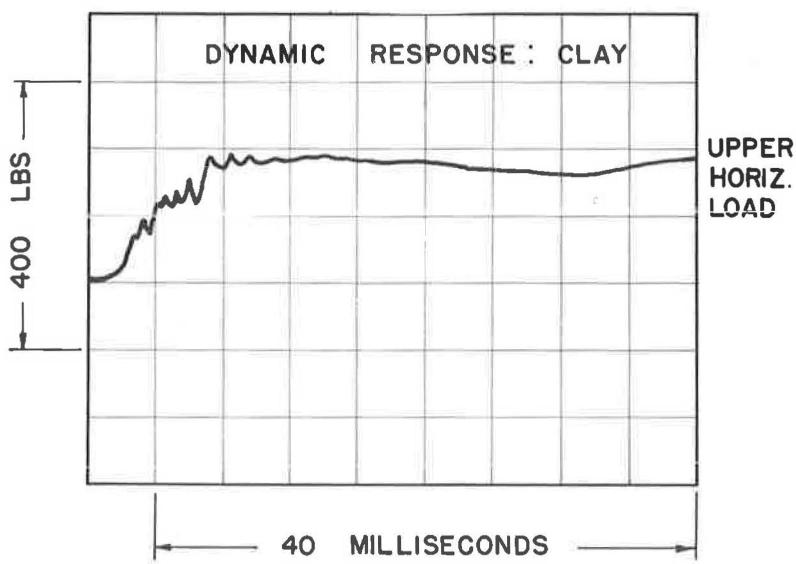

Figure 10. Dynamic response: clay.

imposed on the specimen resulting in a time to failure of approximately 3 msec. From the direction of the forces involved, it was concluded that the peak in the lower horizontal load cell trace was due to the acceleration of the lower tray. Based on this conclusion and by varying the mass of the lower tray, the inertial force as shown was determined. The remaining force, equal to the total force minus the inertial peak, was applied to the specimen as dictated by the agreement between the "action" and "reaction" load cells.

Figure 9 compares the results of the dynamic sand tests, all of which involved times

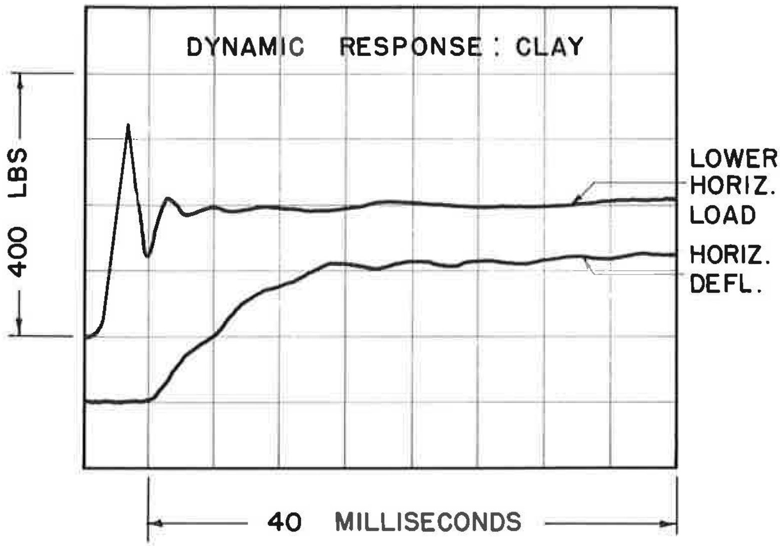

Figure 11. Dynamic response: clay.

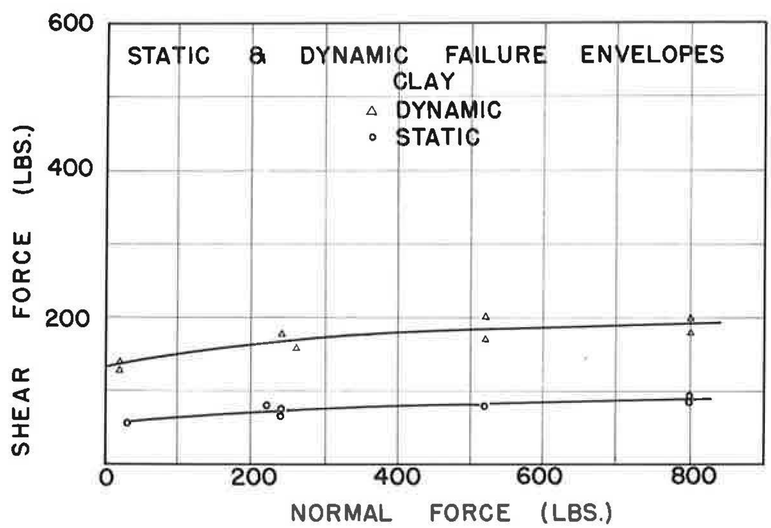

Figure 12. Static and dynamic failure envelopes: clay.

to failure between 0 and 5 msec, and the static failure envelopes. This plot clearly indicates that the strength of the dry Ottawa Sand tested is insensitive to load rate effects, thus verifying the results obtained by Whitman (5) in triaxial compression.

The next phase of the investigation involved essentially a repetition on the Jordan Buff Clay of the previously described static and dynamic test. The static test traces were similar to those in Figures 4 and 5; however, the dynamic trace characteristics differed somewhat from those reported on the sand. Figures 10 and 11 are a typical set of dynamic test results for the compacted clay.

The static and dynamic strength envelopes for the Jordan Buff Clay are shown in Figure 12. The dynamic envelope is comprised of tests with time to failure in the 0 to 5 msec range, whereas the static envelope involved test durations of approximately

0 to 40 sec. An examination of Figure 12 indicates that at any particular value of the normal load, the dynamic shear strength is approximately twice the static value. These results certainly demonstrate the time dependent strength characteristics of the unsaturated clay under consideration; however, the wide spread in test duration should be remembered.

An additional comparison between static and dynamic response is the load deflection characteristics of the soils tested (Fig. 13).

For the compacted clay, the increase in strength associated with the dynamic tests appears to be accompanied by an increase in deflection or strain at peak load. The dry Ottawa Sand, which displayed no strength variations as a function of load rate, reached peak load at a very small deflection in both the static and dynamic cases. These conclusions regarding the load deflection response should be treated as tentative due to the degree of interpretation required in "matching" the individual load and deflection traces.

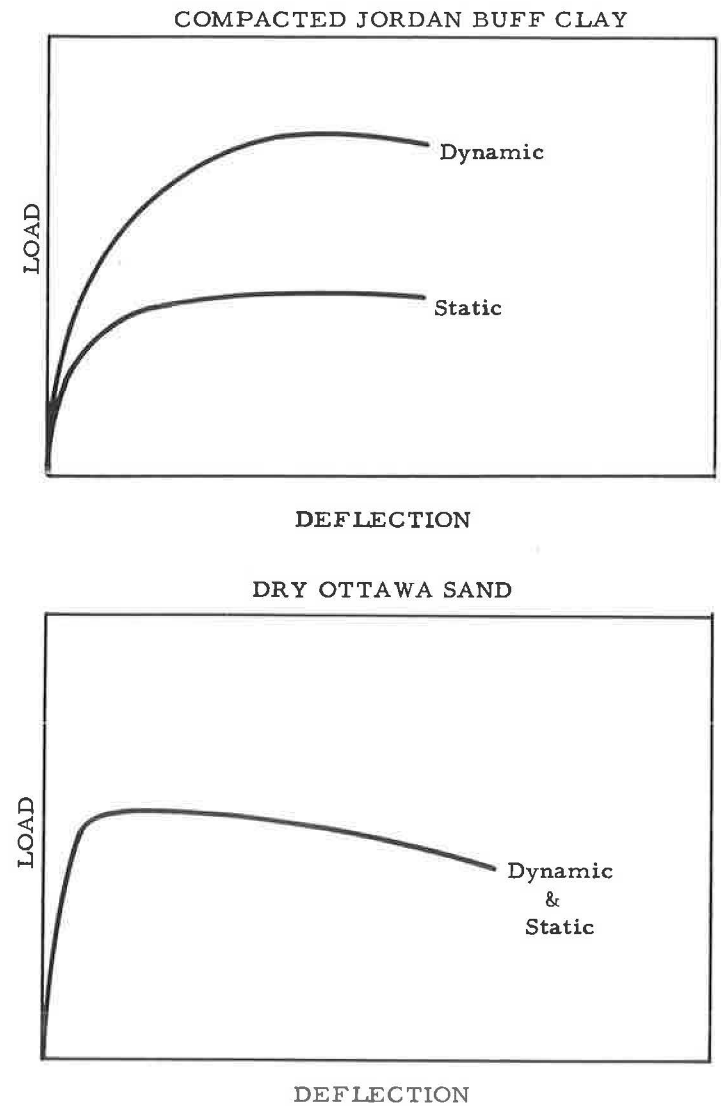

Figure 13. Load displacement relations.

CONCLUSIONS

A direct shear-type device has been developed that is capable of imposing shear loads on a soil specimen over a wide range of loading rates. In the conventional time range, it duplicates the behavior of standard-type direct shear machines.

Preliminary dynamic results appear to corroborate, at least in a qualitative sense, the findings obtained from dynamic triaxial compression tests.

The two-dimensional dynamic capabilities of the apparatus offer the promise of greater insight into the dynamic behavior of soils.

ACKNOWLEDGMENTS

The authors wish to thank the United States Air Force, Air Force Systems Command, Research and Technology Division, Air Force Weapons Laboratory, for permission to use part of the data from Contract AF 29(601)-5174 in the preparation of this paper.

Special recognition should be given to Prof. Carl C. Stevason of the Mechanical Engineering Department of the University of Notre Dame for the machine design of DACHSHUND I.

Richard Wood's literature search on the original design and Theodore Kretschmer's and Vincent Drnevich's assistance in the operational check-out of the device and the testing of soils cannot be overlooked. A debt of gratitude is due Mrs. Ruth Jewett for her patient typing of the manuscript to its finished form.

REFERENCES

1. Burmister, D. M., "The Place of the Direct Shear Test in Soil Mechanics." ASTM Spec. Tech. Publ. 131 (1952).
2. Casagrande, A., and Shannon, W. L., "Strength of Soils Under Dynamic Loads." Trans., ASC, 74:4 (1948).
3. Richardson, A. M., "Effects of Rate of Strain on Stress Strain Behavior of Saturated Soils." M.I.T. Rep. 6, Response of Soil to Dynamic Loadings, U.S. Army Corp of Engineers, AD-272653 (1961).
4. Taylor, D. W., "A Comparison of the Results of Direct Shear and Cylindrical Compression Tests." ASTM Sym. on Shear Testing of Soils (1939).
5. Whitman, R. V., "The Behavior of Soils Under Transient Loadings." Proc. 4th Internat. Conf. on Soil Mechanics and Foundation Engineering (1957).
6. Woods, R. D., "The Dynamics of Impulsively Loaded Soils." U.S. Air Force Tech. Doc. Rep. 63-3050 (1963).
7. Saxe, H. C., Graves, L. D., and Schimming, B. B., "Development of an Apparatus for the Dynamic Direct Shear Testing of Soils." U.S. Air Force Weapons Lab. Tech. Doc. Rep. RTD TDR-63-3055.